CNWRA *A center of excellence in earth sciences and engineering*

A Division of Southwest Research Institute™
6220 Culebra Road • San Antonio, Texas, U.S.A. 78228-5166
(210) 522-5160 • Fax (210) 522-5155

May 24, 2001
Contract No. NRC–02–97–009
Account No. 20.01402.671

U.S. Nuclear Regulatory Commission
ATTN: Dr. Mysore S. Nataraja
Division of Waste Management
TWFN (Mail Stop 7–C6)
Washington, DC 20555

Subject: Repository Design and Thermal-Mechanical Effects Key Technical Issue Intermediate Milestone No. 20.01402.671.110, Process-Level Rockfall Studies for Input to SEISMO Module of the TPA Code—Letter Report

Dear Dr. Nataraja:

Attached is the Center for Nuclear Waste Regulatory Analyses document entitled "Assessment of Seismically Induced Rockfall in the Emplacement Drifts of the Proposed Repository at Yucca Mountain, Nevada." This technical document fulfills the requirements for the subject milestone, which is due May 25, 2001.

This report documents results of the two-dimensional (2D) discontinuous deformation analysis (DDA) on effects of seismic ground motions on rock mass surrounding underground excavations. The major focuses of the study are to (i) determine the appropriateness of using 10-Hz and 3-s duration harmonic wave time histories to represent site-specific ground motion time histories, (ii) identify key parameters that control drift stability, and (iii) assess potential extent and areal coverage of seismically induced rockfall. Harmonic wave time histories with a 10-Hz frequency and a 3-s duration are currently used by the Civilian Radioactive Waste Management System Management and Operating Contractor to study ground control and drift degradation. The 2D DDA results suggest that these harmonic waves may not represent site-specific ground motion time histories. Consequently, site-specific ground motion time histories should be used for analyses. Several observations are obtained from the limited study of seismically induced rockfall:

- Variations of joint parameters (e.g., spacing and length) play an important role in drift stability. The extent of damage ranges from a few small rock blocks that fall into the drifts to a substantial collapse of the drifts.
- Seismic events influence stability through accumulation of permanent deformations around underground excavations.
- Degradation of joint shear strength may substantially decrease the stability of drifts. For consideration of long-term stability of drifts, degradation of joint shear strength over time should be included in the analyses.
- The extent of rockfall is found to be more severe for the rock-mass models with relatively small joint spacings than for the models with relatively large joint spacings. The latter cases contain block sizes often larger than the rock-mass models with relatively small joint spacings. Consequently, they are kinematically more stable.

Washington Office • Twinbrook Metro Plaza #210
12300 Twinbrook Parkway • Rockville, Maryland 20852-1606

The effect of thermal load on rockfall was not considered in the analyses because the DDA computer codes do not have the option of modeling formation of new rock blocks due to thermally induced failure of intact rocks. This mode of failure is plausible for the thermal load and the proposed continuous ventilation during the operations period being considered at the proposed repository and could potentially affect seismically induced rockfall. This condition is particularly important for the large joint spacing cases where the rock masses include relatively large block sizes that are kinematically more stable. Formation of new blocks may offset the stable condition, thus changing maximum rockfall block size. Separate analyses investigating such effects may be beneficial.

If you have any questions on this report, please contact me at (210) 522-5151 or Simon Hsiung at (210) 522-5209.

Sincerely yours,

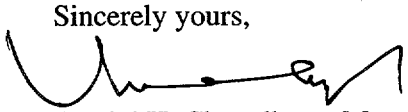

Asadul H. Chowdhury, Manager
Mining, Geotechnical, and
Facility Engineering

ACH/cp

cc: J.Greeves
J. Piccone
W. Reamer
D. DeMarco
B. Meehan
J. Linehan
(w/o enclosure)
E. Whitt
N. Stablein
D. Brooks
D. Galvin
B. Jagannath
T. Ahn
T. McCartin
P. Justus
B. Leslie
J. Pohle
W. Patrick
CNWRA Directors
CNWRA Element Managers
P. Maldonado
T. Nagy (SwRI Contracts)
S. Hsiung
A. Ghosh
D. Gute
G. Ofoegbu
B. Dasgupta
D. Hughson
J. Stamatakos
G. Cragnolino
D. Dunn
S. Mohanty

ASSESSMENT OF SEISMICALLY INDUCED ROCKFALL IN THE EMPLACEMENT DRIFTS OF THE PROPOSED REPOSITORY AT YUCCA MOUNTAIN, NEVADA

Prepared for

U.S. Nuclear Regulatory Commission
Contract NRC–02–97–009

Prepared by

Sui-Min Hsiung
Gen-Hua Shi
Asadul H. Chowdhury

Center for Nuclear Waste Regulatory Analyses
San Antonio, Texas

May 2001

ABSTRACT

Long-term stability of emplacement drifts is of interest in assessing the safety of disposal of high-level waste in the proposed repository at Yucca Mountain, Nevada. Seismicity is a potential disruptive event that needs adequate consideration in assessing the performance of the proposed geologic repository. Rockfall induced by seismicity could damage drip shields and waste packages, affecting their performance. Furthermore, change in drift geometry due to seismically induced rockfall may have an effect on flow into the emplacement drifts and the near-field environment.

The overall objective of this study is to assess the effects of seismic ground motions on the behavior of rock mass surrounding underground excavations. Emphasis is placed on determination of the extent of rockfall. This study also examines if the use of sinusoidal waves with a frequency of 10 Hz and a duration of 3 s by the Civilian Radioactive Waste Management System Management and Operating Contractor is appropriate. This report presents a two-dimensional (2D) discontinuous deformation analysis (DDA) for the above objective using computer codes df0 and dda_ct2. Analyses indicate that sinusoidal waves with a frequency of 10 Hz and a duration of 3 s may not represent site-specific ground motion time histories for ground control or rockfall analyses. The results also show that rock-mass responses to ground motions are dependent on the geometries of the blocky systems analyzed for a given joint set because the inherent variations of the parameters for that joint set. The extent of damage ranges from a few small rock blocks that fall into the drifts to a substantial collapse of the drifts. Analyses confirm observations from the laboratory and field studies that seismic events influence stability through accumulation of permanent deformations around underground excavations. DDA results also indicated that the effect of long-term degradation of joint shear strength would decrease the stability of the drifts. Consequently, long-term degradation of joint shear strength needs to be considered in assessing rockfall potential for the emplacement drifts during the postclosure performance period. DDA results also indicate that a majority of the block sizes for rockfall are small for both the large and small joint spacing cases analyzed with occasional large blocks. Based on limited modeling results, it was found that the maximum rock block size for the large joint spacing cases was approximately 1.1 m^3 per unit drift length and approximately 3.1 m^3 per unit drift length for the small joint spacing cases. The values for the maximum block sizes could change when more modeling results become available. Note that the rock block size is presented in volume per unit drift length in this report because the actual rock block volume falling on one waste package cannot be estimated from a 2D analysis. The rock block volume will depend on the joint spacing in the third dimension. The effect of thermal load on rockfall was not considered in the analyses because the DDA computer codes do not have the option of modeling formation of new rock blocks due to thermally induced failure of intact rocks. This mode of failure is plausible for the thermal load and the proposed continuous ventilation during the operations period being considered and could potentially affect seismically induced rockfall. This condition is particularly important for the large joint spacing cases where the rock masses include relatively large block sizes that are kinematically more stable. Formation of new blocks may offset the stable condition, thus changing maximum rockfall block size. Separate analyses investigating such effects may be beneficial.

CONTENTS

CONTENTS (cont'd)

FIGURES

FIGURES (cont'd)

FIGURES (cont'd)

TABLES

ACRONYMS

2D	two-dimensional
CNWRA	Center for Nuclear Waste Regulatory Analyses
CRWMS M&O	Civilian Radioactive Waste Management System Management and Operating Contractor
DDA	Discontinuous Deformation Analysis
DOE	U.S. Department of Energy
EBS	engineered barrier system
EDA II	Enhanced Design Alternative II
FEM	finite element method
NRC	U.S. Nuclear Regulatory Commission
PGA	peak ground acceleration
PGV	peak ground velocity
PSHA	probabilistic seismic hazard analysis
QA	quality assurance
RSS	Repository Safety Strategy
TPA	Total-system Performance Assessment
TSw2	Topopah Springs Welded Tuff Unit 2
VA	viability assessment
WP	waste package
YM	Yucca Mountain

ACKNOWLEDGMENTS

This report was prepared to document work performed by the Center for Nuclear Waste Regulatory Analyses (CNWRA) for the U.S. Nuclear Regulatory Commission (NRC) under Contract No. NRC–02–97–009. The activities reported here were performed on behalf of the NRC Office of Nuclear Material Safety and Safeguards, Division of Waste Management. The report is an independent product of the CNWRA and does not necessarily reflect the views or regulatory position of the NRC.

The authors thank A. Ghosh, P. Mackin, G.I. Ofoegbu, and B. Dasgupta for their review of the report. The authors are thankful to C. Patton and L. Selvey for assisting with the word processing and preparation of the report and to C. Cudd and B. Long for the editorial reviews.

QUALITY OF DATA, ANALYSES, AND CODE DEVELOPMENT

DATA: All CNWRA-generated original data contained in this report meet quality assurance (QA) requirements described in the CNWRA QA Manual. Sources of other data should be consulted for determining the level of quality for those data.

ANALYSES AND CODES: Analyses in this report were conducted using computer codes df0 and dda_ct2. These two computer codes are for discontinuous deformation analysis of jointed rock media. The computer code df0 is controlled by the CNWRA software QA procedure (TOP–018, Development and Control of Scientific and Engineering Software). The computer code dda_ct2 is currently under development and will be brought under control following TOP–018 once the development work is completed.

EXECUTIVE SUMMARY

Seismicity is a potential disruptive event that needs adequate consideration in assessing the performance of the proposed geologic repository at Yucca Mountain (YM), Nevada. Rockfall induced by seismicity could damage drip shields and waste packages (WPs), affecting their performance. The potential effects of rockfall on the performance of the drip shields and WPs are twofold. The first potential effect of rockfall is to rupture drip shields and WPs by the impact produced by the falling rock. The second aspect is that rockfall may cause damage to the drip shields and WPs leading to accelerated corrosion that may reduce their intended service life.

The proposed repository design employs an engineered barrier system (EBS) in concert with the desert environment and geologic features of YM with the intent of keeping water away from the high-level radioactive waste for thousands of years. The primary component of the proposed EBS is a WP. The U.S. Department of Energy (DOE) Repository Safety Strategy (RSS) identified several principal factors that would be addressed in its performance assessment. Water seepage into drifts is one of the principal factors that could affect the long-term performance of the repository. The DOE RSS identified other factors that may be affected by rockfall and consequent alteration of drift geometry: (i) coupled thermal-mechanical-hydrological-chemical processes, (ii) environment on the drip shields, and (iii) environments on and within the WP.

The new Enhanced Design Alternative II has been adopted recently by the DOE as its site recommendation reference design. This new design includes design features (e.g., drip shields) that reduce the effects of dripping water and rockfall on the performance of WPs.

The impact load caused by a seismically induced rockfall can affect the structural and hydrological performance of the drip shields and the confinement capabilities of the WPs. The current U.S. Nuclear Regulatory Commission Total-system Performance Assessment computer code includes a module called SEISMO. This module evaluates the potential only for direct rupture of WPs from rockfall induced by seismicity based on several simplifying assumptions and without consideration of the possible accelerated degradation of the WPs. The effect of rockfall on drip shield performance is not currently included in the SEISMO module. An effort is under way to reevaluate the assumptions made for the SEISMO module so that the assessment of seismically induced rockfall impacts on drip shield and WP performances can be accomplished in a more reasonable manner.

This report documents the results of determining the size and areal coverage of rockfalls during various ground motions that may occur in the proposed repository. Two-dimensional Discontinuous Deformation Analysis (DDA) computer codes were used by the Center for Nuclear Waste Regulatory Analyses to evaluate seismically induced rockfall for the emplacement drifts located in the Topopah Springs Welded Tuff Unit 2 (TSw2) thermo-mechanical unit. The analyses were based on two types of joint spacings. One joint type represented areas where small joint spacings were dominant, and the other one was associated with areas with large joint spacings, especially in the TSw2 lower lithophysal unit. The joint information used for analysis includes only the joints with measured trace length greater than 1 m. The joints with trace length smaller than 1 m were not available for consideration. The effects of long-term degradation of joint shear strength were also analyzed in this investigation.

The DDA forms blocky systems of rock masses based on cross-sectional profiles of a three-dimensional joint network. A unique tree-cutting technique was used in the DDA to remove joints or portions of joints that do not contribute to the formation of blocks, because the DDA deals only with blocks. Consequently, it is not possible for the DDA to evaluate the effects of new block formations through potential propagation of these joints because of the relatively high stresses that may result from thermal load, long-term degradation of rock strength, or both. The effects of thermal load will depend on temperature and rock mechanical and strength properties. As a result, thermal load was not included in the analyses on rockfall to avoid the potentially misleading results.

In analyzing seismically induced rockfall in the emplacement drifts, realizations of the DDA model were formed from the same joint type, specifically considering the variations associated with joint spacing, joint length, and joint bridge (gap). A Monte Carlo technique was adopted in this study to generate sample realizations. In generating these realizations, the joint spacing, length, and bridge were assumed to be distributed uniformly with certain variations in the mean values of the respective joint parameters. In a full application of the Monte Carlo technique, a sufficient number of realizations should be analyzed to develop a reasonable representation associated with the variations of the joint parameters. The number of realizations necessary to obtain sufficient representation depends on the statistics to be evaluated. In this study, these statistics include extent and block sizes of rockfall. Due to time constraints, a full application of the Monte Carlo technique was not adopted in the analyses.

Site-specific seismic design input for repository design is being developed by the Civilian Radioactive Waste Management System Management and Operating Contractor (CRWMS M&O) through a probabilistic seismic hazard analysis process. Some seismic design input has been used by CRWMS M&O in ground control and drift degradation analyses (e.g., peak ground accelerations and peak ground velocities). Site-specific ground motion time histories were not used by CRWMS M&O in these analyses; instead, sinusoidal velocity waves with amplitudes equal to the appropriate levels of peak ground velocities were used. The frequency assigned for these sinusoidal waves is 10 Hz and the duration is 3 s. DDA results indicated that the effects of the sinusoidal waves with a 10-Hz frequency and 3-s duration used by CRWMS M&O on rock-mass responses are not sufficient to bound those induced by the ground motion time history developed for the Yerba Buena Island Tunnel seismic retrofit program. This finding is expected to be applicable to the site-specific ground motion time histories developed for the proposed YM site. It is the responsibility of CRWMS M&O to demonstrate that the sinusoidal waves used for rock-mass response analysis provide results that bound the seismic time history results.

Rock-mass responses to ground motions appear to be complicated. The DDA results suggested that the responses were dependent on the geometries of the blocky systems analyzed for a given joint set because the inherent variations of the parameters within that joint set. Considering variations associated with the various joint parameters, the extent of damage (characterized by rockfall and accumulation of permanent joint deformation) varied widely from DDA model realization to realization; typically, the damage ranges from a few small rock blocks that fall into the drifts to a substantial collapse of the drifts. This finding suggests that some block geometries are inherently less stable than others. Consequently, analyses should be performed on a sufficient number of realizations to assess the stability of drifts so the conditions for the most critical damage can be identified for ground support design and drift degradation assessment. Rock masses with large joint spacings with respect to drift size were more stable, and the extent of rockfall, in general, was less than for the rock masses with small joint spacings.

DDA results indicated that magnitudes of ground motions were found to affect drift stability. This observation is intuitive. The physical effects could be additional rockfall or accumulation of joint slip as the magnitude increases, and often it is a combination of these two. It should be noted the effect was also found to be geometry-dependent. There were cases where rock masses surrounding the drifts were inherently unstable, and as a result, extensive rockfall occurred even with a small magnitude of ground motion. In other cases, the geometries of the blocky systems were inherently stable. The rock masses in these cases tended to better resist the influence of ground motion.

Observations from the laboratory and field studies indicate that seismic events are likely to influence stability through accumulation of permanent deformations around underground excavations. These observations also suggest the fundamental failure mechanism of an excavation in a jointed rock medium subjected to repeated episodes of seismic events is the accumulation of joint deformations. DDA results confirm these observations. The DDA examined the effects of two episodes of ground motion with identical signals. It was found that the first earthquake induced only minor damage to the drift, and the second earthquake caused significantly more rockfall that actually filled up the excavation. This result supports the conclusion that repeated ground motions could have a detrimental effect on excavation stability.

DDA results indicated that consideration of long-term degradation of joint shear strength would decrease the stability of the drifts, and the effect could be substantial. Consequently, long-term degradation of joint shear strength needs to be considered in assessing rockfall potential for the emplacement drifts during the postclosure performance period.

For the DDA realizations modeled, more than 90 percent of the rock blocks that fell were smaller than 0.8 m^3 per unit drift length and were made of several blocks for the small and large joint spacing cases. The effect of these rockfalls on performance of drip shields and WPs may be small. The maximum rock block size for the large joint spacing cases was approximately 1.1 m^3 per unit drift length and approximately 3.1 m^3 per unit drift length for the small joint spacing cases. Note that the rock block size is presented in volume per unit drift length in this report because the actual rock block volume falling on one waste package cannot be estimated from a two-dimensional analysis. To estimate rock block volume, the joint spacing in the third dimension needs to be considered. Preliminary DDA results also indicated that areal coverage of rockfall (of concern from performance perspective) is relatively small for the large joint spacing cases when compared to the small joint spacing cases.

1 INTRODUCTION

1.1 BACKGROUND

The U.S. Department of Energy (DOE) has been studying the Yucca Mountain (YM) site in Nevada for more than 15 yr to determine its suitability for constructing a geologic repository for the nation's high-level radioactive waste (U.S. Department of Energy, 1998a). The proposed repository design employs an engineered barrier system (EBS) in concert with the desert environment and geologic features of YM with the intent of keeping water away from the waste for thousands of years. The primary component of the proposed EBS is a waste package (WP). Other potential components of the EBS include drip shields, backfill, and emplacement drift seals. The basic concept of geologic disposal at YM is to place carefully prepared and packaged waste in excavated drifts in tuff approximately 300 m below the ground surface and 225 m above the water table in the unsaturated zone. In this condition, the engineered barriers are intended to work with the natural barriers to contain and isolate waste for thousands of years.

Design of the repository, including the EBS and the underground facility, is an evolving process. It changes as more information and knowledge become available. Since the DOE submitted its Viability Assessment (VA) (U.S. Department of Energy, 1998a,b) to the U.S. Congress, the reference design that supported the VA was replaced in early 2000 with the Enhanced Design Alternative (EDA) II. EDA II is the result of an extensive process—License Application Design Selection; and EDA II is also presented in the basis for DOE design selection (Barrett, 1999). EDA II [Civilian Radioactive Waste Management System Management and Operating Contractor (CRWMS M&O), 2000a] includes the following essential features:

- WPs with 2-cm-thick, corrosion-resistant outer barrier and a 5-cm-thick, corrosion-allowance inner barrier to extend service life
- Drip shields intended to limit the amount of dripping water contact and to mitigate the effects of rockfall on WPs
- An option to place backfill before permanent closure

The DOE Repository Safety Strategy (RSS) (CRWMS M&O, 2000b) has identified water seepage into drifts as one of the principal factors that would affect the long-term performance of the repository. Hughson and Dodge, (1999) indicated that a change of drift geometry as a result of rock deformation (in the form of joint displacement) and rockfall, which might cause the geometry of an emplacement drift to become irregular or rugged, could potentially reduce the percolation threshold necessary for water to start dripping into emplacement drifts by more than one order of magnitude. The DOE RSS identified other factors that may be affected by rockfall and consequent alteration of drift geometry: (i) coupled processes-effects on seepage, (ii) environment on the drip shield, and (iii) environments on and within the WP.

For the jointed rock mass at YM, rockfall may be induced by:

- Existence of unstable rock blocks after excavation and before placement of support. The rockfall related to this situation is primarily controlled/determined by the joint pattern and orientation of the openings relative to the orientation of the joint sets in which these openings

are located. Inherently unstable rock blocks that tend to fall immediately or a short period of time after excavation due to gravity loads are called key blocks (Goodman and Shi, 1985). Due to the loss of support, key blocks that fall may trigger the subsequent fall of other rock blocks above the key blocks.

- Long-term deterioration of rock mass during prolonged thermal load. The deterioration of rock mass could come from three sources. The first source is reduction of joint shear strength due to a long-term creeping effect during a high state of shear stresses. The second possible condition is failure of the intact rock block during a high state of stresses. Extensive failure could be possible and has been identified through numerical modeling (Ahola el al., 1996) for the VA reference design. For the EDA II design, the magnitude of thermal load has been reduced and further controlled through preclosure ventilation to remove decay heat. However, after permanent closure, the emplacement drift temperature could still go beyond 100 °C. The state of stresses induced by temperature of this magnitude could cause the rock block to fail. Another important factor is the potential long-term deterioration of rock strength due to a creep effect. Observations indicate that creep effect could reduce rock strength (Griggs, 1939; Hardy, 1969; Scholz, 1968; Wawersik, 1972). Rock strength reduction of 30–50 percent has been reported (Cruden, 1970; Wawersik, 1972). These situations could substantially increase rockfall potential. When the rock mass surrounding the repository begins to cool down, the relaxation of stresses could loosen the rock and thus create further rockfall conditions (Wilder and Yow, 1987).

- Seismically induced ground motion. Seismicity at YM could potentially damage the rock mass surrounding underground excavations and subsequently induce rockfall. Studies indicate that rock mass may be damaged by a single ground motion or through repeated ground motions (Sharma and Judd, 1991). The fundamental mechanics that weaken rock mass surrounding underground excavations involve accumulation of joint shear displacements and temporary reduction of joint normal stresses, which, in turn, reduce joint resistances (Hsiung et al., 1992, 1999; Brown and Hudson, 1974; Barton and Hansteen, 1979).

Seismicity can affect the drip shield and WP performance by rockfall and shaking. The impact load caused by a seismically induced rockfall can affect the confinement capabilities of the WPs and the structural and hydrological performance of the drip shields in two ways. The first is a catastrophic rupture of the WP or drip shield, which may be weakened by corrosion in the latter stage of their design lives. The second way is that rockfall may cause damage to WPs and drip shields that would accelerate corrosion. The current U.S. Nuclear Regulatory Commission (NRC) Total-system Performance Assessment (TPA) code includes a SEISMO module (Mohanty et al., 2000) that evaluates only the potential for direct rupture of WPs from rockfall induced by seismicity based on several simplifying assumptions and without consideration of the degradation of the WPs with time. Performance of the new design feature, drip shields, has not been considered in the NRC performance assessment and will need to be evaluated as well. An effort is under way to reevaluate the assumptions made in the SEISMO module for the assessment of seismically induced rockfall impacts on the performance of WPs and drip shields. This effort focuses on two areas: (i) mechanical response of drip shields and WPs due to rockfall impact and (ii) size and areal coverage of rockfalls due to various ground motions that may occur in the proposed repository. This report focuses on the study of the second item. The study of the first item will be provided in a separate report.

1.2 OBJECTIVE AND SCOPE

This study focuses on analyzing seismically induced rockfall. The objectives of the study are: (i) development of a database for the extent of rockfall, rockfall sizes, and areal coverage of rockfall in the emplacement drifts from various magnitudes of ground motions; and (ii) assessment of the potential change in drift geometry. As discussed earlier, the results from the first item will be used as input to the SEISMO module for the NRC future version of the TPA code to estimate the effects of seismically induced rockfall on WP integrity. The results from the second item will be provided as input to investigate effects on water seepage into emplacement drifts. The latter study will be performed as part of the Thermal Effects on Flow Key Technical Issue. To meet the objectives, specific activities include:

- Estimating changes in geometry and extent of rockfall during various levels of ground motions
- Determining size distribution of rockfalls from various levels of ground motions
- Determining areal coverage of rockfalls from various levels of ground motions
- Estimating the potential for multiple rock blocks to fall in unison.

This report presents the findings of the investigation. The rockfall analyses of emplacement drifts subjected to earthquake ground motion were performed using a two-dimensional (2D) Discontinuous Deformation Analysis (DDA) approach. The effects of long-term degradation of joint shear strength on the extent of rockfall were also evaluated in the study. Furthermore, a study was conducted to investigate the effect of dynamic load characteristics, such as sinusoidal waves versus seismic time history, on rock-mass response.

2 DISCONTINUOUS DEFORMATION ANALYSIS

Long-term stability of emplacement drifts at YM will primarily depend on time-dependent, thermal-mechanical effects. The thermal-mechanical effects are caused by *in-situ* and excavation-induced stresses, thermally induced stresses, and dynamic loads. Because the preclosure operations period (up to several hundred years) and postclosure compliance period (thousands of years) are long, the repository openings are expected to be subjected to repeated seismic events of various magnitudes (Hsiung, et al., 1999).

One of the major consequences of the instability of emplacement drifts in a jointed rock mass is rockfall. Key block analysis provides a means for estimating size and number of unstable rock blocks that could have the potential to fall within a short time after excavation without seismic ground motion (Hsiung et al., 2000). However, seismic ground motions could possibly cause additional rockfall. To evaluate seismically induced rockfall, direct numerical modeling is required.

An intuitive way to assess rockfall potential and the extent of rockfall due to seismicity is by using the discontinuum approach. In this report, two versions of the 2D DDA computer codes, df0 and dda_ct2 (Shi, 1998; Hsiung[1]) are adopted for the analysis. The computer code dda_ct2 is an extension of the computer code df. The major differences between computer codes df0 and dda_ct2 will be discussed briefly in the following sections. DDA allows for direct modeling of fractures/joints that are common in rock media. DDA uses a unique scheme to track nodal (vertex) points of blocks during analysis that makes it an attractive method for structural analysis of complex and fractured geologic media.

2.1 FORMULATION OF DISCONTINUOUS DEFORMATION ANALYSIS

DDA is suited for investigating fractured rock-mass behavior important to many geotechnical and structural problems. DDA is the block system version of the finite element method (FEM). It involves a finite element type of mesh where all elements are real isolated blocks, bounded by preexisting discontinuities (or joints). Although DDA seems to resemble the distinct element method in that it accounts for joint contact behavior, mathematically it parallels FEM in the following aspects (Shi, 1996):

- DDA establishes its equilibrium equations by minimizing the total potential energy of the system
- DDA uses displacements as unknowns for the simultaneous equations
- Stiffness, mass, and loading matrices of individual blocks are calculated independently and added to the global matrix of the entire system.

The blocks simulated in DDA can be of any shape (both convex and concave). An implicit solution algorithm is adopted in DDA. The large displacements of the blocks are accounted for by the use of a time

---

[1]Hsiung, S.M. Discontinuous Deformation Analysis (DDA) with n^{th} order polynomial displacement functions. *38th U.S. Rock Mechanics Symposium, July 7–10, 2001, Washington, DC.* 2001. Submitted for publication.

step scheme: at the end of each time step, the equilibrium is reached by minimizing the total potential energy, and block geometry is updated. The deformed block geometry and resulting state of stresses from the previous time step is used as the initial condition for the next time step.

In the original DDA formulation (Shi, 1993, 1996), it was suggested that a polynomial displacement function could be used to describe the movement of any point in a 2D domain. In developing the computer code for DDA, a first order polynomial displacement function was assumed, so that the stresses and strains within a block in the model were constant. In the first order approximation formulation, the x- and y-direction displacements, (u, v), at any point (x, y) of a block, can be expressed using six displacement variables (Shi, 1996):

$$\begin{pmatrix} u \\ v \end{pmatrix} = \begin{pmatrix} 1 & 0 & -(y-y_0) & x-x_0 & 0 & \dfrac{y-y_0}{2} \\ 0 & 1 & x-x_0 & 0 & y-y_0 & \dfrac{x-x_0}{2} \end{pmatrix} \begin{pmatrix} u_0 \\ v_0 \\ r_0 \\ \varepsilon_x \\ \varepsilon_y \\ \gamma_{xy} \end{pmatrix} \tag{2-1}$$

where

(x_0, y_0)	—	reference point in the block (for convenience, centroid of the block is normally used)
(u_0, v_0)	—	rigid body translation of point (x_0, y_0)
r_0	—	rotation angle of the block with respect to point (x_0, y_0) and
ε_x, ε_y, and γ_{xy}	—	normal and shear strains of the block.

Equation (2-1) can be generalized as

$$\begin{pmatrix} u_i \\ v_i \end{pmatrix} = [W_i][D_i] = \begin{pmatrix} t_{11}^i & t_{12}^i & t_{13}^i & t_{14}^i & t_{15}^i & t_{16}^i \\ t_{21}^i & t_{22}^i & t_{23}^i & t_{24}^i & t_{25}^i & t_{26}^i \end{pmatrix} \begin{pmatrix} d_{1i} \\ d_{2i} \\ d_{3i} \\ d_{4i} \\ d_{5i} \\ d_{6i} \end{pmatrix} \tag{2-2}$$

where the subscript i denotes the ith block, $[W_i]$ is the transformation function, and $[D_i]$ contains the variables defined earlier.

Hsiung[2] introduced a more generalized formulation to permit the original DDA computer code to accept any order of polynomial displacement functions. In the generalized formulation, the displacements *(u,v)* at any point *(x,y)* in a block can be represented using the approximation of an n^{th} order polynomial displacement function:

$$u = \sum_{\ell=0}^{n} \sum_{m=0}^{\ell} d_{2\left(m+\sum_{k=1}^{\ell} k\right)+1} x^{\ell-m} y^{m}$$
$$v = \sum_{\ell=0}^{n} \sum_{m=0}^{\ell} d_{2\left(m+\sum_{k=1}^{\ell} k\right)+2} x^{\ell-m} y^{m} \qquad (2\text{-}3)$$

where n is the order, ℓ is an integer from 0 to n, m is an integer from 0 to ℓ, and d_j are the coefficients of the polynomial function. Eq. (2-3) can be expressed as

$$\begin{pmatrix} u \\ v \end{pmatrix} = \left[W_i\right]_{2\times\left(\sum_{\ell=1}^{n+1} 2\ell\right)} \left[D_i\right]_{\left(\sum_{l=1}^{n+1} 2\ell\right)\times 1} \qquad (2\text{-}4)$$

where the subscript i represents the i^{th} block, $\left[W_i\right]$ is a collection of the $x^{\ell-m} y^{m}$ terms in Eq. (2-3) and a $2 \times \sum_{\ell=1}^{n+1} 2\ell$ matrix; and $\left[D_i\right]$ is the collection of coefficients of the polynomial function, d_j, and a $\sum_{\ell=1}^{n+1} 2\ell \times \ell$ matrix.

Assuming that a system contains N number of blocks, the total potential energy Π_s of the system has the form

$$\Pi_s = \frac{1}{2}[D_s]^T[K_s][D_s] + [D_s]^T[F_s] + C \qquad (2\text{-}5)$$

[2]Hsiung, S.M. Discontinuous Deformation Analysis (DDA) with nth order polynomial displacement functions. *38th U.S. Rock Mechanics Symposium, July 7–10, 2001, Washington, DC.* 2001. Submitted for publication.

where

$$[D_s] = \begin{bmatrix} D_1 \\ D_2 \\ \vdots \\ D_N \end{bmatrix} \tag{2-6}$$

is a matrix containing displacement variables of the system;

$$[K_s] = \begin{bmatrix} K_{11} & K_{12} & \cdots & K_{1N} \\ K_{21} & K_{22} & \cdots & K_{2N} \\ \vdots & \vdots & \ddots & \vdots \\ K_{N1} & \cdots & \cdots & K_{NN} \end{bmatrix} \tag{2-7}$$

is the system stiffness matrix (Shi, 1996); and C is the energy produced by friction forces between blocks. If an n^{th} order displacement function is chosen, there are $\sum_{\ell=1}^{n+1} 2\ell$ displacement variables/unknowns for each block in the system. As a result, each element itself in matrices $[D_s]$ and $[F_s]$ is a $1 \times \sum_{\ell=1}^{n+1} 2\ell$ matrix and each element in $[K_s]$ is a $\sum_{\ell=1}^{n+1} 2\ell \times \sum_{\ell=1}^{n+1} 2\ell$ matrix.

By minimizing the total potential energy of the system, a set of simultaneous equations can be obtained

$$[K_s][D_s] = [F_s] \tag{2-8}$$

The stiffness matrix $[K_s]$ and the force matrix $[F_s]$ take the contribution from the elastic strains, displacement and load boundary conditions, initial stresses, force inertia, thermal stresses, and contacts between blocks. The general forms of the formulations for these contributions for the n^{th} order approximation are similar to those for the first order approximation except that appropriate transformation functions should be used. Some of the formulations are presented in the following sections.

2.1.1 Block Stiffness Matrix

The strain energy Π_e for block i is

$$\Pi_e = \iint \frac{1}{2}[\varepsilon_i][\sigma_i]dxdy \tag{2-9}$$

where σ_i is the stress matrix and ε_i is the strain matrix of block *i*. The stress-strain relationship can be presented as

$$[\sigma_i] = [E_i][\varepsilon_i] \tag{2-10}$$

For a plane stress condition

$$[E_i] = \frac{E}{1-\nu}\begin{bmatrix} 1 & \nu & 0 \\ \nu & 1 & 0 \\ 0 & 0 & \frac{1-\nu}{2} \end{bmatrix} \tag{2-11}$$

where E is Young's Modulus and ν is Poisson's ratio. To represent a plain strain condition, E can be replaced by $E/(1-\nu^2)$ and ν should be replaced by $\nu/(1-\nu)$. The strains $[\varepsilon_i]$ can be determined by

$$\begin{bmatrix} \varepsilon_x \\ \varepsilon_y \\ \gamma_{xy} \end{bmatrix} = \begin{bmatrix} \frac{\partial u}{\partial x} \\ \frac{\partial v}{\partial y} \\ \frac{\partial u}{\partial y} + \frac{\partial v}{\partial x} \end{bmatrix} = [B_i][D_i] \tag{2-12}$$

The $[B_i]$ matrix can be obtained by taking the derivative of the elements in the transformation function $[W_i]$ with respect to appropriate variables indicated in Eq. (2-12) and is a $3 \times \sum_{\ell=1}^{n+1} \ell$ matrix. With Eq. (2-12), Eq. (2-10) can be expressed by

$$[\sigma_i] = [E_i][B_i][D_i] \tag{2-13}$$

Substituting Eqs. (2-12) and (2-13) into Eq. (2-9), the strain energy of block *i* will be

$$\Pi_e = \iint \frac{1}{2}[D_i]^T[B_i]^T[E_i][B_i][D_i]dxdy \tag{2-14}$$

The contribution of the stiffness matrix to the overall stiffness matrix from block *i* is determined by minimizing Eq. (2-14)

$$[K_{ii}] = \iint [B_i]^T[E_i][B_i]dxdy \tag{2-15}$$

It should be noted that the elements in $[B_i]$ matrix contain $x^{n_1} y^{n_2}$ terms, where n_1 and n_2 are integers equal to or greater than zero. Consequently, integration of Eq. (2-15) is not straightforward. Shi (1994) presented the analytical solutions that make integration of any polynomial term possible. Chen and Ohnishi (1999) further reduced the solutions to a more manageable form.

2.1.2 Initial Stress

The initial stresses $[\sigma_i^0]$ in block i at the beginning of a time step are

$$[\sigma_i^0] = [E_i][\varepsilon_i^0] = [E_i][B_i][D_i^0] \tag{2-16}$$

The potential energy Π_{σ^0} for the initial stresses in block i is

$$\begin{aligned} \Pi_{\sigma^0} &= \iint [\varepsilon_i][\sigma_i^0] dxdy \\ &= \iint [D_i]^T [B_i]^T [E_i][B_i][D_i^0] dxdy \end{aligned} \tag{2-17}$$

The contribution of the initial stresses in block i to the overall force matrix is calculated by minimizing Eq. (2-17) and is expressed as

$$[F_i] = -\iint [B_i]^T [E_i][B_i] dxdy [D_i^0] \tag{2-18}$$

2.1.3 Body Force

For a constant body force (f_x, f_y) in block i, the associated potential energy Π_b of a constant body force is

$$\Pi_b = -\iint \begin{bmatrix} u & v \end{bmatrix} \begin{bmatrix} f_x \\ f_y \end{bmatrix} dxdy \tag{2-19}$$

Substituting Eq. (2-4) into Eq. (2-19), the potential energy equation can be rewritten as

$$\Pi_b = -\iint [D_i]^T [W_i]^T \begin{bmatrix} f_x \\ f_y \end{bmatrix} dxdy \tag{2-20}$$

Minimizing Eq. (2-20), the contribution of the body force in block i to the overall force matrix is

$$[F_i] = \iint [W_i]^T dxdy \begin{bmatrix} f_x \\ f_y \end{bmatrix} \tag{2-21}$$

2.1.4 Displacement Constraints

As a boundary condition, specific points in a system may be fixed to prevent movement. This constraint can be achieved by applying stiff springs. Assuming the resulting residual displacement of the fixed point in block i after a time step is (u, v) and two springs with a stiffness of p are applied to this point (one is along the x direction and the other y direction), the spring forces $\begin{bmatrix} f_x^s & f_y^s \end{bmatrix}$ at the fixed point are

$$\begin{bmatrix} f_x^s \\ f_y^s \end{bmatrix} = \begin{bmatrix} -pu \\ -pv \end{bmatrix} \tag{2-23}$$

It should be noted that the magnitude of the residual displacement depends on the spring stiffness applied. The larger the spring stiffness is, the smaller the residual displacement. The strain energy Π_s associated with the springs is

$$\begin{aligned} \Pi_s &= \frac{p}{2} \begin{pmatrix} u & v \end{pmatrix} \begin{pmatrix} u \\ v \end{pmatrix} \\ &= \frac{p}{2} [D_i]^T [W_i]^T [W_i] [D_i] \end{aligned} \tag{2-24}$$

The contribution to the system stiffness matrix from the fixed point can be obtained by minimizing Eq. (2-24)

$$[K_{ii}] = p[W_i]^T [W_i] \tag{2-25}$$

2.1.5 Inertia Force

Because the DDA method is based on a dynamic approach, inertia force plays an important role in block motion. When a block moves in dynamic mode, the initial velocity of this block at the beginning of a time step should be equal to its velocity at the end of the previous time step. Newton's second law of motion is used to regulate the block movement. For the time-dependent displacement (u, v) of any point in the i^{th} block, the associated inertia force per unit area (f_x, f_y) is

$$\begin{pmatrix} f_x \\ f_y \end{pmatrix} = -M \frac{\partial^2}{\partial t^2} \begin{pmatrix} u(t) \\ v(t) \end{pmatrix} \tag{2-26}$$

where M is the mass per unit area. The potential energy Π_I for the inertia force can be written as follows.

$$\Pi_I = \iint M\begin{pmatrix} u & v \end{pmatrix}\begin{bmatrix} \frac{\partial^2 u(t)}{\partial t^2} \\ \frac{\partial^2 v(t)}{\partial t^2} \end{bmatrix} dxdy \tag{2-27}$$

Equation (2-27) can be expressed in terms of displacement variables and transformation function

$$\Pi_I = \iint M[D_i]^T[W_i]^T[W_i]\frac{\partial D_i(t)}{\partial t^2} dxdy \tag{2-28}$$

Expanding the partial derivative term in Eq. (2-28) based on the Taylor series using a time step increment Δ and omitting the higher order terms, the partial derivative term can be shown as

$$\frac{\partial^2 D_i(t)}{\partial t^2} = \frac{2}{\Delta^2}[D_i] - \frac{2}{\Delta}\frac{\partial D_i(t)}{\partial t} \tag{2-29}$$

where $\frac{\partial D_i(t)}{\partial t}$ is the velocity V_0at the end of the previous time step. Minimizing Eq. (2-28), the contribution of the stiffness matrix to the overall stiffness matrix from block *i* from the inertia force is

$$[K_{ii}] = \frac{2M}{\Delta^2}[W_i]^T[W_i]dxdy \tag{2-30}$$

and the force matrix contribution to the overall force matrix is

$$[F_i] = \frac{2M}{\Delta}\left(\iint [W_i]^T[W_i]dxdy\right)[V_0] \tag{2-31}$$

2.2 CONTACT JUDGING

To model a blocky system, a complete solution has to satisfy both equilibrium and compatibility conditions (Ma, 1999). DDA uses an open-close iteration criterion to fulfill the compatibility conditions between blocks by solving a set of algebraic inequalities through iterations within a given time step (Shi, 1996). The open-close iteration process continues until no tension or penetration occurs at all conditions of contact modes before the calculation proceeds to the next time step. Based on natural contact phenomena, three basic contact modes can be identified: open, sliding, and locking.

Assume point P_1 has the coordinate (x_1, y_1) and line $\overline{P_2P_3}$ has the coordinates (x_2, y_2) and (x_3, y_3) at the two end points (solid lines in figure 2-1). After deformation, points P_1, P_2, and P_3 changed their positions to P_1', P_2', and P_3' as shown in figure 2-1. The displacements for points P_1, P_2, and P_3 are (u_1, v_1), (u_2, v_2), and (u_3, v_3), respectively. The contact condition of P_1 versus line $\overline{P_2P_3}$ can be described by the inequality (Shi, 1996)

$$\Delta = \begin{vmatrix} 1 & x_1 + u_1 & y_1 + v_1 \\ 1 & x_2 + u_2 & y_2 + v_2 \\ 1 & x_3 + u_3 & y_3 + u_3 \end{vmatrix} < 0 \qquad (2\text{-}32)$$

where Δ is the determinant. When Δ is positive, P_1 has no contact with $\overline{P_2P_3}$. Otherwise, P_1 is in contact with $\overline{P_2P_3}$. The distance d between P_1 and $\overline{P_2P_3}$ after deformation can be approximated assuming small deformation using

$$d = \frac{\Delta}{\sqrt{(x_2 - x_3)^2 + (y_2 - y_3)^2}} \qquad (2\text{-}33)$$

In DDA, Coulomb's Law is applied to assess the contact conditions between blocks. At every iteration, each contact is evaluated to determine if

- The normal contact force at the contact is greater than or equal to the contact tensile strength
- The shear contact force is smaller than the contact shear strength multiplied by the half length of the block edge where this contact is located, when the normal contact force is compressive
- The shear contact force is greater than or equal to the contact shear strength multiplied by the half length of the block edge where this contact is located, when the normal contact force is compressive.

If the first condition is satisfied, the contact is judged as open and no normal spring is applied. When the second condition is met, the contact is essentially locked such that no sliding between point P_1 and line $\overline{P_2P_3}$ has occurred. In this condition, both normal and shear stiffnesses are simulated using normal and shear springs at the contact. If the third condition is satisfied, P_1 slides along $\overline{P_2P_3}$: a normal spring is added and a pair of friction forces at the contact are added to the system force matrix $[F_s]$. The contribution of

the added contact springs should be included in the system stiffness matrix $[K_s]$ to account for the kinematics between blocks in the system. Details regarding how to determine the contribution of joint contact to the system force and stiffness matrices can be found elsewhere (Shi, 1993, 1996).

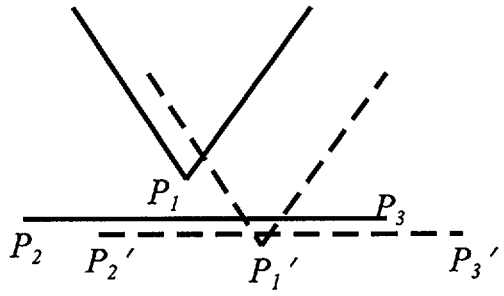

Figure 2-1. Contact Determination

3 DATA INPUT AND MODEL GEOMETRY

3.1 JOINT DATA INPUT

The joint pattern information including orientation, spacing, and length used in this analysis for the Topopah Spring Welded Tuff Unit 2 (TSw2) thermo-mechanical unit is given in tables 3-1 and 3-2. The data presented in table 3-1 were estimated from the Exploratory Studies Facility fracture mapping data, and those listed in table 3-2 were derived from the Drift Degradation Analysis (CRWMS M&O, 2000c) for the TSw2 lower lithophysal unit. The information presented in both tables includes only the joints with measured trace length larger than 1 m. The joint spacings for the joint sets listed in table 3-1 were smaller than those listed in table 3-2. To facilitate discussion, the DDA runs with their models developed using the joint information from table 3-1 are called small joint spacing cases and those models developed using the joint information from table 3-2 are called large joint spacing cases. A fracture geometry analysis report prepared by CRWMS M&O (2000e) documenting the fracture geometry for TSw2 (including joint information for the four subunits of the TSw2) became available at the later stage of this analysis. However, the joint patterns for each individual subunit were not included in this study. It may be worthwhile to evaluate seismically induced rockfall considering the joint patterns for each TSw2 subunit.

The bridge length is the gap between the end points of two adjacent collinear joint lines. This value was also assumed, because no data are currently available. Bridge length is normally a smaller value relative to the joint length. Without bridge length, a joint could become persistent if variation in joint spacing was not considered. Bridge length somewhat controls the formation of blocks. Smaller or negative bridge length improves the chance of a block forming. A negative joint bridge length was assumed in this analysis for the TSw2 lower lithophysal unit to improve the chance for block formation.

Table 3-1. Joint information for Topopah Spring Welded Tuff Unit 2 with small joint spacings

Joint Set Number	Dip Angle, Degrees	Dip Direction, Degrees	Mean Length, m	Mean Bridge Length, m	Mean Spacing, m
1	79	270	1.8	0.3	0.3
2	81	230	2.4	0.3	0.3
3	5	45	1.8	0.5	0.5

Table 3-2. Joint information for Topopah Spring Welded Tuff Unit 2 lower lithophysal unit

Joint Set Number	Dip Angle, Degrees	Dip Direction, Degrees	Mean Length, m	Mean Bridge Length, m	Mean Spacing, m
1	82	145	2.1	-0.3	1.6
2	79	180	1.7	-0.3	3.2
3	5	315	3.4	-0.3	0.6

3.2 MODEL GEOMETRY

To consider variations associated with the joint properties, a Monte Carlo technique was adopted to generate sample joint patterns. Each sample generated is an equally likely realization of joints that honor the information in tables 3-1 and 3-2. In generating these realizations, the joint spacing, length, and bridge length were assumed to be uniformly distributed and varied ±35 percent about the mean values of the respective parameters. The fracture geometry analysis report prepared by CRWMS M&O (2000e) shows that the joint spacings and trace lengths for the four lithostratigraphic subunits of TSw2 are mostly lognormally distributed, and some are exponentially distributed. Depending on the lower and upper limits used to constrain sampling, the assumption of uniform distribution used in this analysis could potentially underestimate the maximum block size, yet overestimate the number of relatively large blocks available. Uncertainties in joint dip angle and dip direction were not incorporated in most of the analyses presented in this report to avoid producing overly complicated DDA block models. Figures 3-1 through 3-3 show three example realizations of joint distributions generated stochastically for constructing DDA block models. All three realizations used the same joint information listed in table 3-1. The joint lines in the figures are bounded by the inner edges of the boundary frame on all sides.

The joint distribution realizations similar to those in figures 3-1 through 3-3 were further processed to form blocks for DDA. A tree-cutting procedure was used to remove joints or portions of joints that did not contribute to the formation of blocks because DDA deals with blocks only. This procedure also allows removing joint segments that are smaller than a user-defined value by merging the end points of the segments. The detailed discussion on the tree-cutting procedure is in Shi (1996). Figures 3-4 through 3-6 show three DDA block realizations developed using the joint patterns shown in figures 3-1 through 3-3 after nonintersecting joints were removed. Notice that the rock blocks formed for the three realizations contain many different shapes with any number of vertices. These shapes are often complex. Many of the blocks are concave. It can also be observed that the block sizes associated with the three models vary. The ultimate shapes of the blocks are controlled by the persistency of the joints. If the joints are persistent (i.e., joint lengths are relatively long), more regular shaped blocks are likely to be formed.

The circular space in the figures represented an excavation 5.5 m in diameter (e.g., figure 3-1). The azimuth of the orientation of the excavation simulated was 75 degrees; the excavation was assumed to be horizontal. The frame placed outside the blocky system was intended to provide horizontal and vertical displacement constraints: displacements were not allowed in the direction normal to either side of the frame (see figure 3-1). Rock blocks in contact with the inner edges of the boundary frame were allowed to slide along the contacted edge.

The dimensions for all DDA model realizations discussed in this report were 18-m wide and 16-m high as shown in figure 3-1. The results presented in sections 4 and 5 show that the maximum extent of rockfall was well within the model domain. It is recognized that the model dimension used in this study assumes a drift spacing of 18 m, which is smaller than the 81-m drift spacing for EDA II. Relatively higher stresses in the pillars are to be expected for the former model dimension than for the latter. As a result, the drifts for the former may be less stable than the drifts for the latter; hence, the potential for rockfall is relatively higher. Consequently, it is expected that the rockfall results from this study should provide acceptable approximations of the expected rockfall.

The emplacement drift was assumed to be approximately 275 m beneath the ground surface. The distance from the top of the model to the top of the emplacement drift was 7.25 m. The additional overburden was accounted for in the DDA block models as initial stresses for both vertical and horizontal directions. The horizontal initial stress was estimated based on Poisson's effect. The vertical initial stress used in the analyses was 600 ton/m^2 and the horizontal initial stress was 300 ton/m^2. The effect of excavation was not modeled in the DDA analysis.

3.3 BLOCK AND JOINT MATERIAL PROPERTIES

Table 3-3 provides the material properties used for the DDA computations extracted from a CRWMS M&O report (2000c). In this analysis, the rock blocks for all DDA models were assumed to behave elastically.

The joint cohesion used for TSw2 in the CRWMS M&O report (2000c) was 0.1 MPa, which was scaled down from 0.86 MPa reported in the YM Site Geotechnical Report (CRWMS M&O, 1997a). In this analysis, zero cohesion was assigned to the joints in all joint sets. The friction angle used in this study was 39 degrees, which is slightly smaller than the 41 degrees used in Drift Degradation Analysis (CRWMS M&O, 2000c). The value used by the CRWMS M&O was considered relatively high as compared to the average value (38.6 degrees) obtained by an early Center for Nuclear Waste Regulatory Analyses (CNWRA) study sponsored by the NRC Office of Research (Hsiung et al., 1994). The normal and shear stiffnesses for joint contact were 50,000 and 20,000 ton/m^2, respectively.

3.4 INPUT EARTHQUAKE TIME HISTORY

Several approaches are available to analyze response of a drift subjected to seismic load. The fundamental approach is to superimpose static analysis results with the estimated seismically induced stress or displacement to determine the extent of disturbed zones. A more advanced approach simulates propagation of seismic waves through rock media. In DDA, simulation of earthquake ground motions was approximated by applying the forces generated from ground accelerations directly to the blocks as body forces. This approach is proposed by Newmark (1965) to evaluate the effects of earthquakes on dams and embankments. Newmark states that "the resistance to earthquake shock motion of a block of soil or rock that slides on a surface is a function of the shearing resistance of the material under the conditions applicable in the earthquake" and, for simplicity, the resistence can be calculated by a force acting at the center of gravity of the sliding block. This force can be determined easily from the acceleration time history of a ground motion.

The Newmark approach was adopted by Shi (1999) to study stability of blocky rock slopes, and the same concept is adopted in this study to investigate potential rockfall of the emplacement drifts. In the

Table 3-3. Rock block material properties

Unit Weight, ton/m^3	2.27
Young's Modulus, ton/m^2	3,000,000
Poisson's Ratio	0.21

analyses, the ground accelerations applied to the blocks were the same throughout the model without phase differences (i.e., wave propagation is not modeled). It is recognized that the resulting rock-mass response without considering the phase differences may be different from that considering the phase differences. For a shear wave velocity of approximately 3,000 m/s (CRWMS M&O, 2000d), a seismic wave traveling from one corner diagonally to the opposite corner of the model takes approximately 0.008 s. The travel time within the zone of interest will even be smaller. The effect of this small travel time on the overall rock-mass response in the model domain was neglected in this study. It should be noted that the modeling approach adopted in this study represented an approximation for the problem at hand.

At the time of this analysis, the site-specific time history of earthquakes from YM was not available: the acceleration time history developed by the California Department of Transportation for the Yerba Buena Island Tunnel seismic retrofit program (Shi, 1999; Law and Lam, 1999) was used for input loads. This time history contains ground accelerations for all three directions. This time history record is 50 s, out of which the record from 10 to 30 s was used in this study. The accelerations during this period encompass the major portion of the ground motion.

Figure 3-7 shows the extracted data along the east, south, and vertical directions and the associated resultant acceleration. The data points are at an interval of 0.005 s. The resultant acceleration shown in the figure was for information purposes and was not used as input for the analyses. The horizontal and vertical accelerations applied to the DDA models were the projected values using the acceleration values in the three directions shown in figures 3-7a, 3-7b, and 3-7c. The resultant accelerations for the cross section are provided in figure 3-8. The three components (figures 3-7a, 3-7b, and 3-7c) of the earthquake signal were scaled in this study when necessary to represent different magnitudes of earthquakes.

In section 4, sinusoidal waves of different frequencies and durations also were used to assess whether it is reasonable to use appropriate sinusoidal wave forms to approximate site-specific ground motion time history when analyzing the stability of underground excavations.

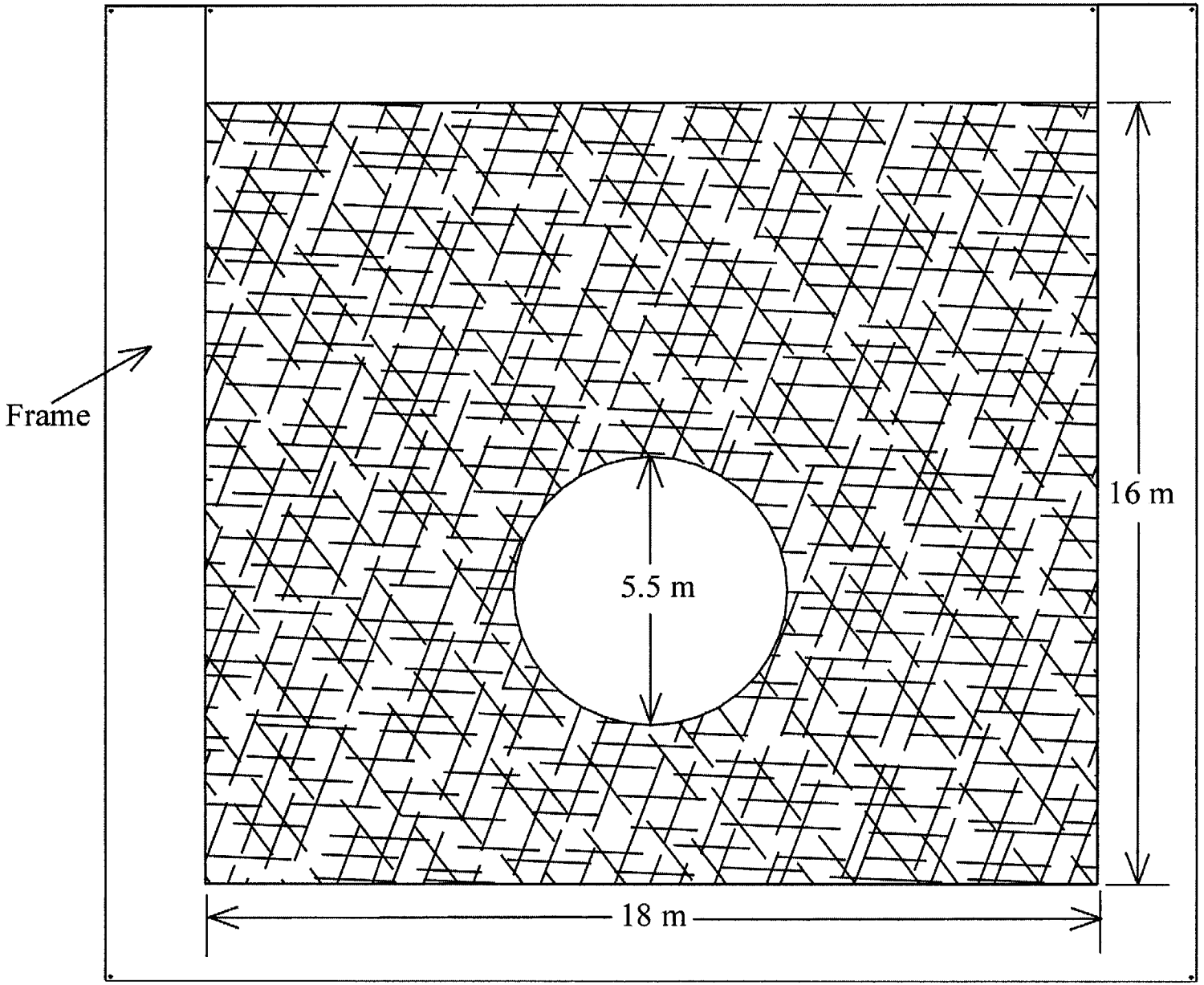

Figure 3-1. Joint distribution example 1 using data from table 3-1

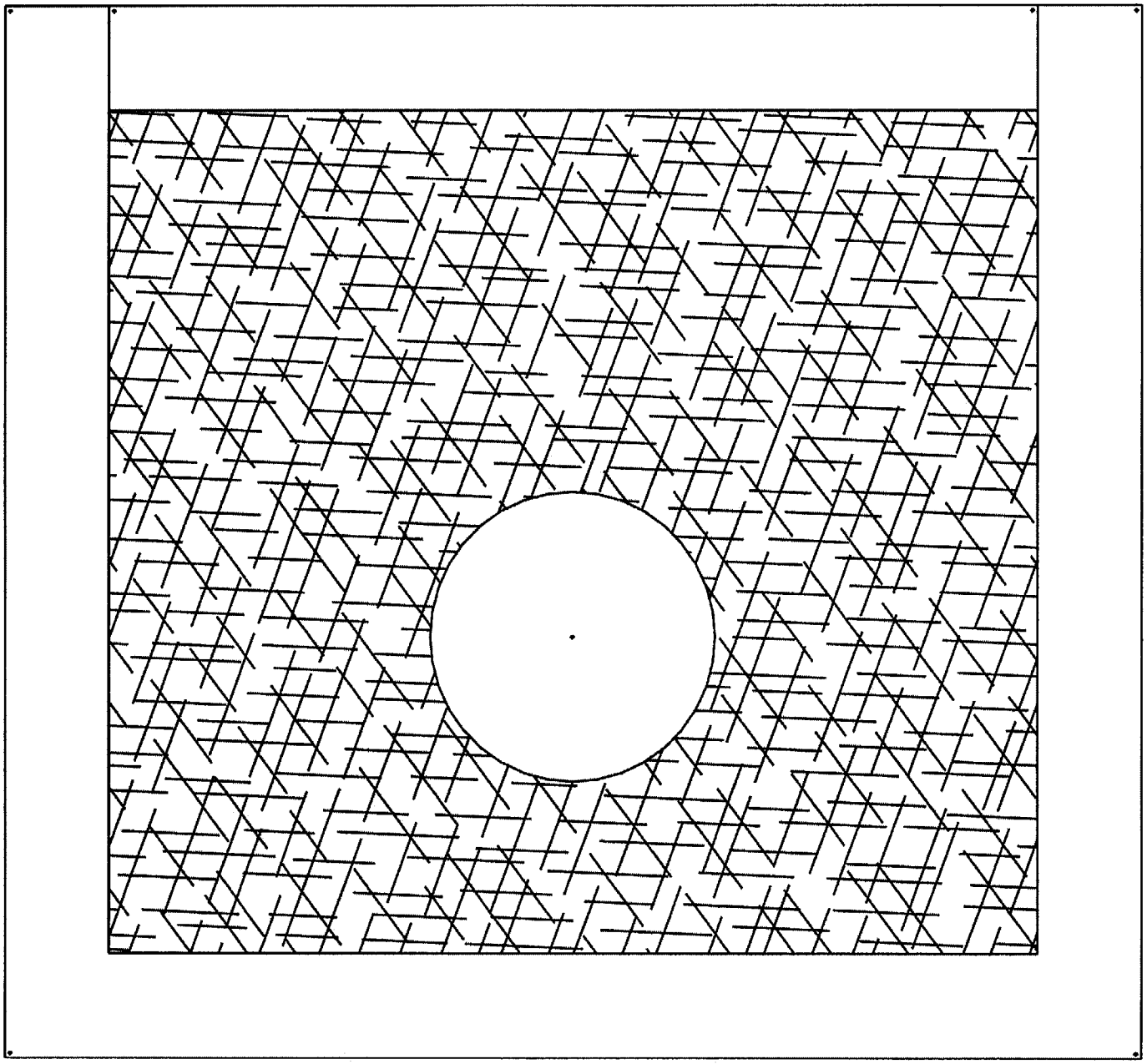

Figure 3-2. Joint distribution example 2 using data from table 3-1

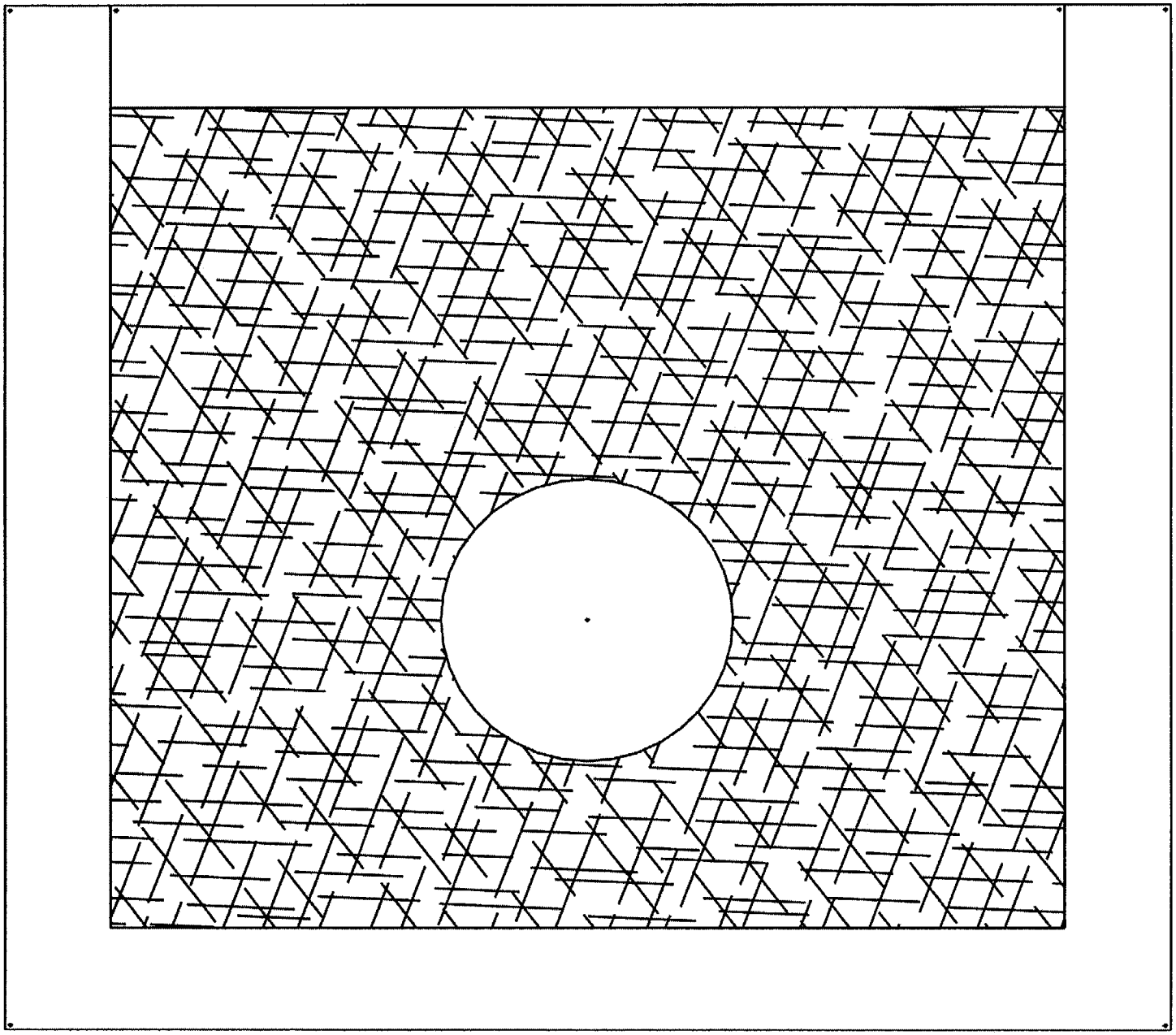

Figure 3-3. Joint distribution example 3 using data from table 3-1

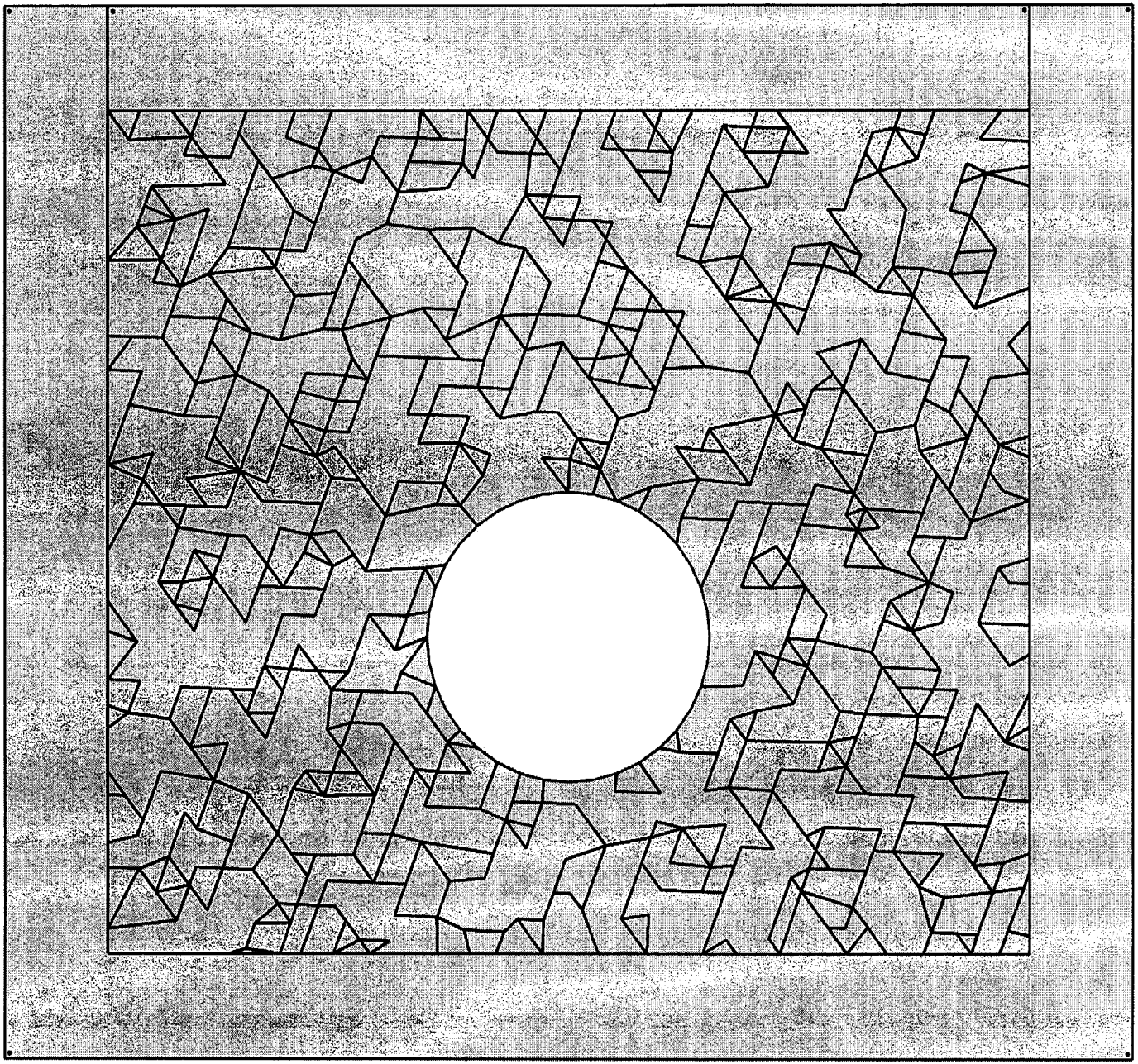

Figure 3-4. Discontinuous Deformation Analysis model formed using joint distribution in figure 3-1

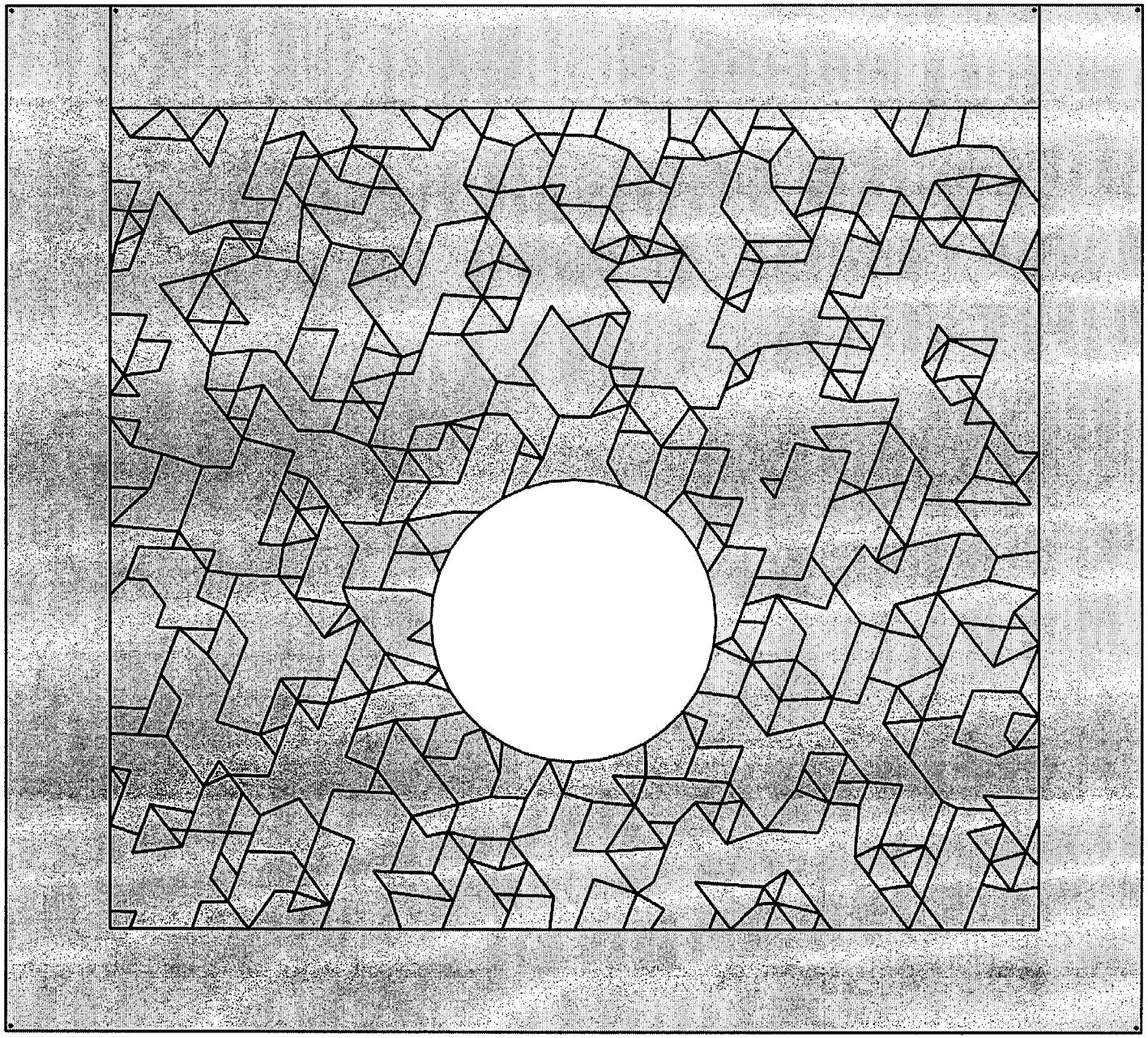

Figure 3-5. Discontinuous Deformation Analysis model formed using joint distribution in figure 3-2

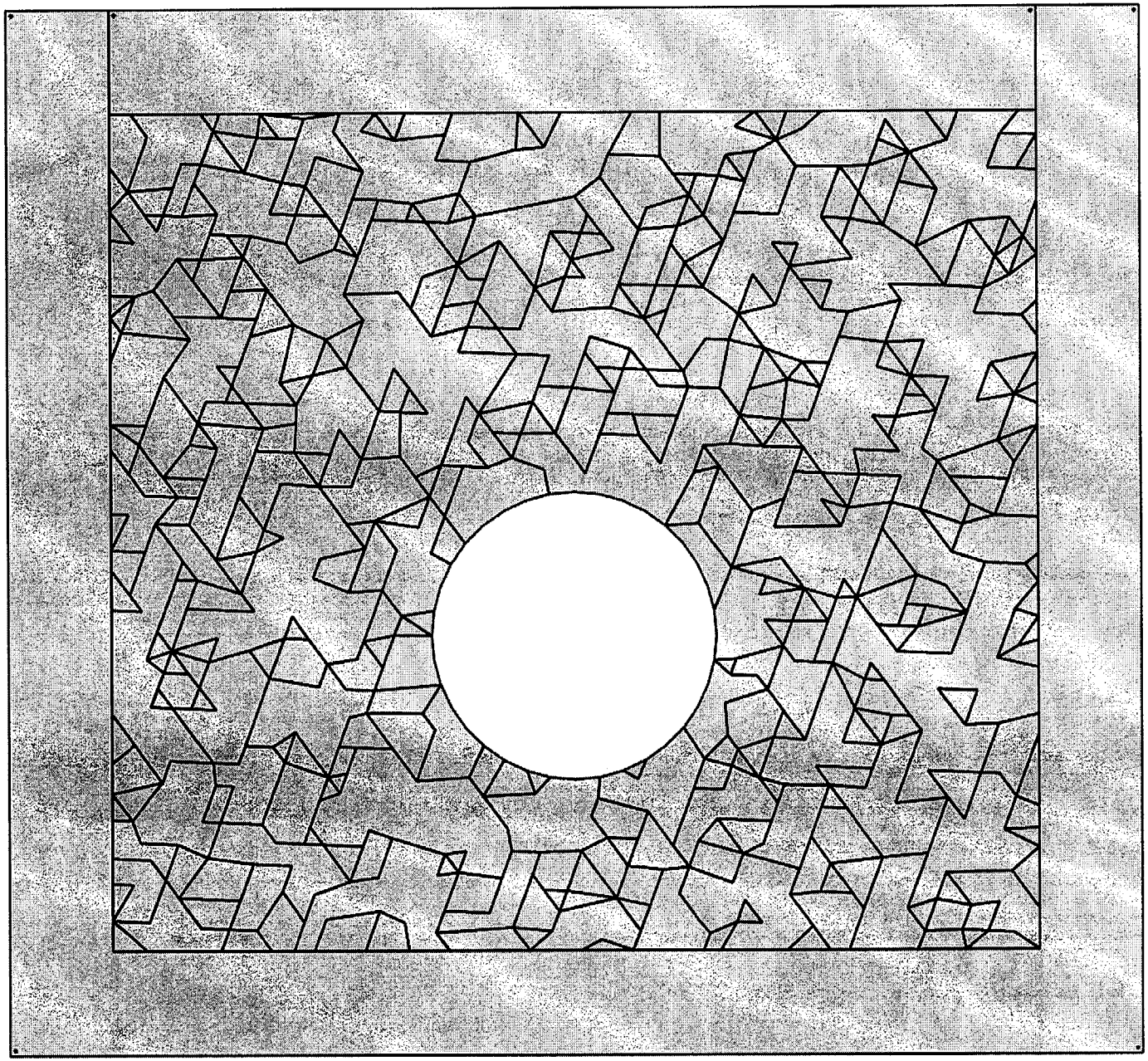

Figure 3-6. Discontinuous Deformation Analysis model formed using joint distribution in figure 3-3

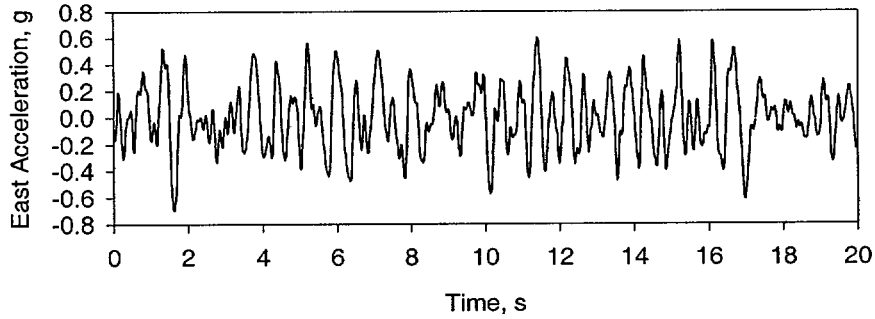

(a) Acceleration in the East Direction

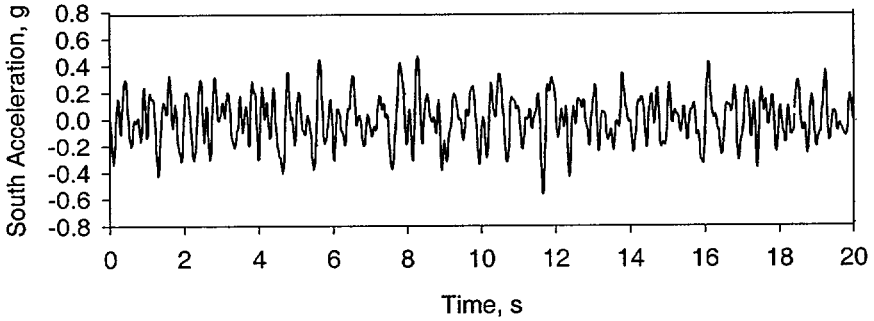

(b) Acceleration in the South Direction

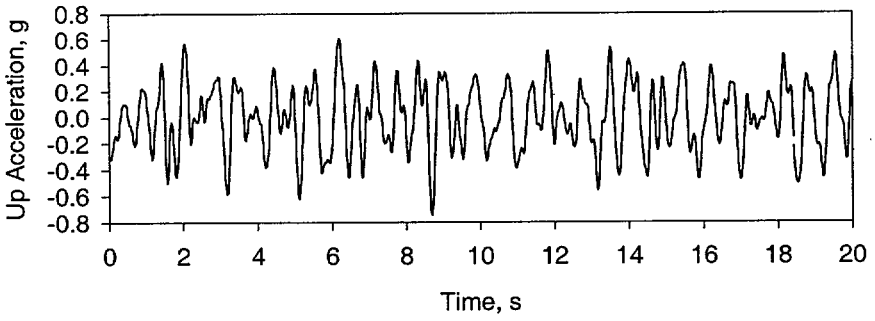

(c) Acceleration in the Vertical Direction

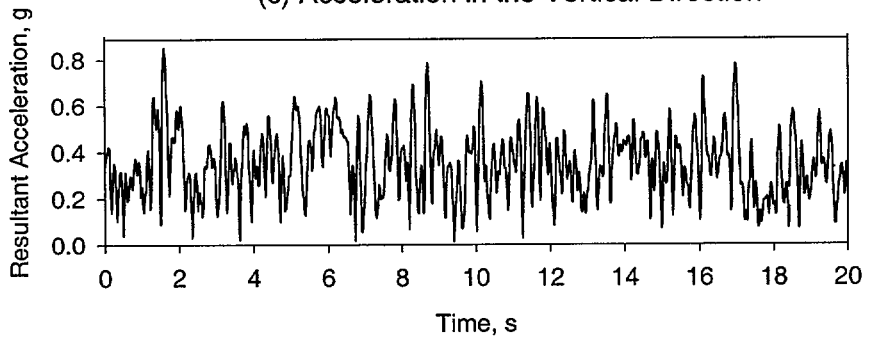

(d) Resultant Acceleration

Figure 3-7. Earthquake acceleration time history

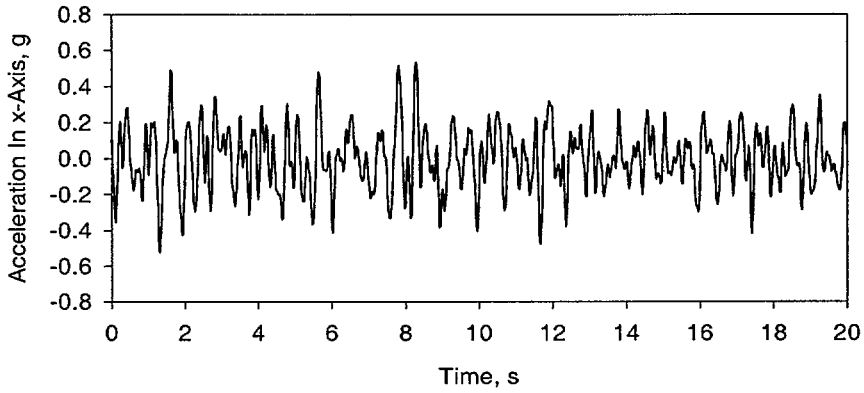

(a) Acceleration in x-Axis

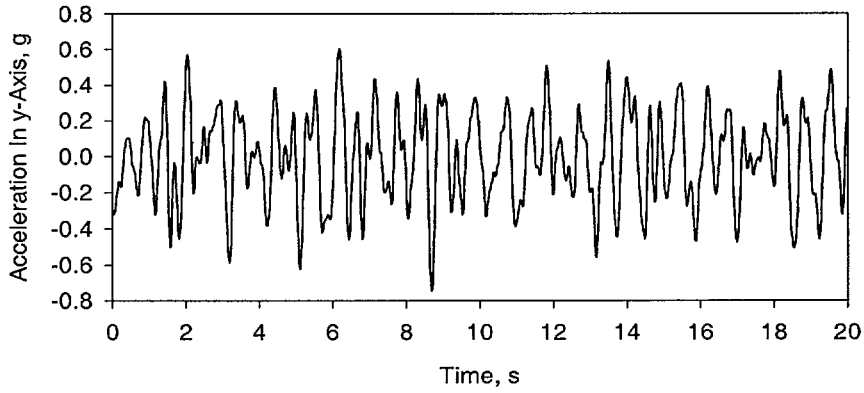

(b) Acceleration in y-Axis

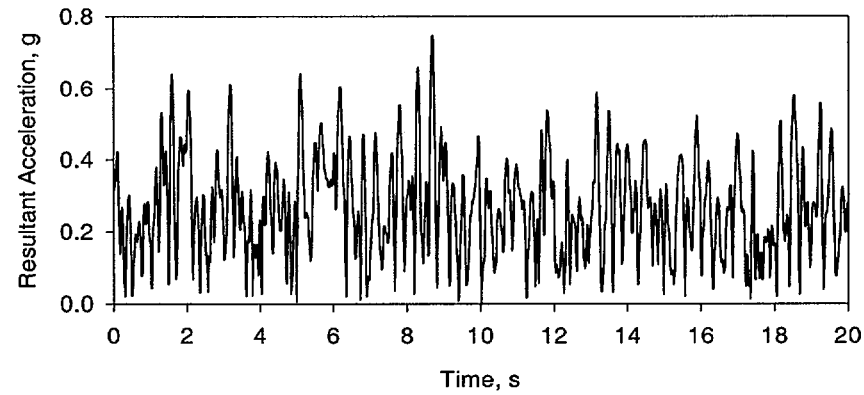

(c) Resultant Acceleration

Figure 3-8. Earthquake ground acceleration projected onto the Discontinuous Deformation Analysis model cross section

4 EFFECT OF DYNAMIC LOAD CHARACTERISTICS ON ROCK-MASS RESPONSE

Response of the rocks surrounding excavations to ground motions is complex. Studies indicate that a rock mass may be damaged by ground motions (Brown and Hudson, 1974; Sharma and Judd, 1991; Hsiung et al., 1992, 1999). This damage can be characterized by cracking, spalling, excessive joint shear displacement, and rockfall. The form and extent of damage may be related to the characteristics of earthquake time history and rock media, state of stresses including thermal stress, and the type and extent of supports used.

The technology available for dynamic analysis on response of jointed rock media over time is recent. Consequently, the effects of the characteristics of seismic signals on the behavior of jointed rock media are not well understood. The problem is further complicated by the fact that time domain ground motion data in the areas of interest often are not available. On occasion, a harmonic-based time history with one dominant frequency is used as a substitute. The appropriateness of adopting this approach has not been addressed adequately. In this report, the potential effects of the characteristics of seismic signals on rock-mass damage and stability are evaluated and discussed.

4.1 USE OF HARMONIC WAVES IN ANALYZING EMPLACEMENT DRIFT STABILITY

CRWMS M&O conducted a probabilistic seismic hazard analysis (PSHA) using site related geologic and fault/faulting data through an expert elicitation process (1998). The purposes of the PSHA are to assess the seismic hazards to the site and subsequently develop site-specific seismic design input for repository design. The PSHA has been completed and CRWMS M&O is preparing a report to document seismic design input developed from the results.

Some information related to the seismic design input has already been used by CRWMS M&O in various activities. For example, peak ground velocities (PGVs) corresponding to Categories 1 and 2 design inputs are being used to assess ground control of emplacement drifts (CRWMS M&O, 2000d), and both the PGVs and peak ground accelerations (PGAs) for a 10,000-yr return period were used in the analyses of drift degradation after permanent closure (CRWMS M&O, 2000c).

However, site-specific ground motion time histories were not used specifically in all these analyses. Instead, simplistic sinusoidal velocity waves with amplitudes equal to the appropriate levels of PGVs were used. The frequency of these sinusoidal waves is 10 Hz and the duration is 3 s.

While recognizing that typical earthquakes generally contain a broad range of frequencies, CRWMS M&O (2000d) indicated that the use of a 10-Hz wave is appropriate. CRWMS M&O (2000d) further noted that a sinusoidal wave with a duration of 3 s at a frequency of 10 Hz would generate conservative results based on the following reasons:

- The wave form used would result in 30 vibrational cycles. CRWMS M&O (2000d) stated that this number of vibrational cycles should produce conservative results in analyzing rock-mass responses at the repository horizon because "the rock formation does not show significant nonlinear behavior during seismic loading."

- The wave is sinusoidal in shape, hence, it leads to repeated cycles of peak ground motion at the level of PGV. Compared to a PGV that occurs only once in the time history of a typical earthquake, the use of a sinusoidal wave form is conservative.

However, no evidence or technical basis was provided by CRWMS M&O to support the idea that a sinusoidal wave with 10 Hz in frequency and 3 s in duration can replace the site-specific ground motion time history. In other words, no analysis was provided to demonstrate that the sinusoidal wave form used for drift stability and degradation analyses will produce rock-mass damage equal to or greater than that generated using the site-specific ground motion time history.

4.2 EFFECTS OF CHARACTERISTICS OF SEISMIC SIGNAL

To assess the reasonableness of the CRWMS M&O (2000d) approach, several DDA runs were conducted at the CNWRA, and the results are discussed in this section. These results are based on two DDA model realizations generated using the joint information listed in table 3-1. These two realizations are shown in figures 4-1 and 4-2. The block mechanical properties and joint strength properties used for both realizations were the same.

As discussed earlier, a typical earthquake ground motion normally excites a broad range of frequencies. The fundamental question is whether the sinusoidal waves with a 10-Hz frequency and 3-s duration used by CRWMS M&O (2000c,d) for its ground control and drift degradation analyses bound the site-specific ground motion time histories. If so, the use of those sinusoidal waves should be acceptable. Otherwise, either the site-specific ground motion time histories should be used or, alternatively, the sinusoidal waves should be modified to include a lower frequency content, use more than 30 cycles, or employ a combination of both.

At the time of this analysis, the site-specific time history of earthquakes from YM was not available. The acceleration time history developed by the California Department of Transportation for the Yerba Buena Island Tunnel seismic retrofit program (Shi, 1999; Law and Lam, 1999), as shown in figure 3-7, was used to determine if the effects of this ground motion time history can be bounded by the effects from the 10 Hz, 3 s sinusoidal wave. To make modeling conditions equivalent, only the acceleration time history along the east direction in figure 3-7 was used. This signal was scaled in such a manner that the maximum amplitude was 0.43 g, and the signal was applied to the DDA models in the horizontal direction, as was the sinusoidal wave.

Figures 4-3 and 4-4 show the extent of rockfall for the DDA model in figure 4-1 after the rock mass in this model was subjected to the sinusoidal and the earthquake ground acceleration signals. The extent of damage was similar for both cases. The earthquake ground motion signal appears to induce relatively more damage in the roof area, while the sinusoidal wave appears to cause more damage in the side wall area. The reason for less damage in the side wall is that the unstable rock blocks located in the side wall were pushed back to their original position during earthquake shaking. Figure 4-5 illustrates this, showing the rock block movements in the side wall after approximately 10 s of shaking. Note that several rock blocks in the side wall were moving into the drift. However, the falling rock blocks above those rock blocks in the side wall were in a position that prevented the latter from further moving into the drift, and these were eventually pushed back into the side wall as shown in figure 4-6. For the 10-Hz sinusoidal wave, this condition was impossible to develop due to shaking at a constant frequency: the rock blocks both in the roof and side wall moved into

the drift at a comparable rate. Additionally, comparing figures 4-5 and 4-7, it can be seen that the two rock blocks located at the lower right corner of the drift in figure 4-5 were kept in position by the fallen rock blocks, while this is not the case for the model in figure 4-7. These two blocks further prevented the side wall from bulging out for the earthquake signal case, while support of these two blocks to the side wall was lost for the harmonic wave case. This observation suggests that a rock mass surrounding an underground excavation may respond differently to seismic waves with different frequency contents.

Figures 4-8 and 4-9 illustrate the extent of rockfall for the DDA model in figure 4-2 after this model was subjected to the sinusoidal and earthquake ground acceleration signals. Significantly more rockfall/damage to the drift was experienced for the case using the earthquake acceleration ground motion (figure 4-9) than for using the sinusoidal wave. This finding suggests that the use of a sinusoidal wave with 10-Hz frequency and 3-s duration may not be appropriate for the purpose of ground control and drift degradation analyses. It is recognized that the earthquake acceleration time history used in this analysis will differ from the site-specific YM time history. However, the major frequency content may not be significantly different. Consequently, the conclusion drawn from this analysis is likely still to be valid relative to the site-specific ground motion time histories.

It should be noted that the investigation performed in this report considers only one component of the incident seismic wave. The other two components could potentially affect rock-mass response as well. When developing a bounding sinusoidal wave form that can be used for ground control assessment, the effects of all three components of the site-specific ground motion time history should be included to reduce uncertainty.

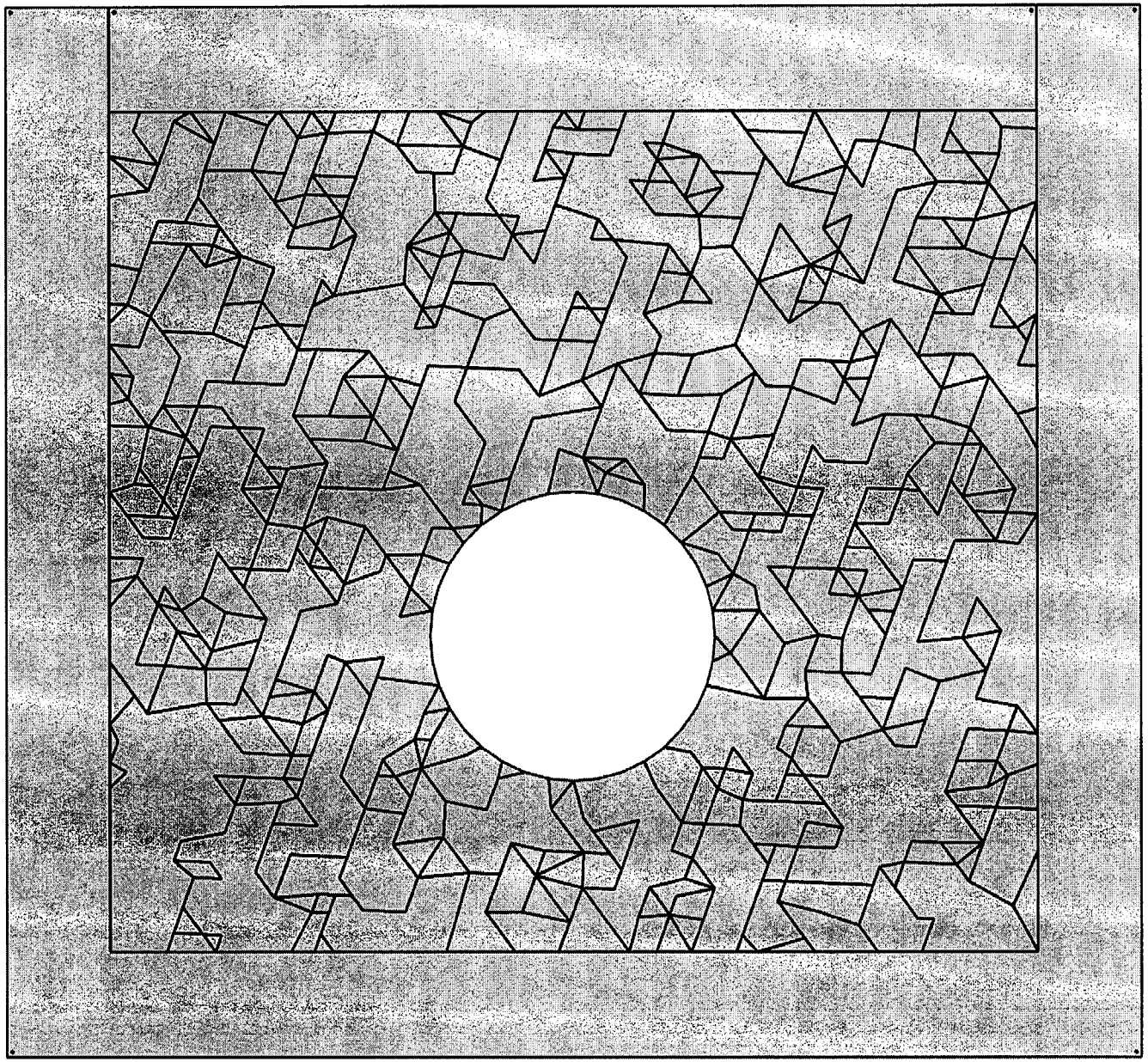

Figure 4-1. Discontinuous Deformation Analysis model realization 1

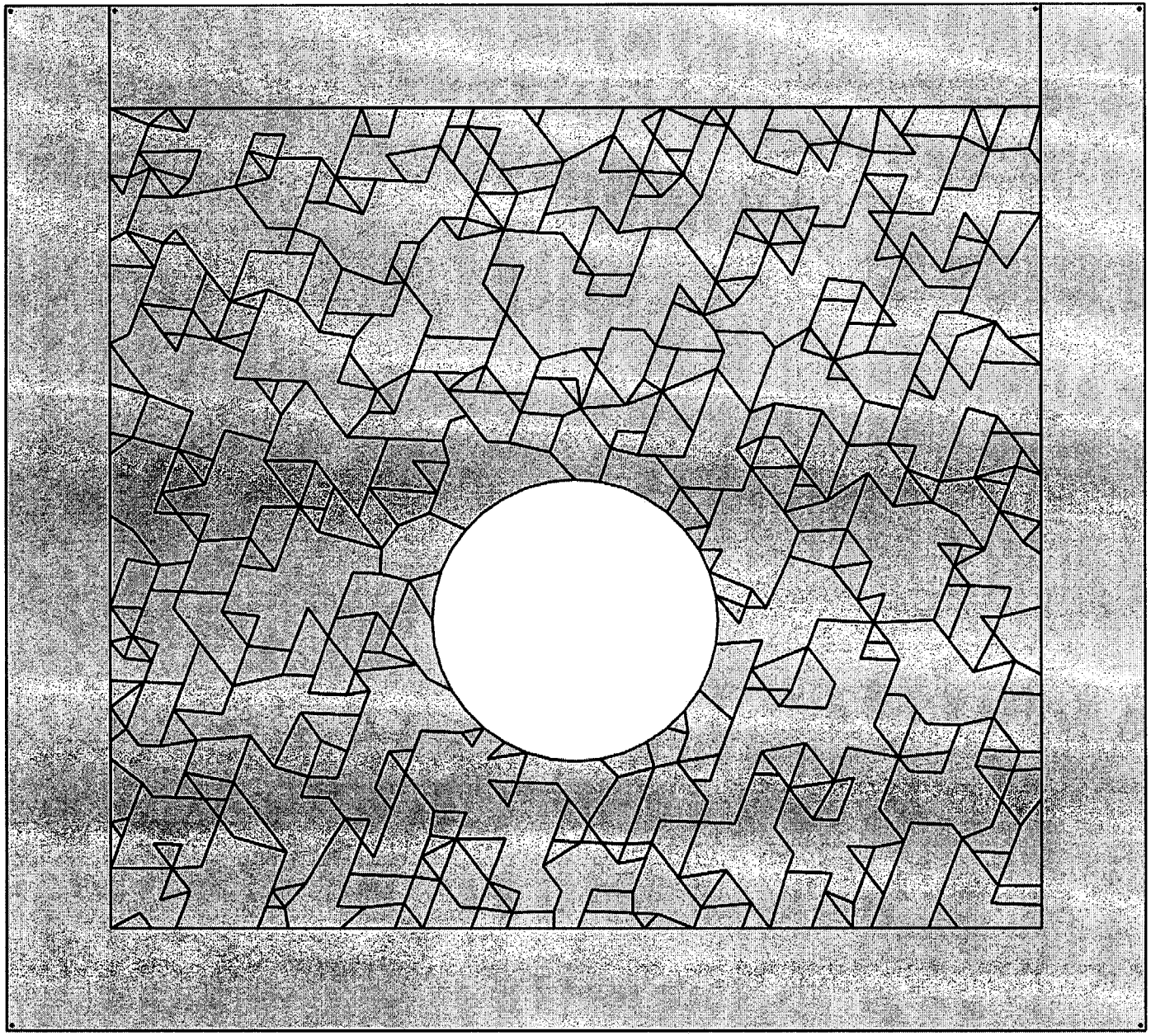

Figure 4-2. Discontinuous Deformation Analysis model realization 2

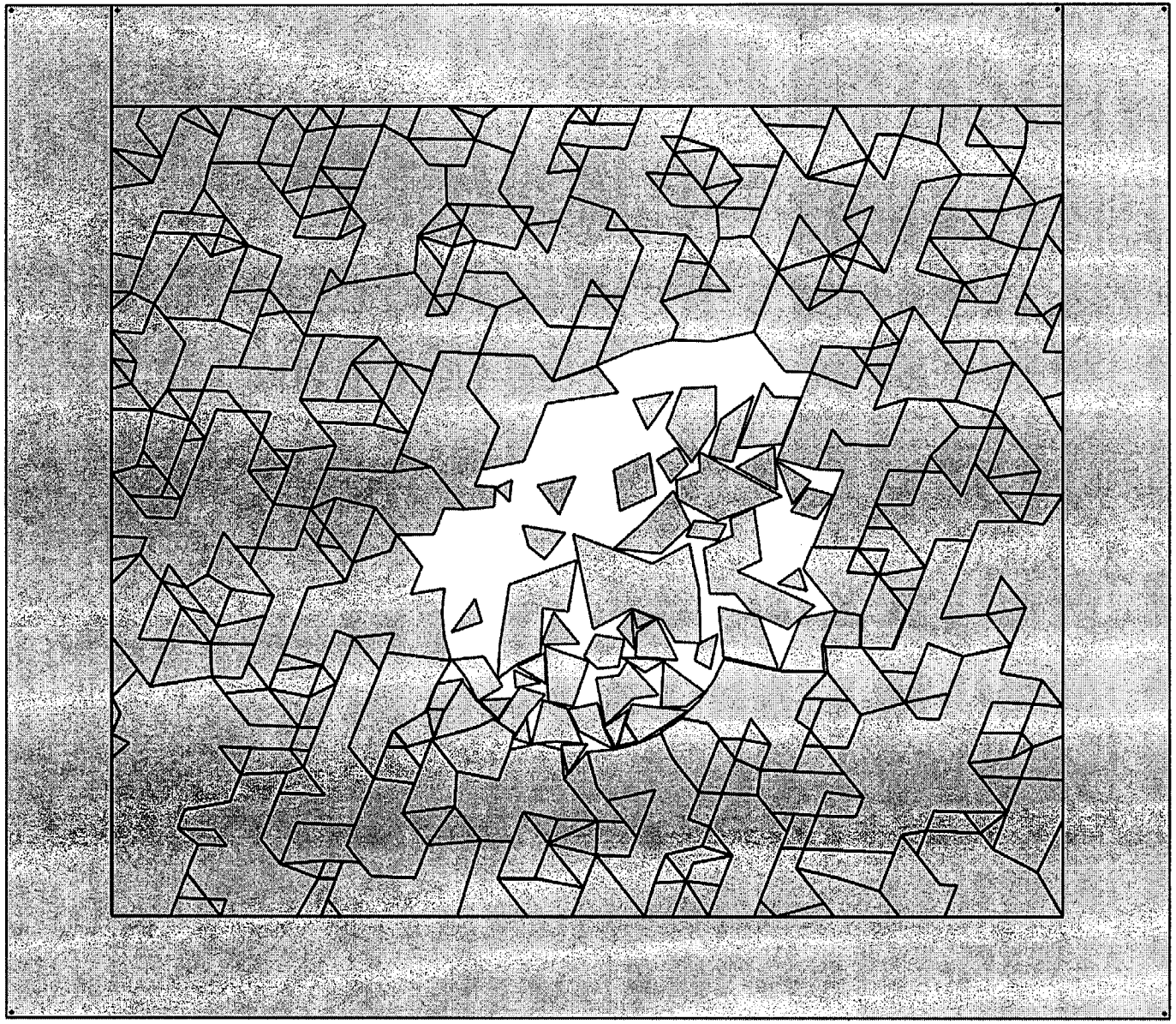

Figure 4-3. Response of rock-mass model in figure 4-1 to a sinusoidal wave with a 0.43-g peak ground acceleration, 10-Hz frequency, and 3-s duration

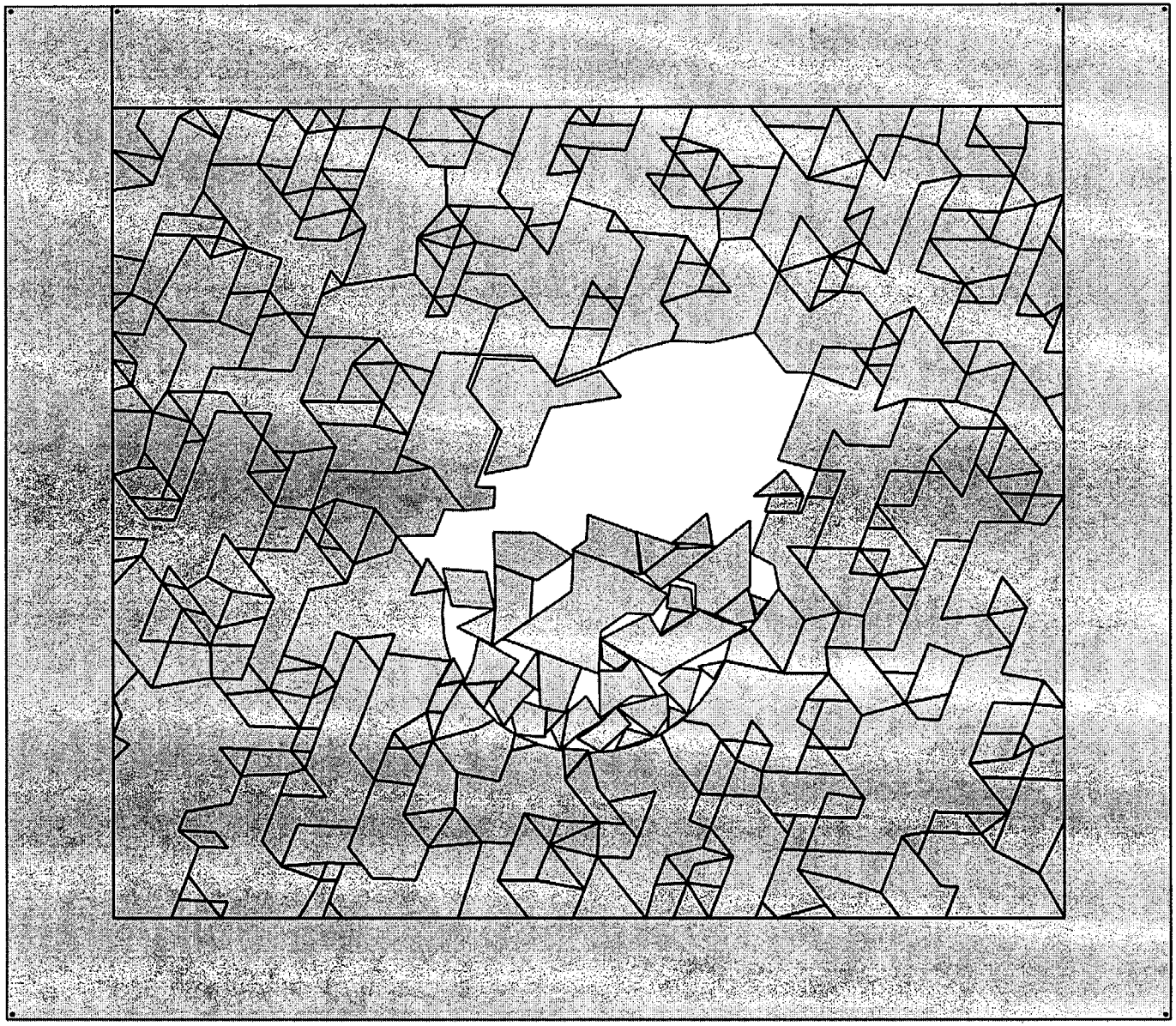

Figure 4-4. Response of rock-mass model in figure 4-1 to the acceleration ground motion in the east direction shown in figure 3-8

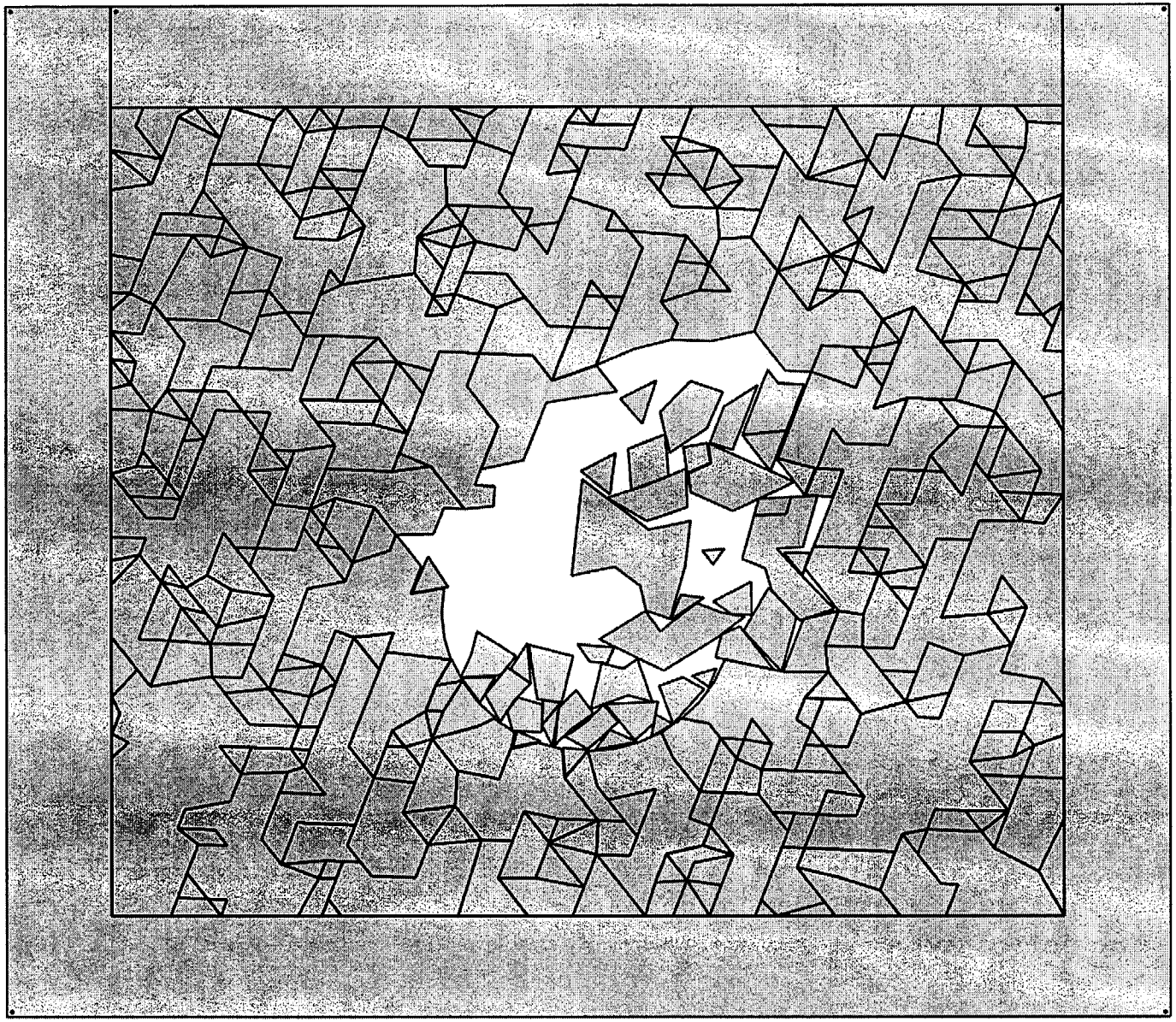

Figure 4-5. Response of rock-mass model in figure 4-1 to the seismic signal shown in figure 3-8 after about 10 s of shaking

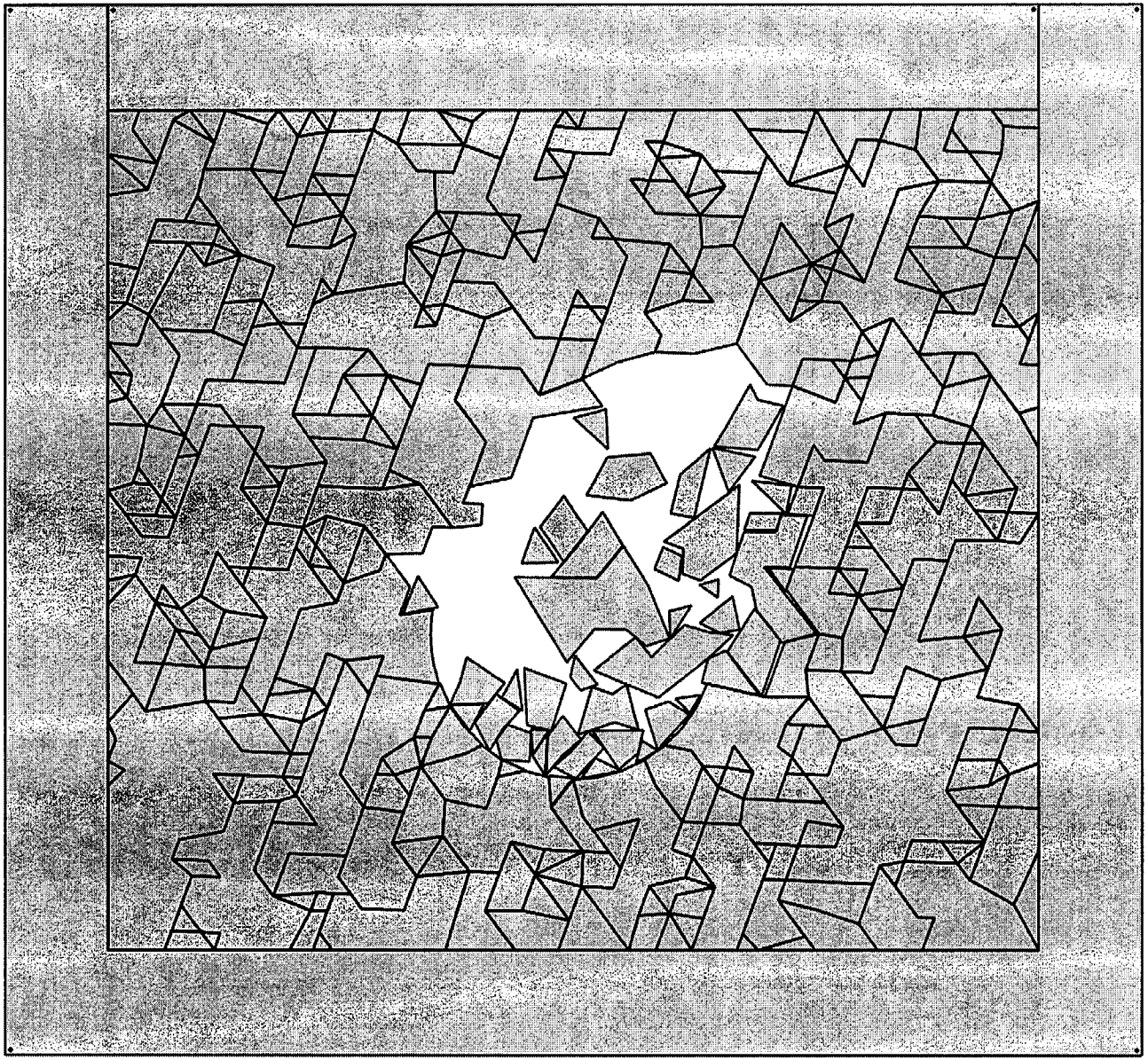

Figure 4-6. Response of rock-mass model in figure 4-1 to the seismic signal shown in figure 3-8 after about 10.5 s of shaking

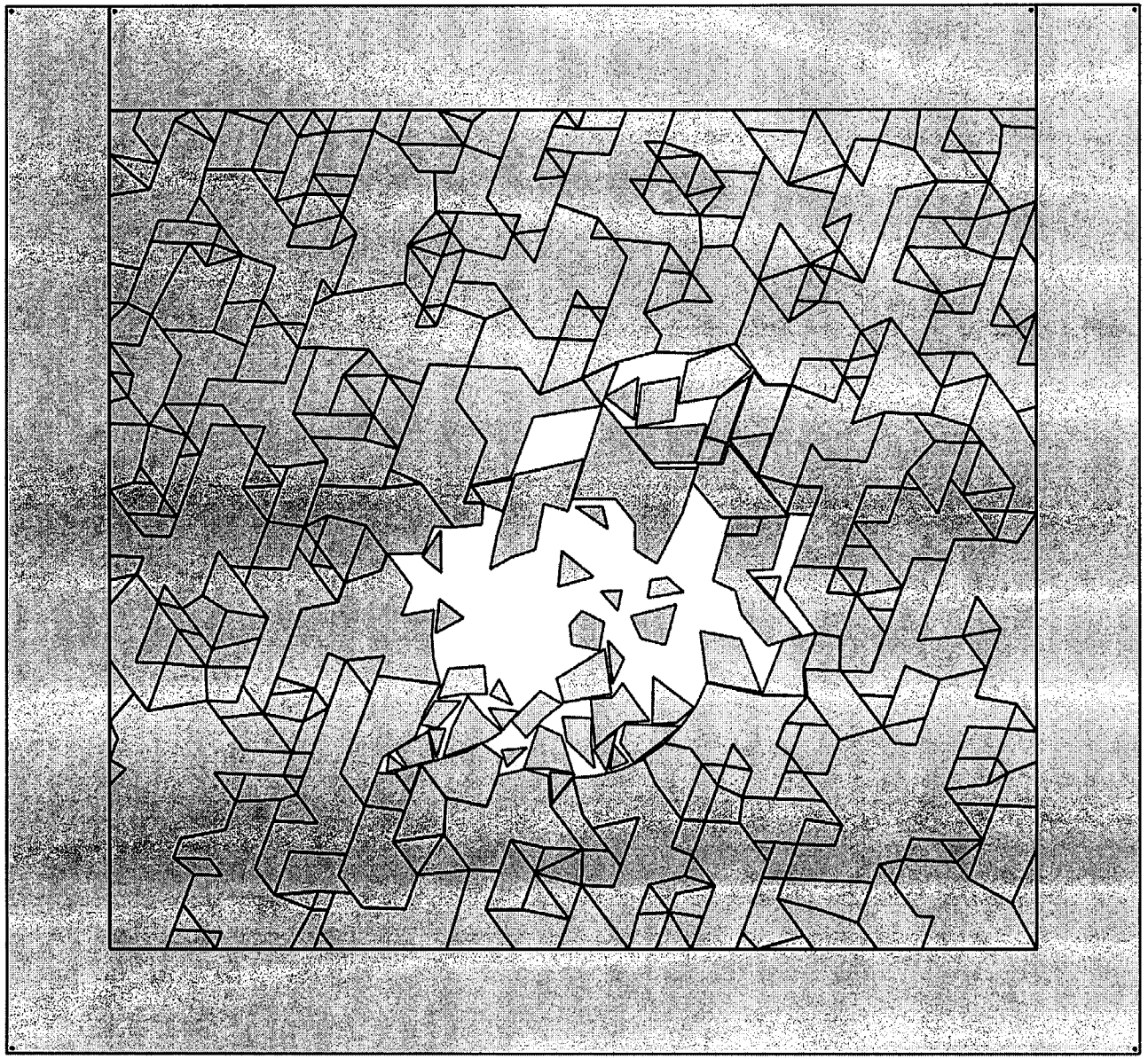

Figure 4-7. Response of rock-mass model in figure 4-1 to a sinusoidal wave with a 0.43-g peak ground acceleration, 10-Hz frequency, and 3-s duration after about 2.3 s of shaking

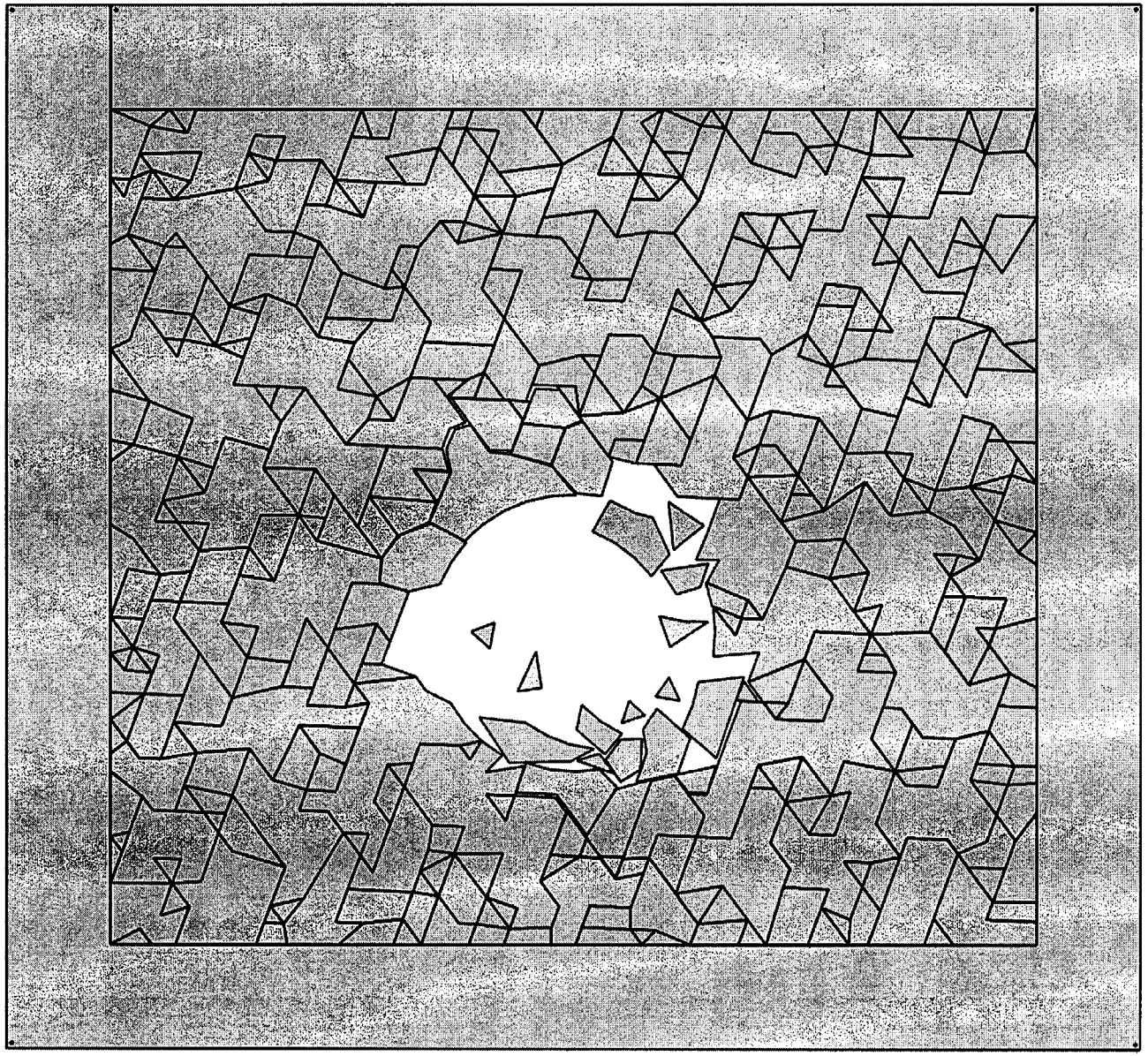

Figure 4-8. Response of rock-mass model in figure 4-2 to a sinusoidal wave with a 0.43-g peak ground acceleration, 10-Hz frequency, and 3-s duration

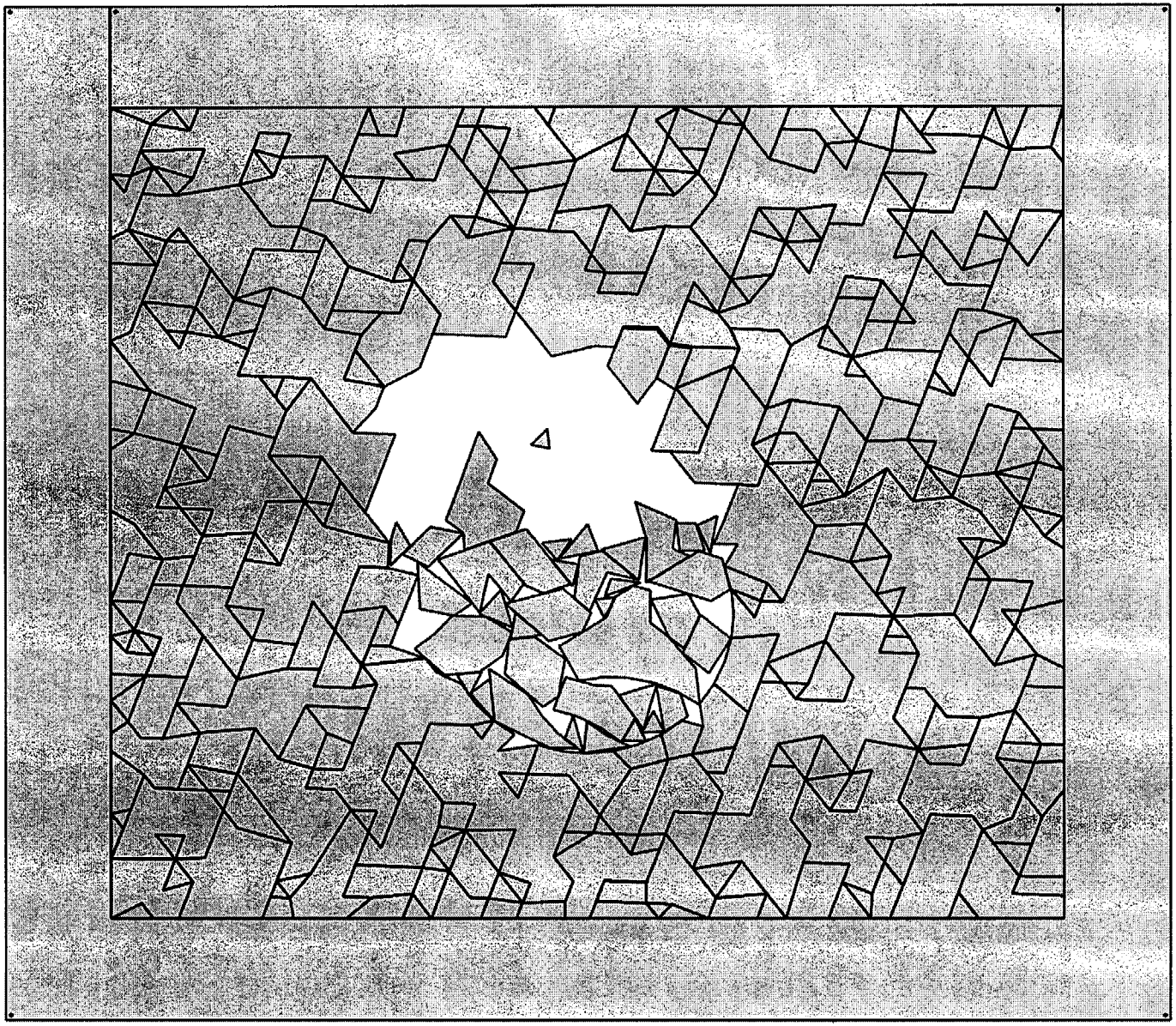

Figure 4-9. Response of rock-mass model in figure 4-1 to the seismic signal shown in figure 3-8 after 20 s of shaking

5 SEISMICALLY INDUCED ROCKFALL

5.1 EFFECTS OF BLOCK GEOMETRY ON EXTENT OF ROCKFALL

In the jointed rock media where systems of rock blocks are formed, damage such as spalling, excessive joint shear displacement, and rockfall may be of concern under earthquakes if excavations are not sufficiently supported during the preclosure period or when the ground supports lose their effectiveness after permanent closure. The damage may be further influenced by geometries of blocks surrounding excavations. In section 4, the effects of block geometries on rockfall and drift stability were discussed briefly. More results on potential geometry effects are presented in this section.

As discussed in section 3.1, the joint parameters considered in the analysis included joint dip direction, joint dip angle, joint spacing, joint length, and bridge (gap) length. The mean values of these parameters are listed in tables 3-1 and 3-2. A Monte Carlo technique was adopted to generate sample joint patterns. In generating these joint patterns, the joint spacing, length, and gap were assumed to be uniformly distributed within a range about ±35 percent of the mean values for the respective parameters. In a full application of the Monte Carlo technique, a sufficient number of realizations should be analyzed. For determining the sufficient number of realizations, one may plot selected statistics (e.g., mean damage, distribution of sizes of rockfall) versus number of realizations. When these statistics stop varying as the number of realizations, one has enough samples. In this report, the previously mentioned technique was not used to determine the a sufficient number of realizations required due to time constraint. However, analyses are continuing so that a sufficient number of realizations will be obtained for future use.

In the current EDA II design, the thermal load is designed to be 60 MTU/acre. The EDA II design also includes ventilation with an intent to keep the emplacement wall temperature below the boiling point during the preclosure period. However, the drift wall temperature is likely to increase and reach a maximum of approximately 120–130 °C within a few hundred years after permanent closure. Depending on the level of temperature and the rock mechanical and strength properties, high thermal stresses could potentially cause slips on existing joints and fracture the rock blocks so that new blocks will form.

With the designed thermal load and no ventilation applied, substantial failure due to thermally induced stresses in the rock mass surrounding the emplacement drifts could result. Application of continuous ventilation will reduce the extent of the failure zones. However, failure may still exist. This thermally induced failure may have effects on seismically induced rockfall in two ways. First, slips on joints could initiate instability. For the blocks located in the roof area, excessive slips on vertical to subvertical joints could cause instability. It is the excessive slip of horizontal to subhorizontal joints that may cause instability for blocks located in the side walls. Thermally induced stresses tend to generate slips on horizontal joints for blocks in the roof and slips on vertical joints for blocks in the side wall. Consequently, the effects of these types of joint slips on stability of the rock blocks in the roof and side wall areas may not be as significant. Second, formation of new blocks through fracturing may create new unstable conditions. These conditions can occur if the thermally induced stresses are sufficiently high to overcome the strength of the blocks.

The DDA computer codes cannot simulate formation of new blocks due to fracturing of the existing blocks. It is difficult to investigate thermal effects on rockfall without considering formation of new blocks given that the current thermal load design may induce thermal stresses sufficiently high to fracture intact

blocks. Consequently, it was decided not to include thermal load analyses in this report to avoid producing misleading results.

In the following two subsections, DDA results for the rock-mass responses due to the seismic signal shown in figure 3-8 are presented. All results reflect rock-mass conditions after 20 s of shaking, unless specified otherwise.

5.1.1 Small Joint Spacing Case

Twelve realizations of DDA models developed using the joint sets in table 3-1 were analyzed for their responses to seismic ground motions, and the results are presented here. Figures 5-1 through 5-10 illustrate 10 stochastically generated DDA realizations. The remaining two are given in figures 4-1 and 4-2.

The effects on the unsupported excavations for these realizations of joint patterns due to the seismic ground motions provided in figure 3-8 are shown in figures 5-11 through 5-22. The maximum peak acceleration or PGA associated with the ground motions in figure 3-8 is approximately 0.75 g. As can be observed, the extent of damage varied widely among the simulated rock-mass models. The extent of rockfall ranges from a few rock blocks (e.g., figures 5-14 and 5-15) to a major collapse of the drift (e.g., figures 5-13, 5-18, and 5-22). In some cases, substantial joint slip is observed for the rock blocks in the roof area (e.g., figure 5-14) that created a potentially unstable condition: a subsequent earthquake with some intensity may induce additional rockfall.

These results indicate clearly that the variations associated with the joint parameters play an important role in the stability of underground excavations when subjected to seismic ground motions. Furthermore, these results identify the potential effects of inherent variability in rock media on excavation stability. If these variations are not accounted for in an analysis, critical responses may not be captured properly. As a result, the stability of excavations may be over or underestimated, leading to an insufficient or uneconomical design of ground support. To assess earthquake damage and subsequently determine adequate support requirements, the responses of a sufficient number of realizations should be examined to quantify the range of possible damage. Proper support requirements then can be derived to contain damage. Damage indicators selected should be consistent with the nature of the problem analyzed.

Figures 5-23 through 5-25 show the rock-mass response for the DDA model in figure 4-2. The time histories used as input for these figures are provided in figure 3-8 with scaling factors of 1/5, 2/5, and 1/2 (so that each had a PGA about 0.15 g, 0.3 g, and 0.375 g). Compare the extent of rockfall in these figures with that in figure 5-22, where the PGA was 0.75 g. It is clear that the excavation subjected to a larger magnitude of ground motion (figures 5-22 and 5-25) suffers much more damage (in terms of extent of rockfall) than the excavation subjected to smaller ground motion (figures 5-23 and 5-24).

The observation that larger earthquakes cause more damage to underground structures is consistent with the field observations reported elsewhere (Sharma and Judd, 1991; Hsiung et al. 1992). However, it should be noted that the extent of damage or whether or not higher magnitudes of earthquakes will cause more damage depends greatly on rock block geometries. While higher magnitudes of ground motions cause more damage to the DDA model in figure 4-2 as shown in figures 5-22 and 5-23, the extent of damage during different magnitudes of ground motions is essentially the same for the DDA models in figures 4-1 and 5-9.

Figures 5-26 and 5-27 show the rock-mass damage subjected to a ground acceleration time history with a 1/5 scaling factor applied to figure 3-8 for the models in figures 4-1 and 5-9. The corresponding rock-mass response subjected to a ground acceleration time history equal to that in figure 3-8 is illustrated in figures 5-21 and 5-19. It can be noticed that major rockfall associated with each model occurred at a small earthquake ground motion with the model in figure 4-1 suffering more damage than the model in figure 5-9; an indication these rock blocks are inherently unstable and are being held in place by joint friction. An increase in the magnitude of ground motion to a PGA of 0.75 g did not induce any more rockfall for either of the DDA models in figures 4-1 and 5-9.

Figure 5-28 shows the responses of the rock-mass model in figure 4-2 after two earthquake ground motions. These two earthquakes were applied to the model one after the other. The acceleration time histories used for both earthquakes were the same and are given in figure 3-8. The amplitudes for the time history were scaled down so that the PGA is 0.15 g. The response to the first earthquake can be found in figure 5-23. As can be observed, the first episode of the earthquake induced only minor damage to the drift (i.e., a small number of blocks and some slip along the joints for the blocks on the roof). Additional damage can be observed after the second ground motion (figure 5-28 versus figure 5-23); significantly more rockfall took place to actually fill the entire excavation. The result demonstrates that repeated ground motions could have a detrimental effect on excavation stability.

Compared to figure 5-24, the results in figure 5-28 seem to suggest that two relatively smaller magnitude earthquakes may be more detrimental to the stability of a drift than one relatively larger one. This observation seems also to imply that the number of cycles of shaking may be one of the more important factors that influence rock-mass behavior. More work appears to be needed to verify this observation. However, it should be emphasized that the validity of this observation will depend greatly on block geometry. In other words, some realizations using the same joint information may be relatively less sensitive to repeated earthquake ground motions than others; just as some block geometries are less sensitive to ground motions than others.

On close examination of figure 5-23, accumulation of joint deformation can be seen at the top left side of the excavation after the first earthquake. This accumulation weakened the rock mass considerably even though the excavation remained stable. As a result, additional joint deformation accumulated in the same region during the second episode of ground motion and eventually triggered rockfall because the remaining joint strength could no longer hold the rock blocks in place (figure 5-28). This finding confirms further the observations both in the laboratory and the field that seismic events are likely to influence stability through accumulation of permanent deformations around underground excavations (Brown and Hudson, 1974; Barton and Hansteen, 1979; Hsiung et al. 1999). This finding also supports the notion that the fundamental failure mechanism for an excavation in a jointed rock medium subjected to repeated episodes of seismic events is accumulation of joint deformations (Hsiung et al., 1992, 1999).

5.1.2 Large Joint Spacing Case

Twelve realizations for the joint sets in table 3-2 were studied. Figures 5-29 through 5-40 show these stochastically generated DDA realizations using the joint set information in table 3-2. Notice that the block geometries in these figures are quite different from those shown in figures 5-1 through 5-10 for smaller joint spacings. It can also be observed that the DDA realizations for the large joint spacing cases contained a

substantial number of rock blocks with sizes bigger than the rock blocks in the DDA realizations for the small spacing cases. The presence of these larger rock blocks has a greater influence on drift stability as is discussed later.

The acceleration time history used in the analysis for this subsection is shown in figure 3-8; no scaling to the amplitudes was applied.

Figures 5-41 through 5-52 show the results of rock-mass response to earthquake ground motion for the DDA models shown in figures 5-29 through 5-40. Examining figures 5-41 through 5-52, one can generally conclude that rockfall potential was significantly more restricted for cases with large joint spacings than for cases with small joint spacing. In other words, the number of rock blocks falling into the drift was much less than for the small joint spacing cases; and the block sizes of the falling rocks were, in general, smaller as well. This is because the large blocks in the large joint spacing cases were kinematically more stable; only those small size blocks, which were kinematically less stable, could fall. In the limited cases studied, the majority of rockfall was started from side walls instead of from the roof area, except for one model (figure 5-52) where almost all rockfall was produced from the roof area, and the associated rock block sizes also were relatively larger than for the rest of the cases.

In close examination of the DDA model realizations in figures 5-29 through 5-40, it can be seen that the rock blocks around the drifts are in such positions that the blocks falling into drifts would be kinematically difficult. This situation may be responsible for the relatively stable conditions observed for the realizations in figures 5-29 through 5-40. It should be noted that the realizations formed for the large joint spacing cases are based on the joint information with measured joint trace lengths greater than 1 m. If the joints with joint trance length smaller than 1 m are included in the database, the possibility of forming blocks with relatively smaller sizes than the block sizes shown in figures 5-29 through 5-41 may increase. Consequently, the resulting realizations may become less stable and more rockfall will be expected. This study did not consider the joints with trace length smaller than 1 m because this information is not available.

5.2 LONG-TERM DEGRADATION OF ROCK MASS

5.2.1 Mechanism For Long-Term Degradation

As discussed in section 1, long-term degradation of rock mass at YM under prolonged thermal load could result from two sources: (i) reduction of joint shear strength due to long-term creeping effects or other modes of deterioration during a high state of stresses and (ii) long-term deterioration of rock strength due to a creeping effect under a sustained high state of stresses that leads to failure of intact rocks. These conditions could substantially increase the potential for rockfall. Item (ii) will cause intact rocks to fracture through either newly formed fracture planes or propagation of the preexisting nonpersistent (not throughgoing) joints in rock blocks. This failure mechanism is similar to that caused by thermally induced block failure. Normally, the failure mechanism for the latter is more likely than that for the former because failure usually follows the weakest path. Reduction of joint shear strength increases rockfall potential for the existing rock blocks. Fracturing of intact rock blocks may form new blocks that could create rockfall conditions that otherwise may not exist previously, even after the long-term degradation of joint shear strength.

As discussed earlier, the current DDA codes do not have options for simulating fracturing of intact rocks for conditions described in item (ii) in the previous paragraph. Consequently, their effects were not investigated in this study. Only the effects related to item (i) were examined.

5.2.2 Long-Term Degradation of Joint Friction

In the analysis, the process of degradation of joint shear strength was not modeled. It was assumed that at a certain point in the degradation process, joint shear strength will be reduced from its original value to a relatively smaller one. This analysis used that reduced value directly from the start of simulation. The reduced value for joint friction angle used in this analysis was 30 degrees, about 23 percent reduction from its original 39 degrees.

Figure 5-53 shows the rock-mass response for the DDA model in figure 4-2 after approximately 7.5 s of shaking. The PGA for the acceleration time history input was 0.3 g. Compare the extent of rockfall experienced in this figure with the rockfall experienced in figure 5-24. It is clear that degradation of joint shear strength plays a role in drift stability. Although there were some permanent accumulations of shear deformations along joints for the rock blocks located in the left upper corner of the drift (figure 5-24), for the condition where the joint friction angle was not reduced, the drift was relatively stable except for a few rockfalls. This subtle stable condition could change if the joint friction angle were allowed to degrade as indicated in figure 5-53. The rock blocks near the upper left corner drift overcame the degraded joint shear strength and triggered a massive rockfall that extended deep into the left upper corner of the drift.

A similar observation also can be made by comparing the dynamic response of a rock mass during the condition for which no degradation took place (figure 5-19) to the dynamic response of the same rock mass where the joint shear strength was substantially degraded (figure 5-54). Based on these results, it would seem prudent to include consideration of long-term joint strength degradation in assessing stability and rockfall of underground excavations depending on the intended service life of the excavations, because degraded excavations are more susceptible to earthquake damage.

5.3 ROCKFALL ANALYSIS USING HIGHER ORDER DISPLACEMENT DEFORMATION FUNCTION

The DDA results presented so far in this report are based on the first order polynomial displacement function approximation. Using this approximation, the strains in each block are constant. This first order approximation is equivalent to a triangular element in FEM. As discussed earlier, Hsiung[1] extended the DDA code to include the option of selecting a polynomial displacement function of any order at run time. The first and second order displacement functions were used in two DDA block models to compare the difference in results (figure 5-20 versus figure 5-55 and figure 5-25 versus figure 5-56). Figures 5-20 and 5-25 give the rock-mass responses using the first order polynomials and figures 5-55 and 5-56 for the second order polynomials. The results indicate that the second order polynomials resulted in an excavation more stable than

[1]Hsiung, S.M. Discontinuous Deformation Analysis (DDA) with n^{th} order polynomial displacement functions. *38th U.S. Rock Mechanics Symposium, July 7–10, 2001, Washington, DC.* 2001. Submitted for publication.

if the first order polynomial displacement function was used. As shown in figure 5-20 (a first order polynomial solution), the shear displacements and separations of joints in rocks at the top right side of the excavation were more pronounced that those in figure 5-55 (a second order polynomial solution). On a separate DDA model realization (figure 4-2), substantially more damage/rockfall to the drift was experienced in figure 5-25 (a first order solution) than in figure 5-56 (a second order solution). This behavior is reasonable because DDA blocks become more deformable when higher order polynomial functions are used. Consequently, the results presented in the previous sections using the first order displacement function should provide reasonable bounding cases for investigating seismically induced rockfall for emplacement drifts.

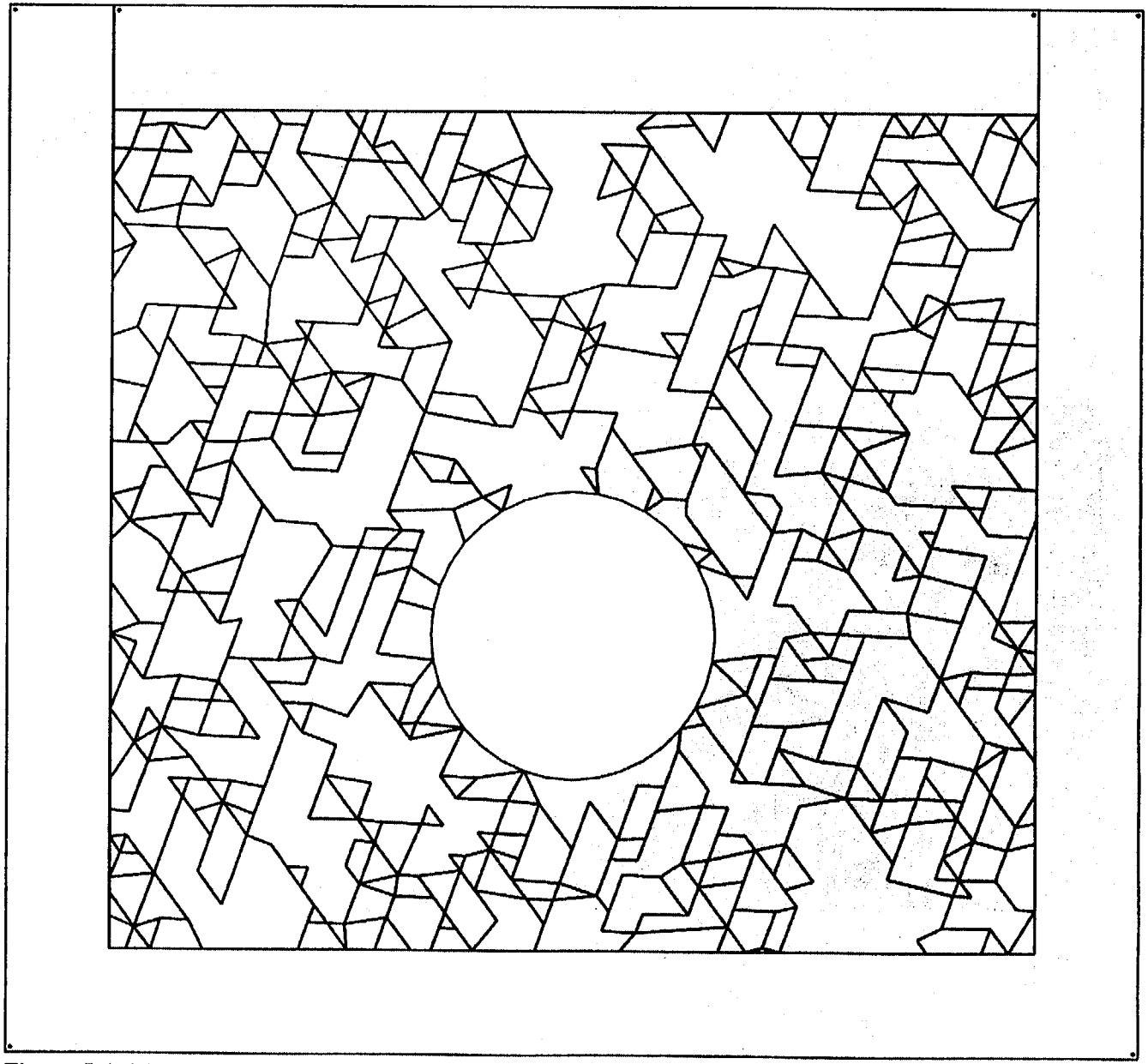

Figure 5-1. Discontinuous Deformation Analysis model realization 3 for small joint spacings

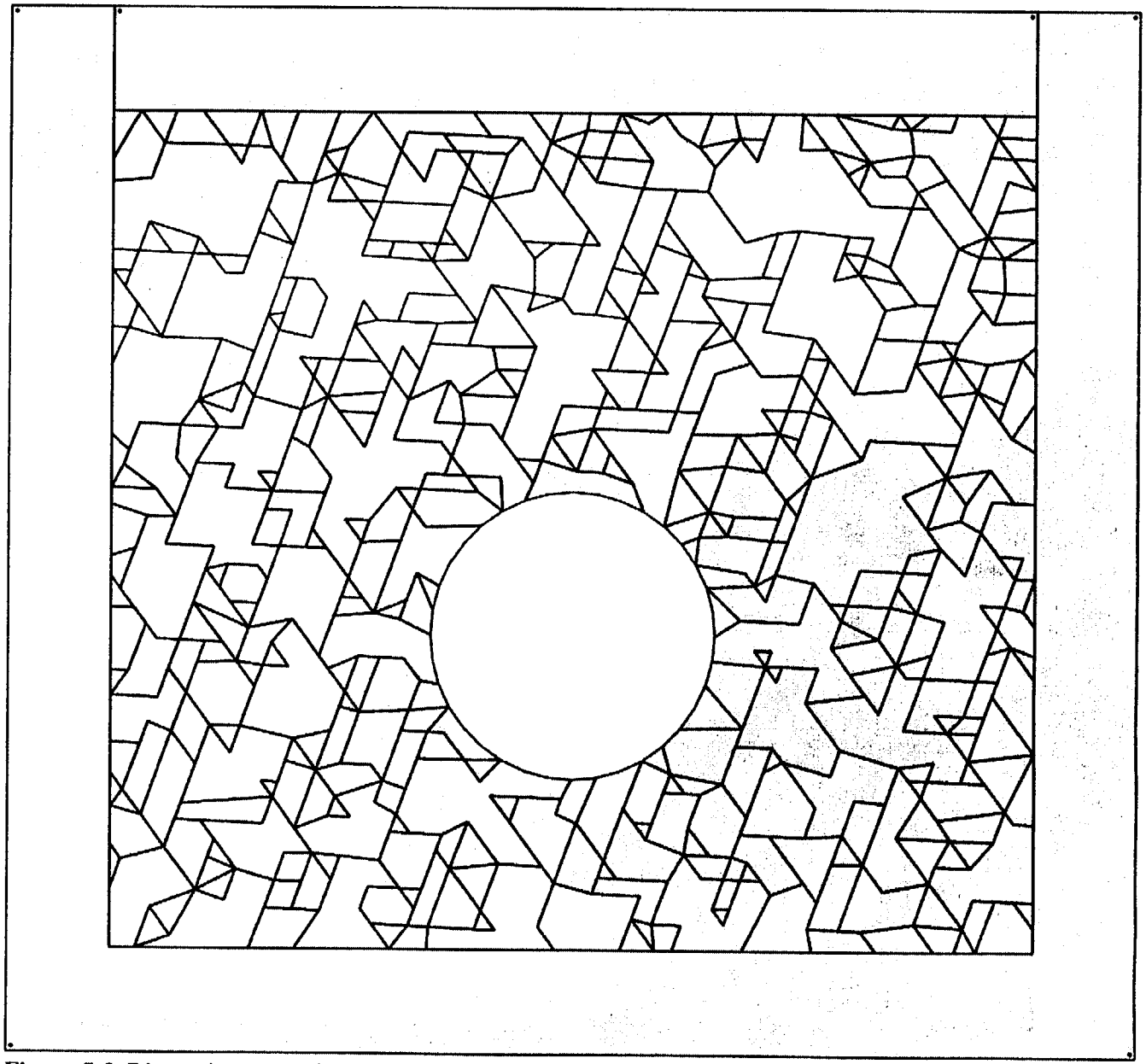

Figure 5-2. Discontinuous Deformation Analysis model realization 4 for small joint spacings

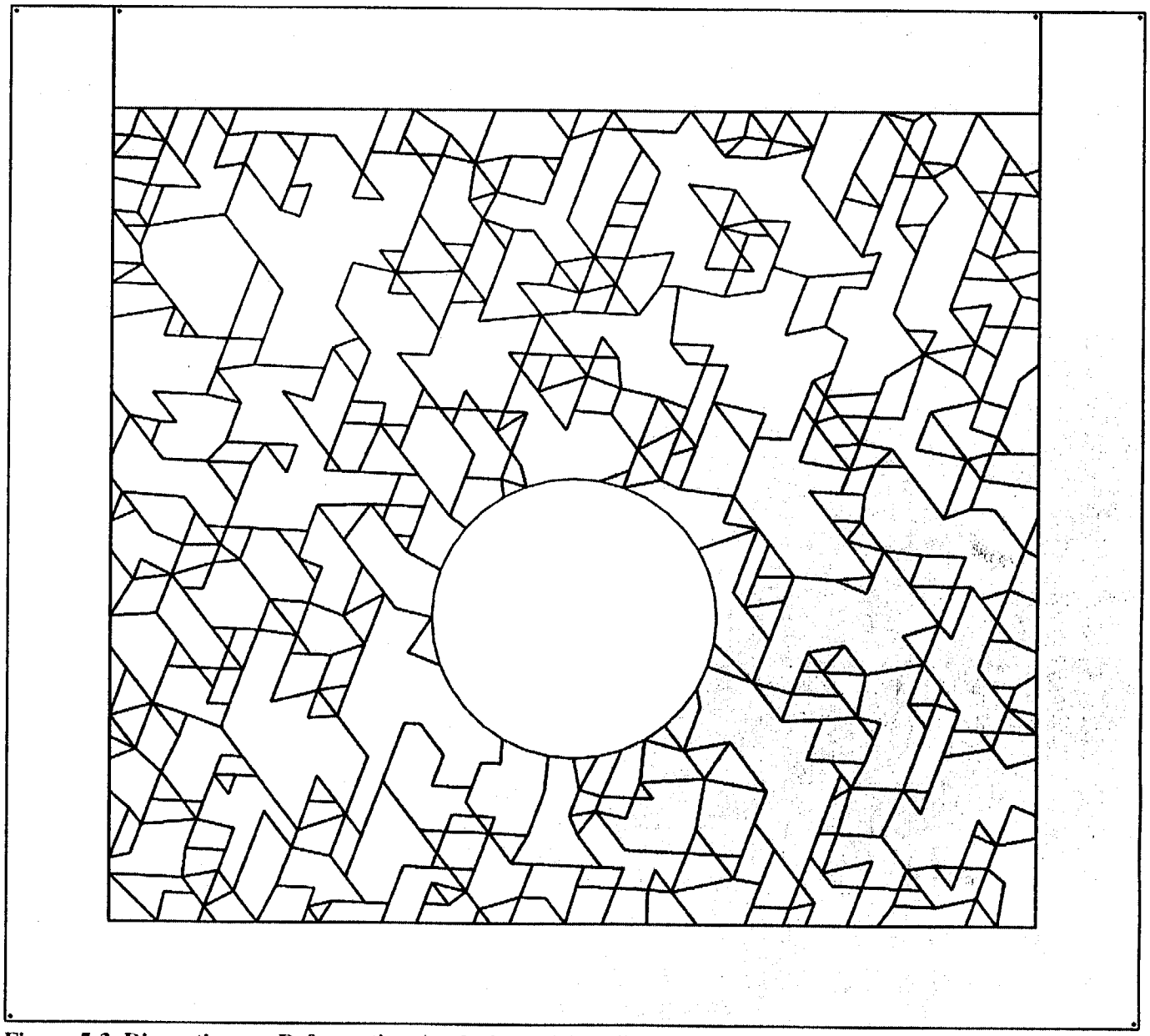

Figure 5-3. Discontinuous Deformation Analysis model realization 5 for small joint spacings

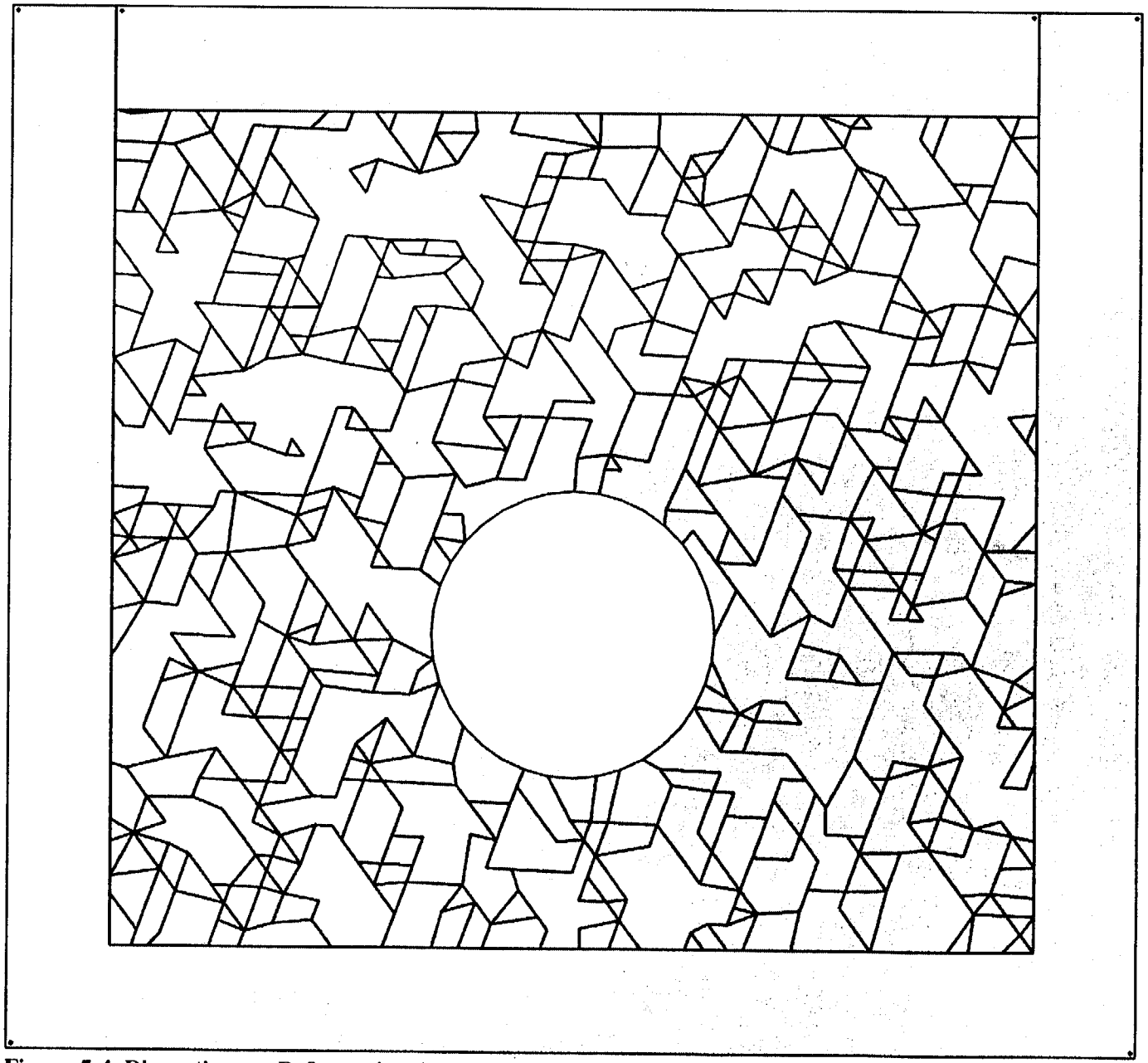

Figure 5-4. Discontinuous Deformation Analysis model realization 6 for small joint spacings

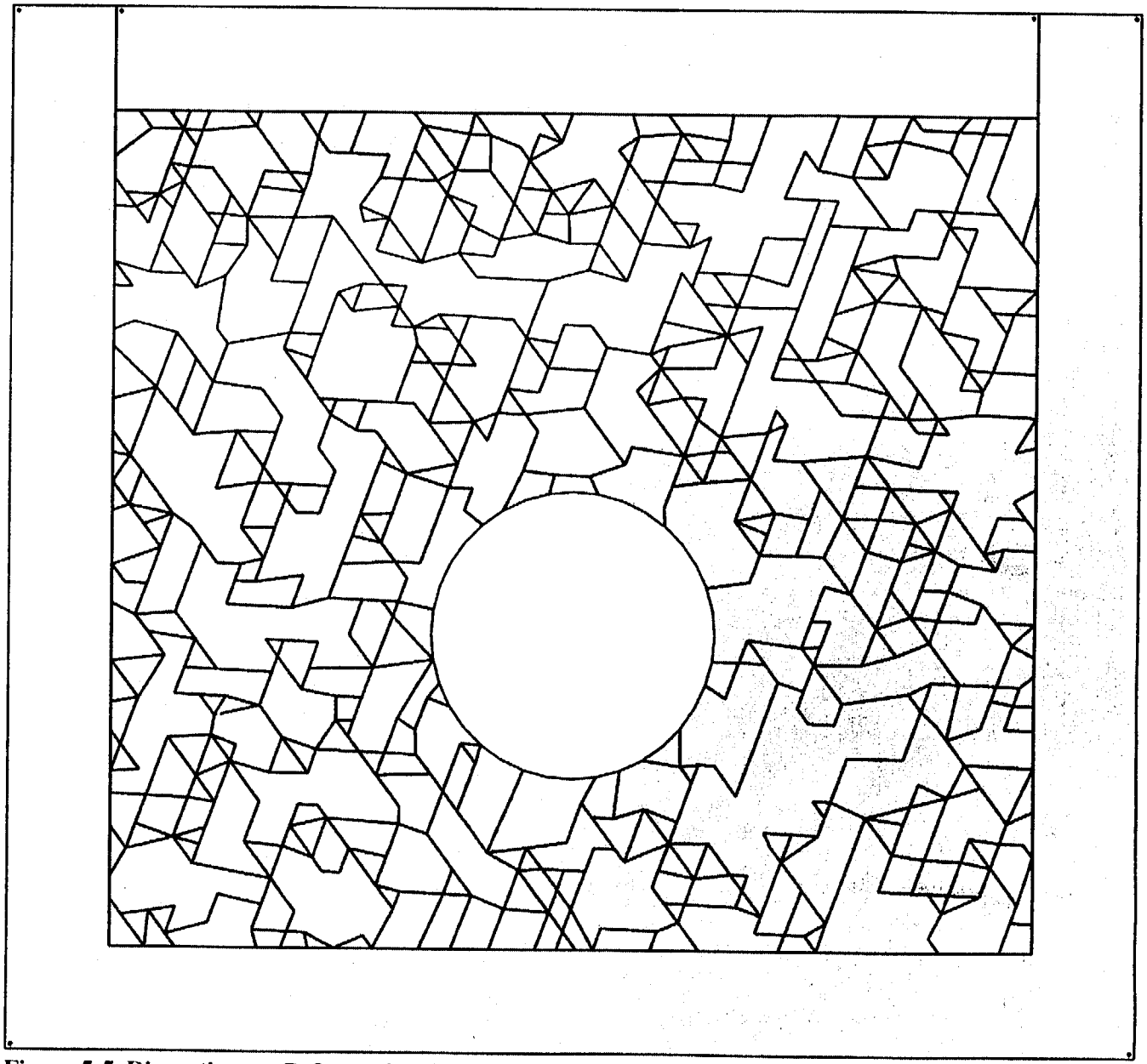

Figure 5-5. Discontinuous Deformation Analysis model realization 7 for small joint spacings

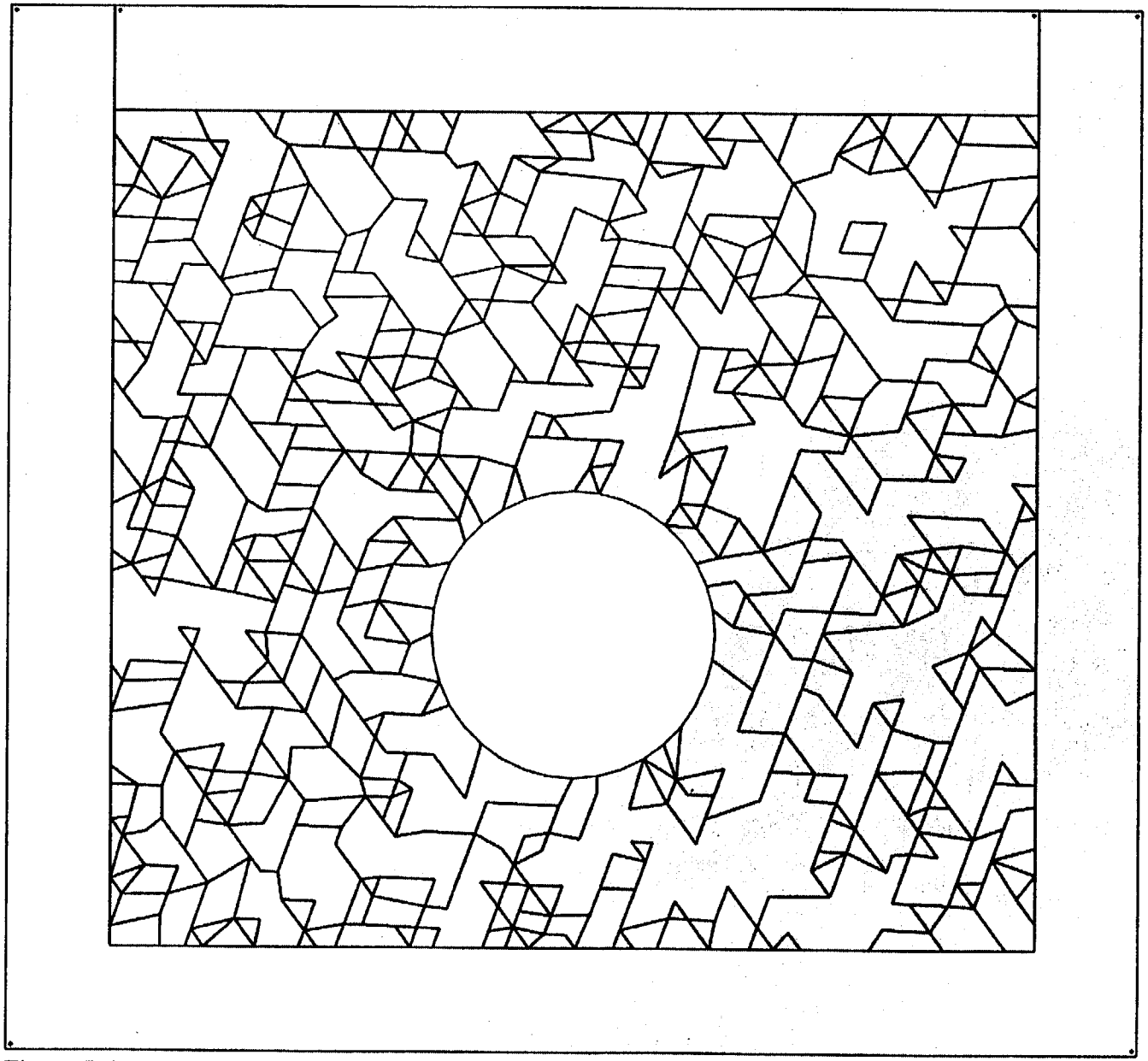

Figure 5-6. Discontinuous Deformation Analysis model realization 8 for small joint spacings

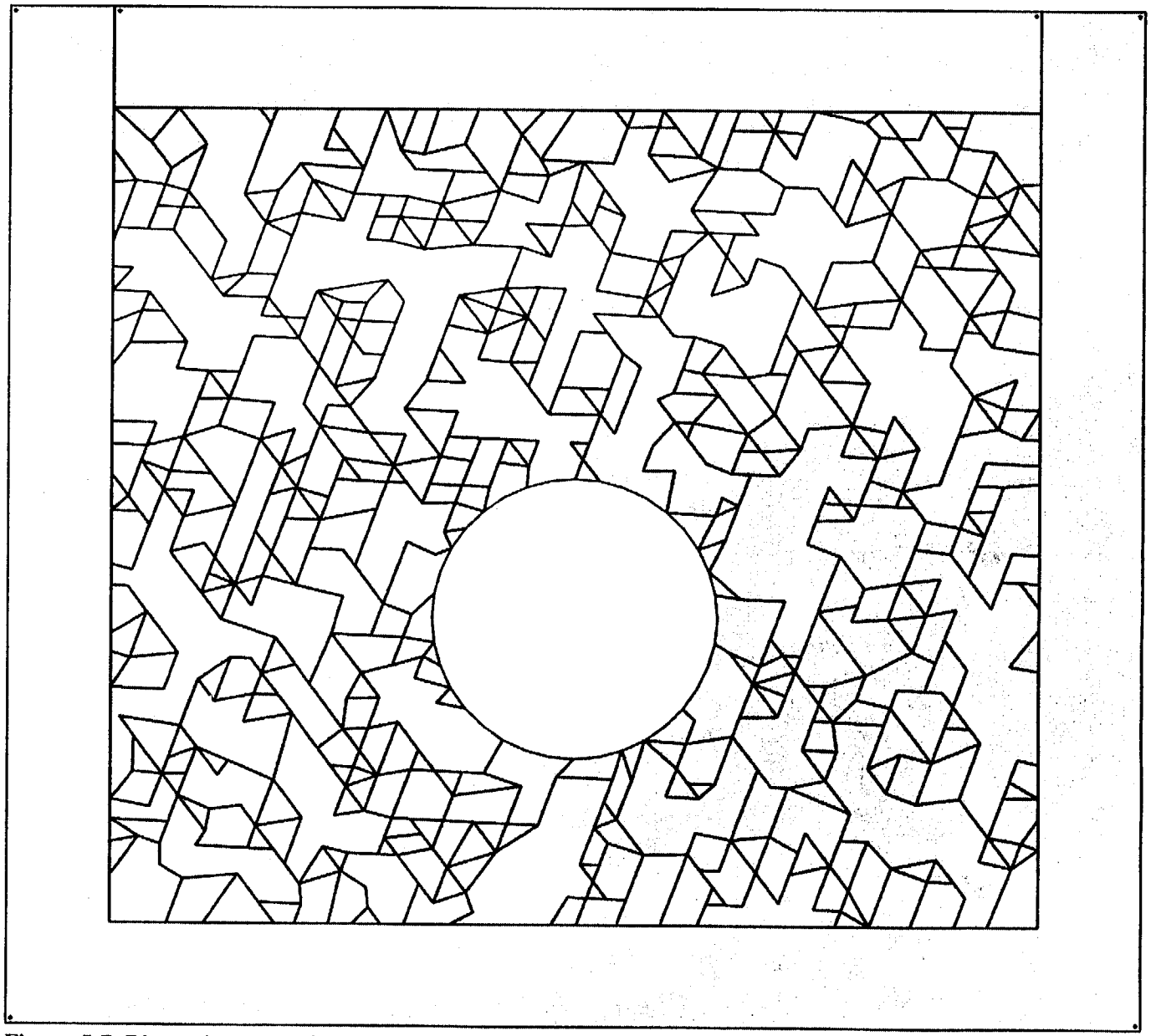

Figure 5-7. Discontinuous Deformation Analysis model realization 9 for small joint spacings

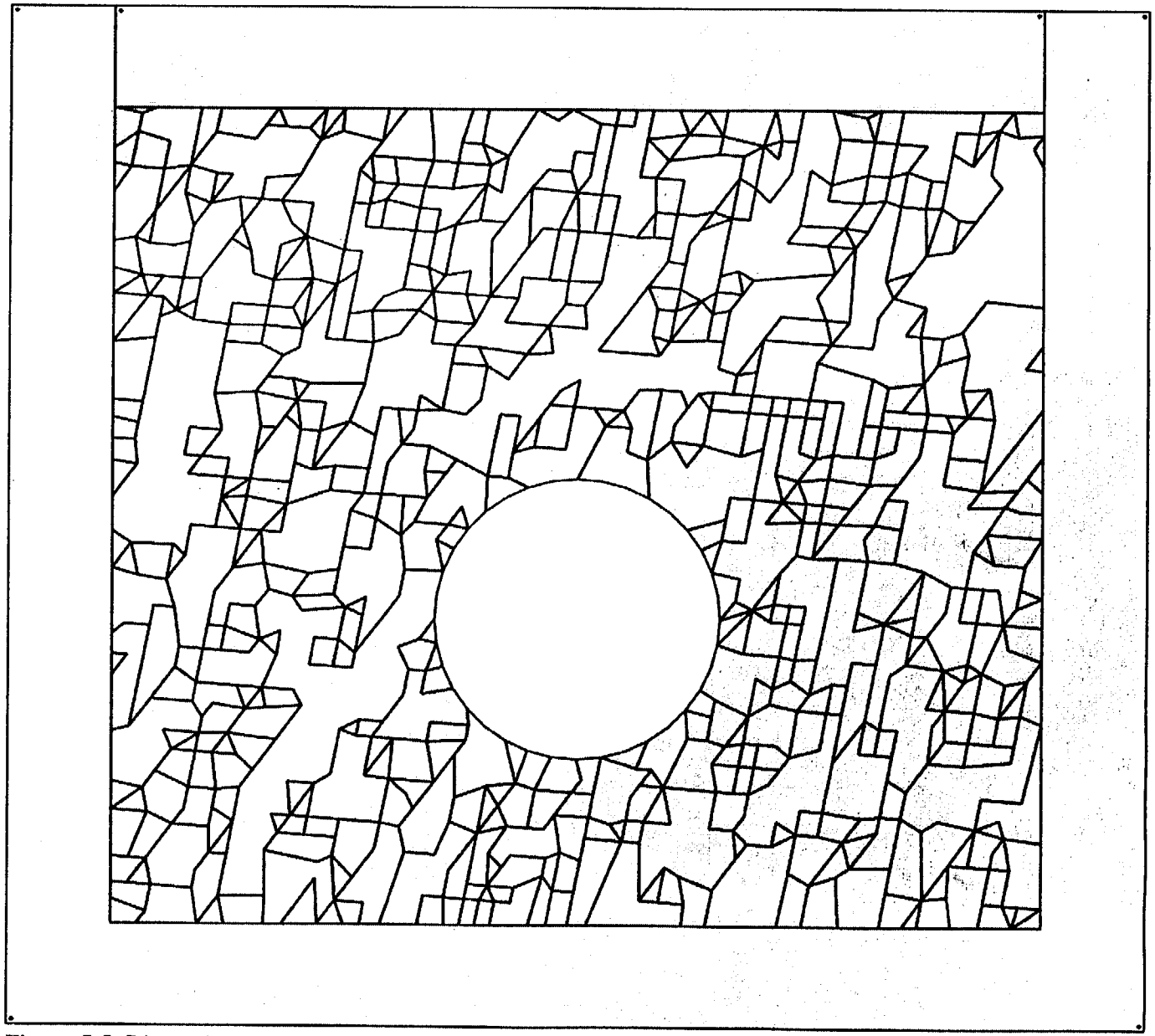

Figure 5-8. Discontinuous Deformation Analysis model realization 10 for small joint spacings

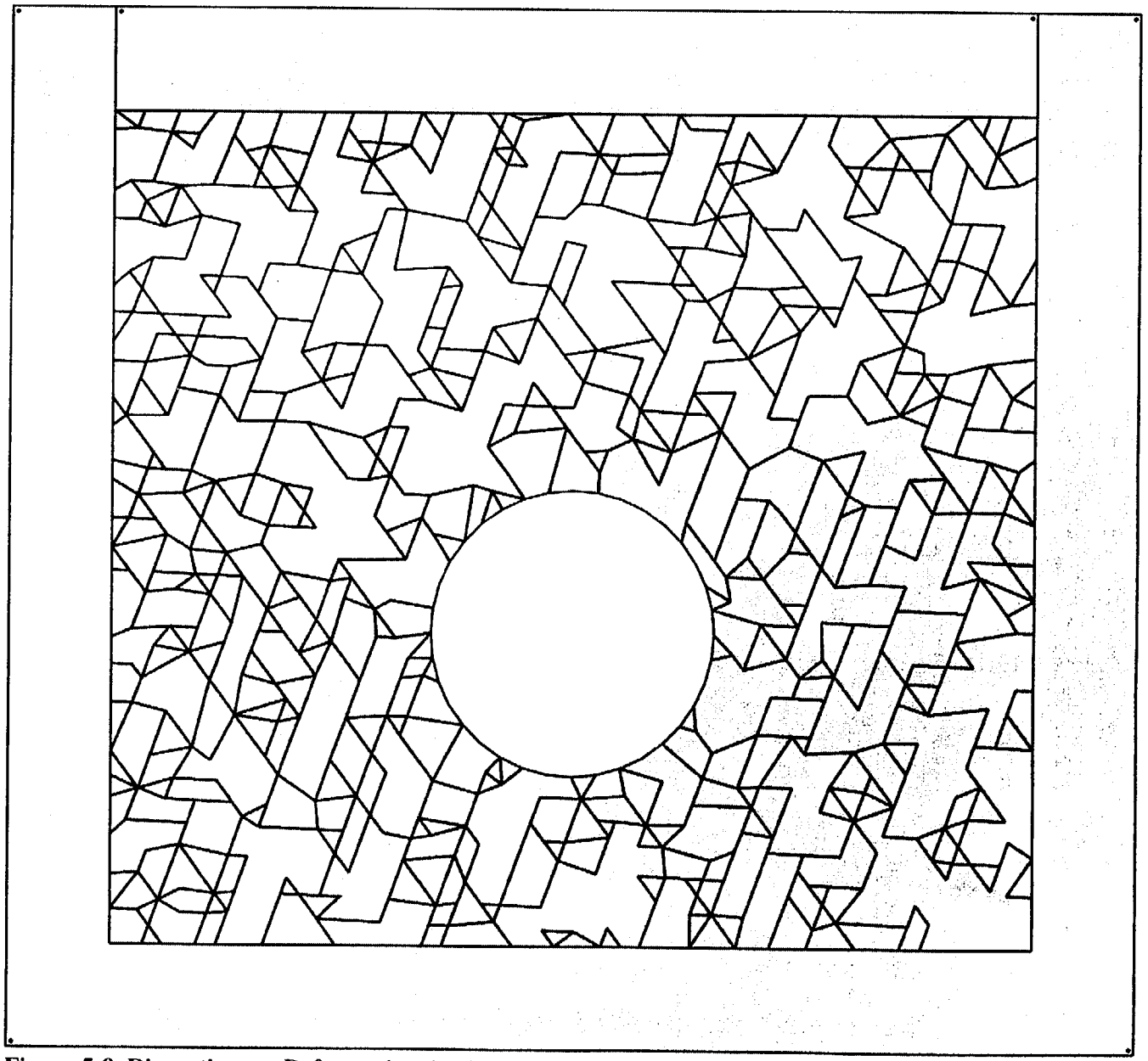

Figure 5-9. Discontinuous Deformation Analysis model realization 11 for small joint spacings

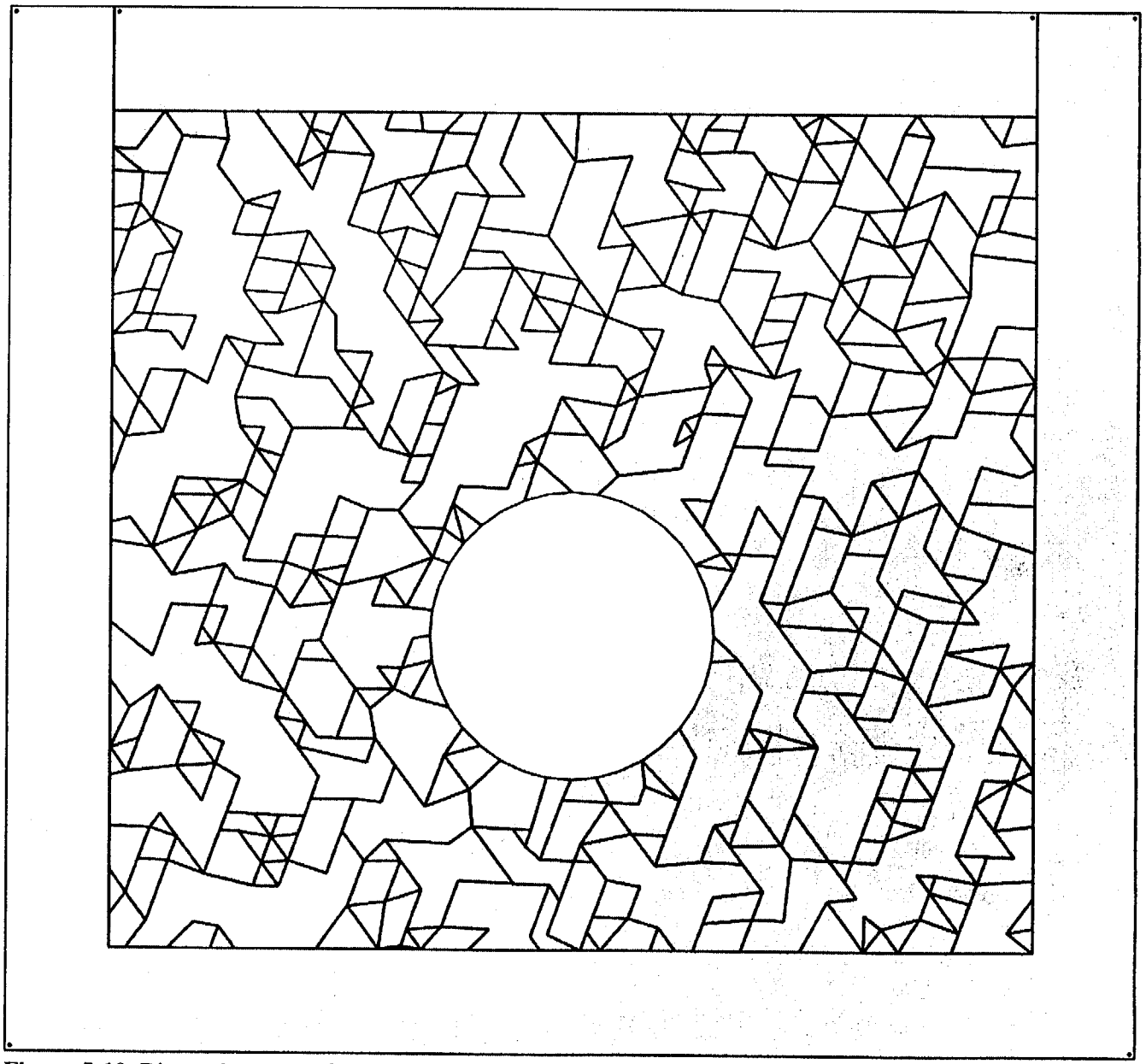

Figure 5-10. Discontinuous Deformation Analysis model realization 12 for small joint spacings

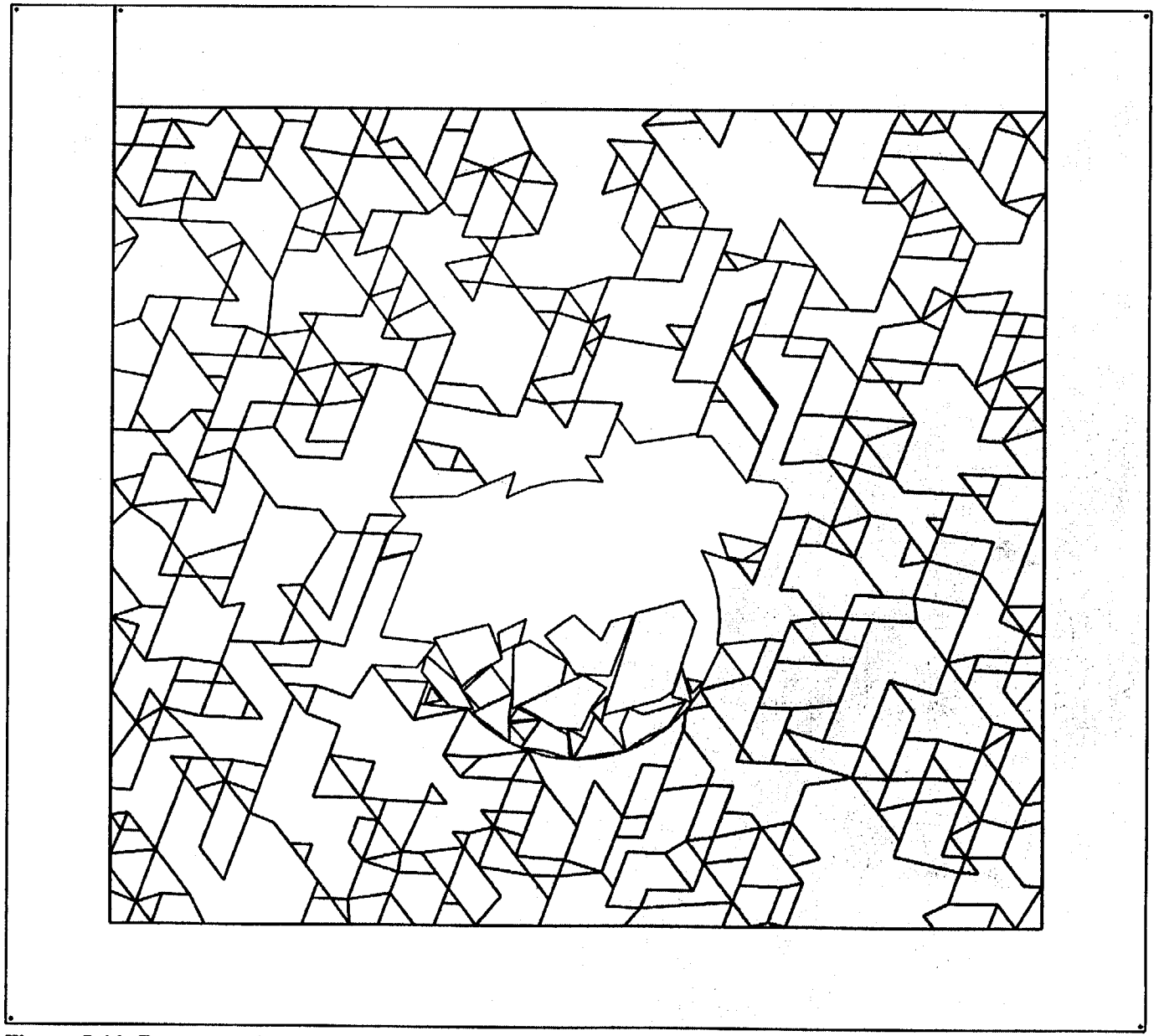

Figure 5-11. Response of rock-mass model in figure 5-1 to the seismic signal shown in figure 3-8

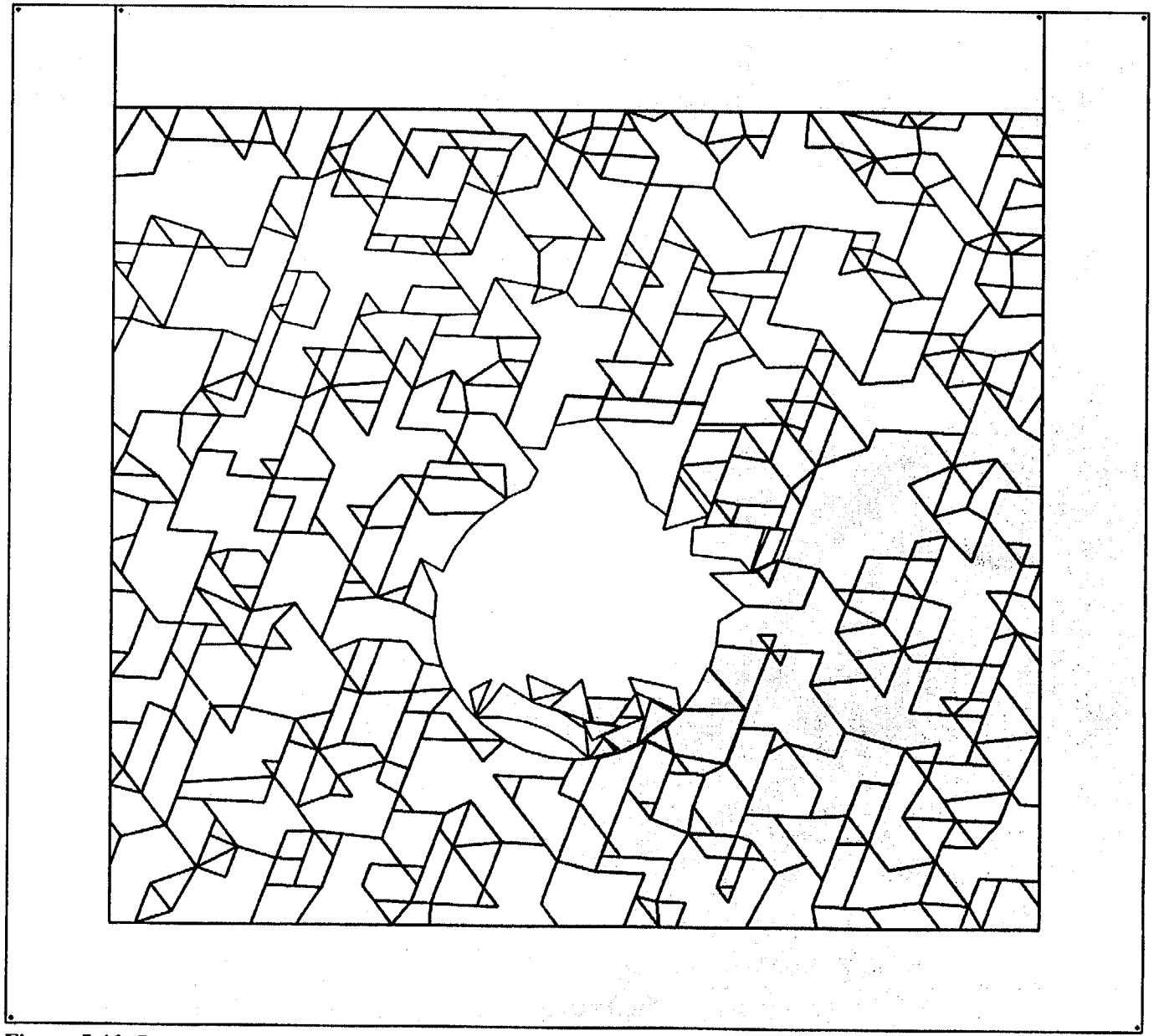

Figure 5-12. Response of rock-mass model in figure 5-2 to the seismic signal shown in figure 3-8

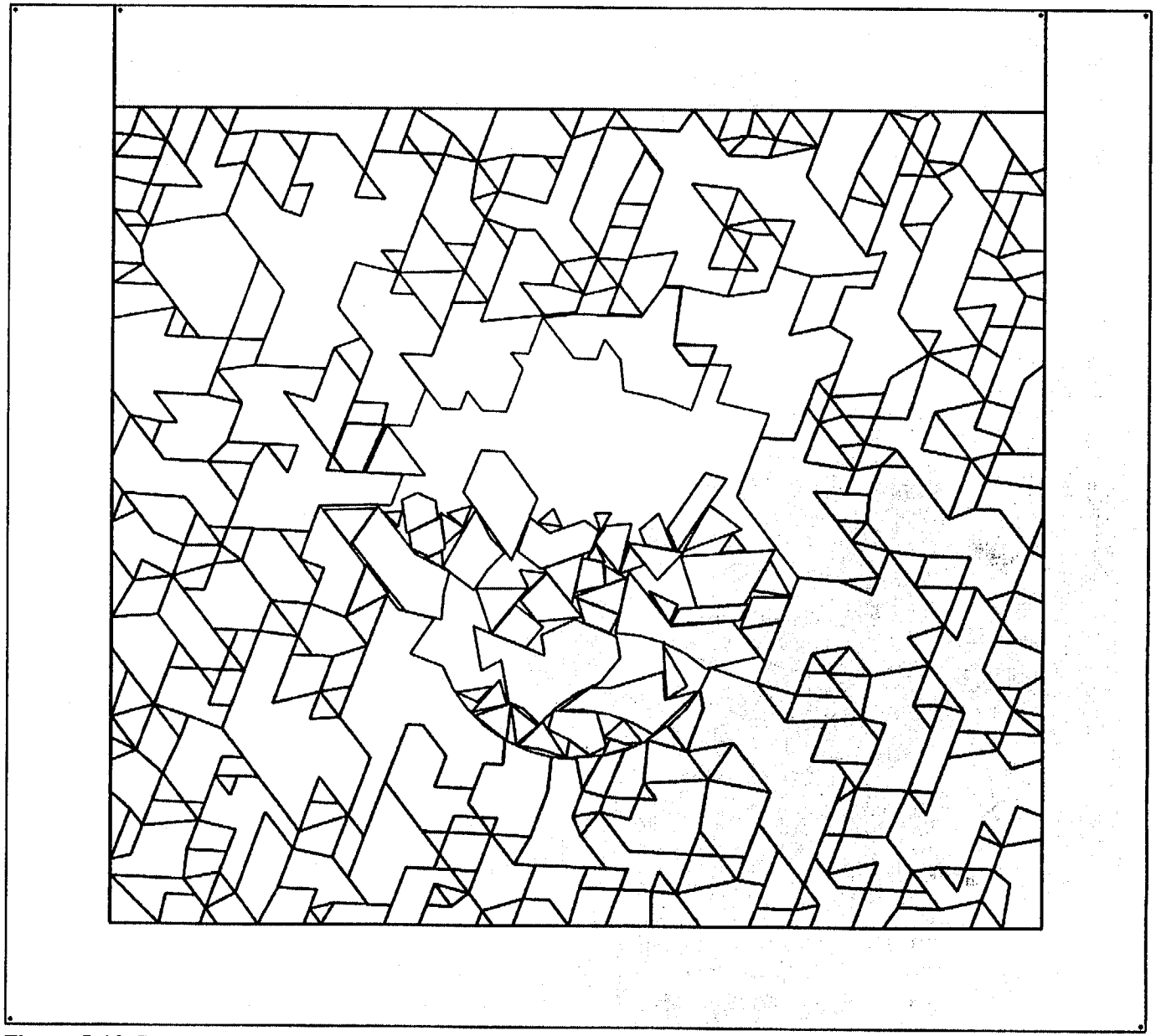

Figure 5-13. Response of rock-mass model in figure 5-3 to the seismic signal shown in figure 3-8

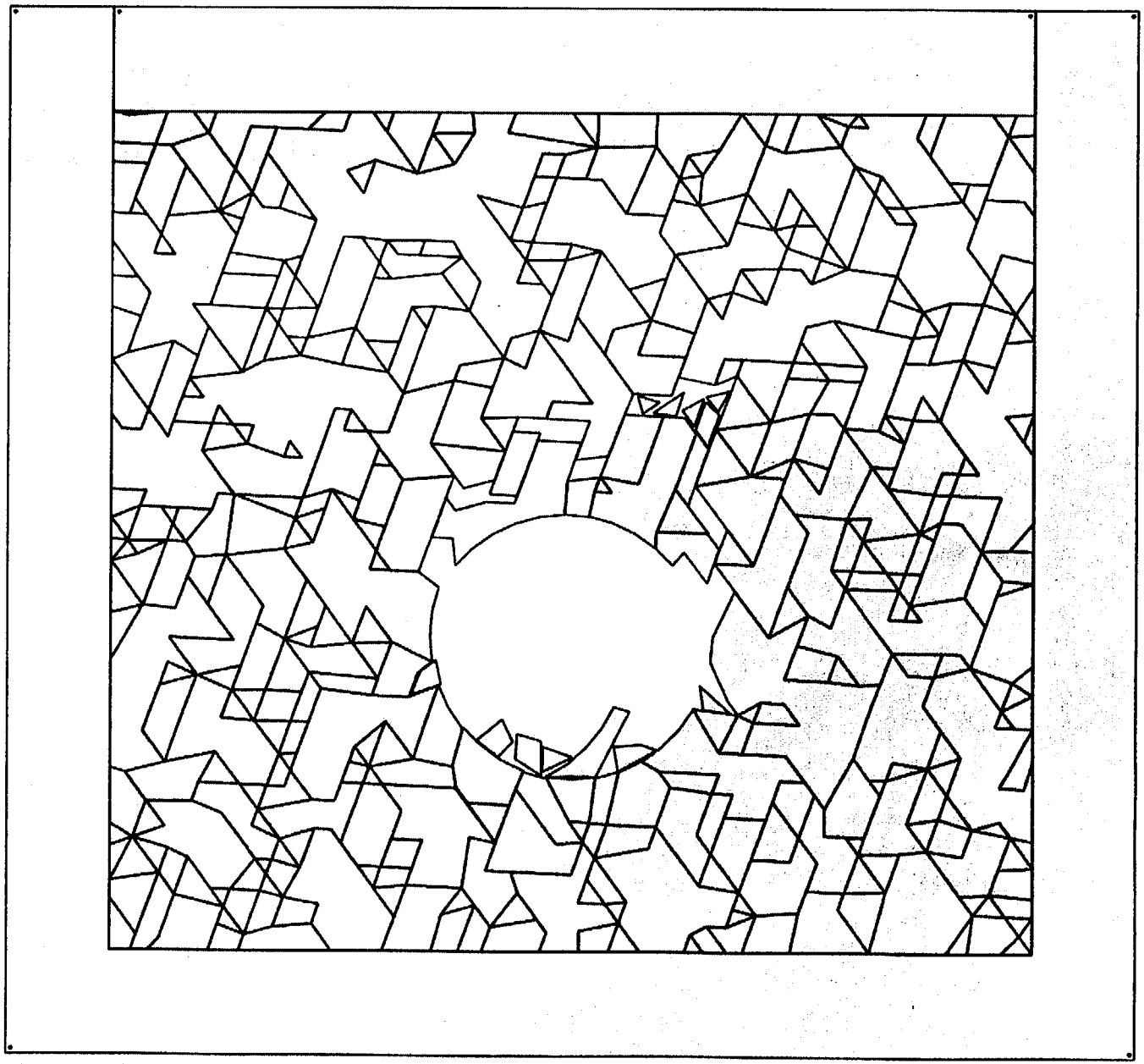

Figure 5-14. Response of rock-mass model in figure 5-4 to the seismic signal shown in figure 3-8

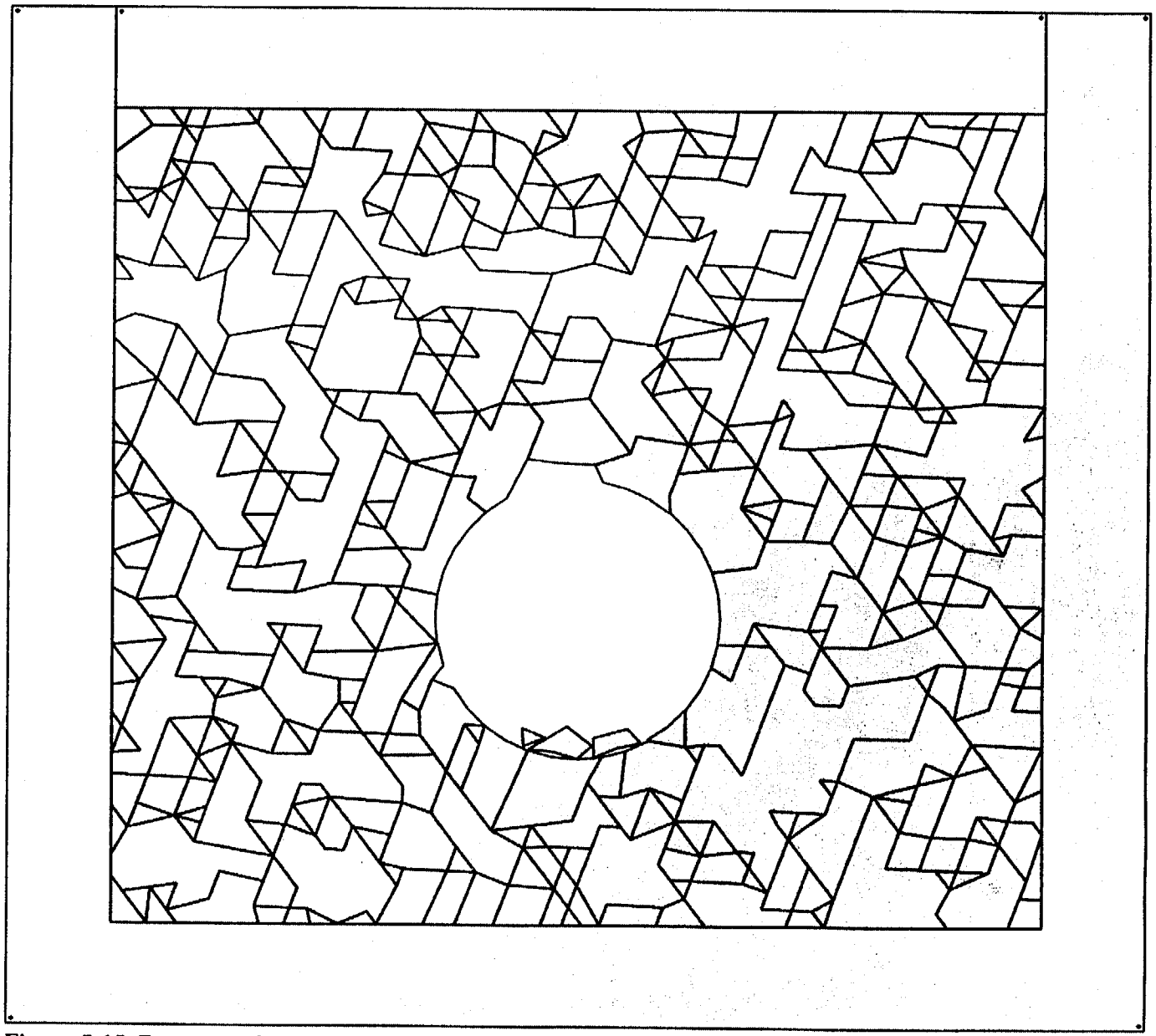

Figure 5-15. Response of rock-mass model in figure 5-5 to the seismic signal shown in figure 3-8

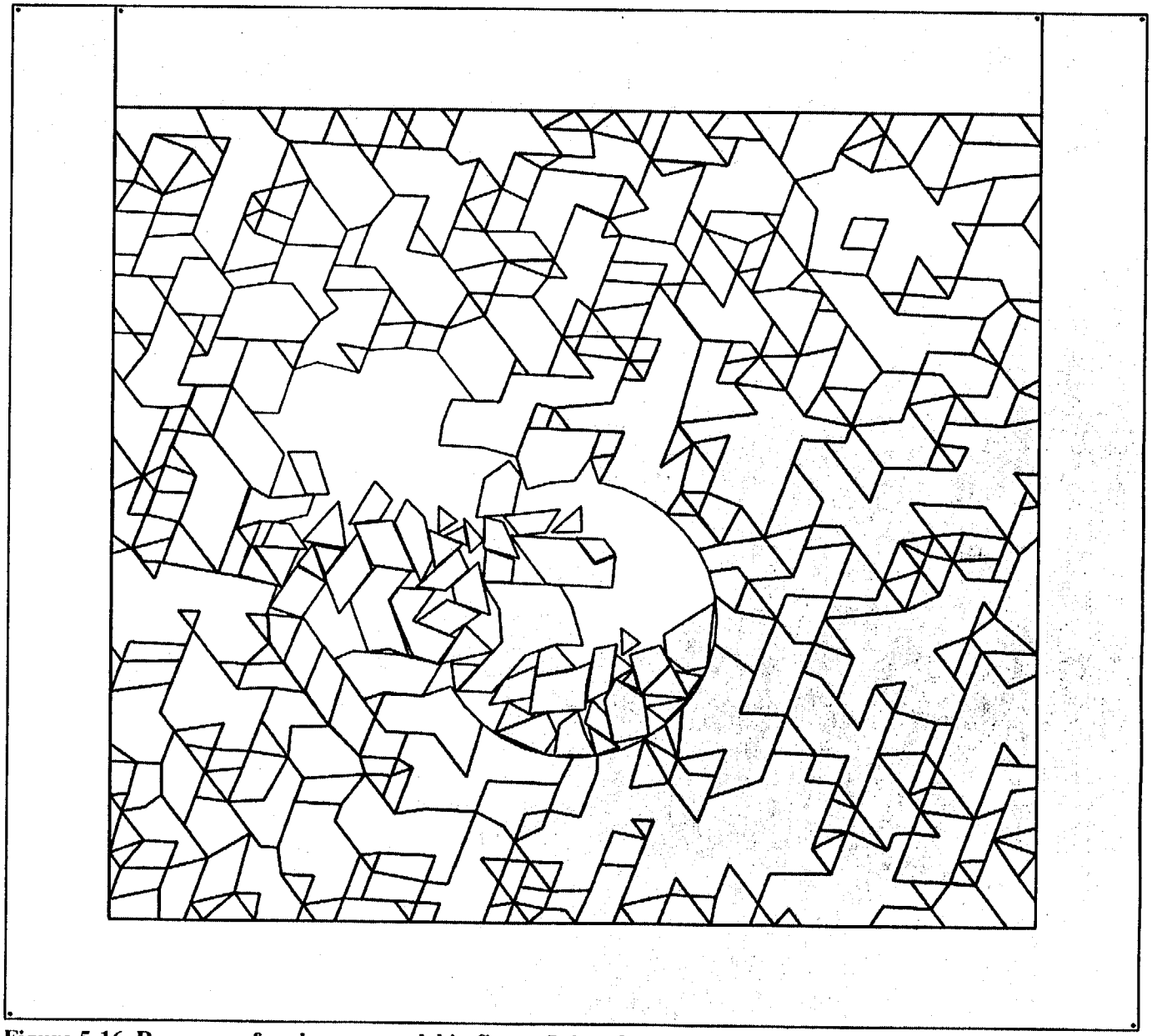

Figure 5-16. Response of rock-mass model in figure 5-6 to the seismic signal shown in figure 3-8

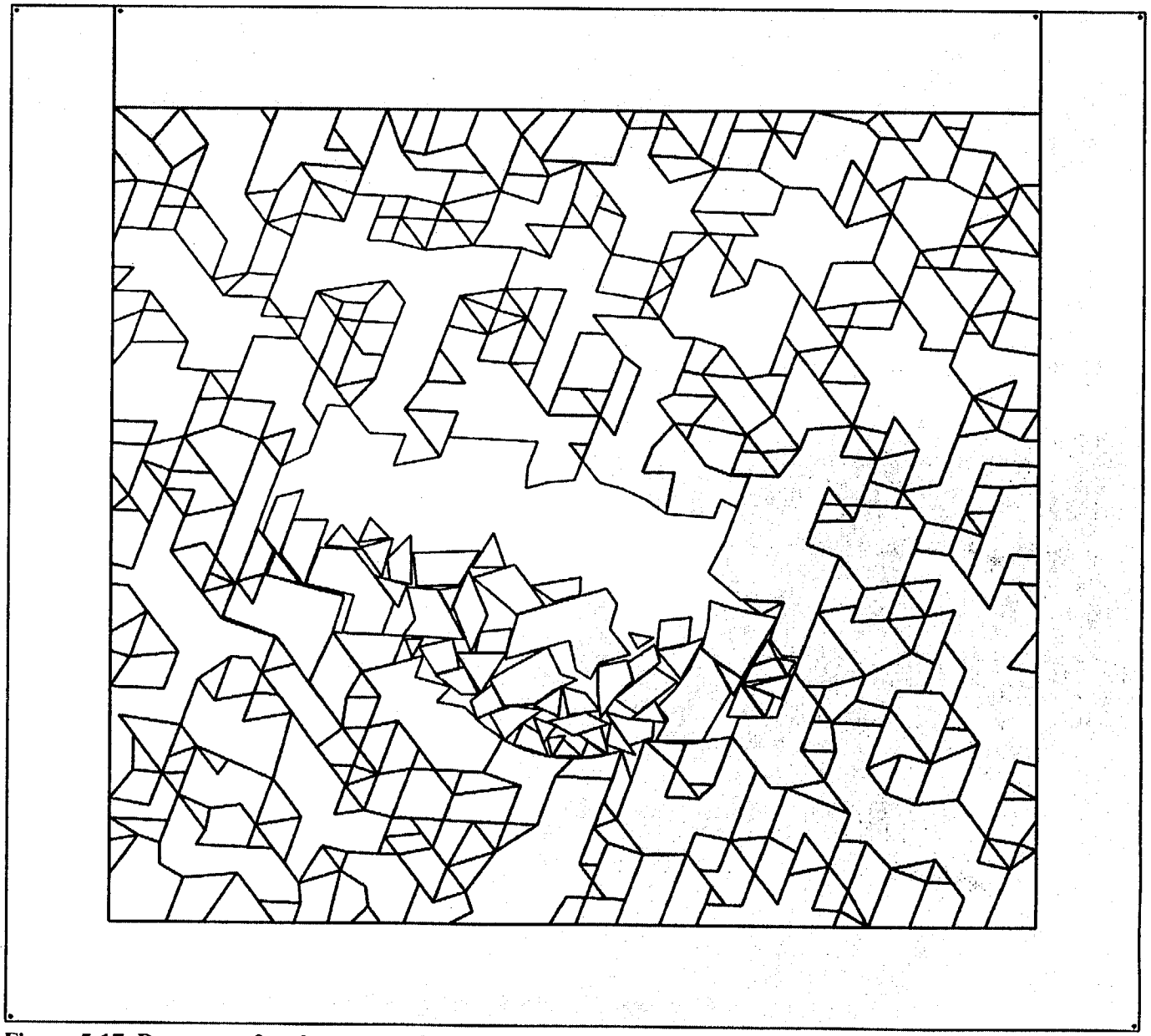

Figure 5-17. Response of rock-mass model in figure 5-7 to the seismic signal shown in figure 3-8

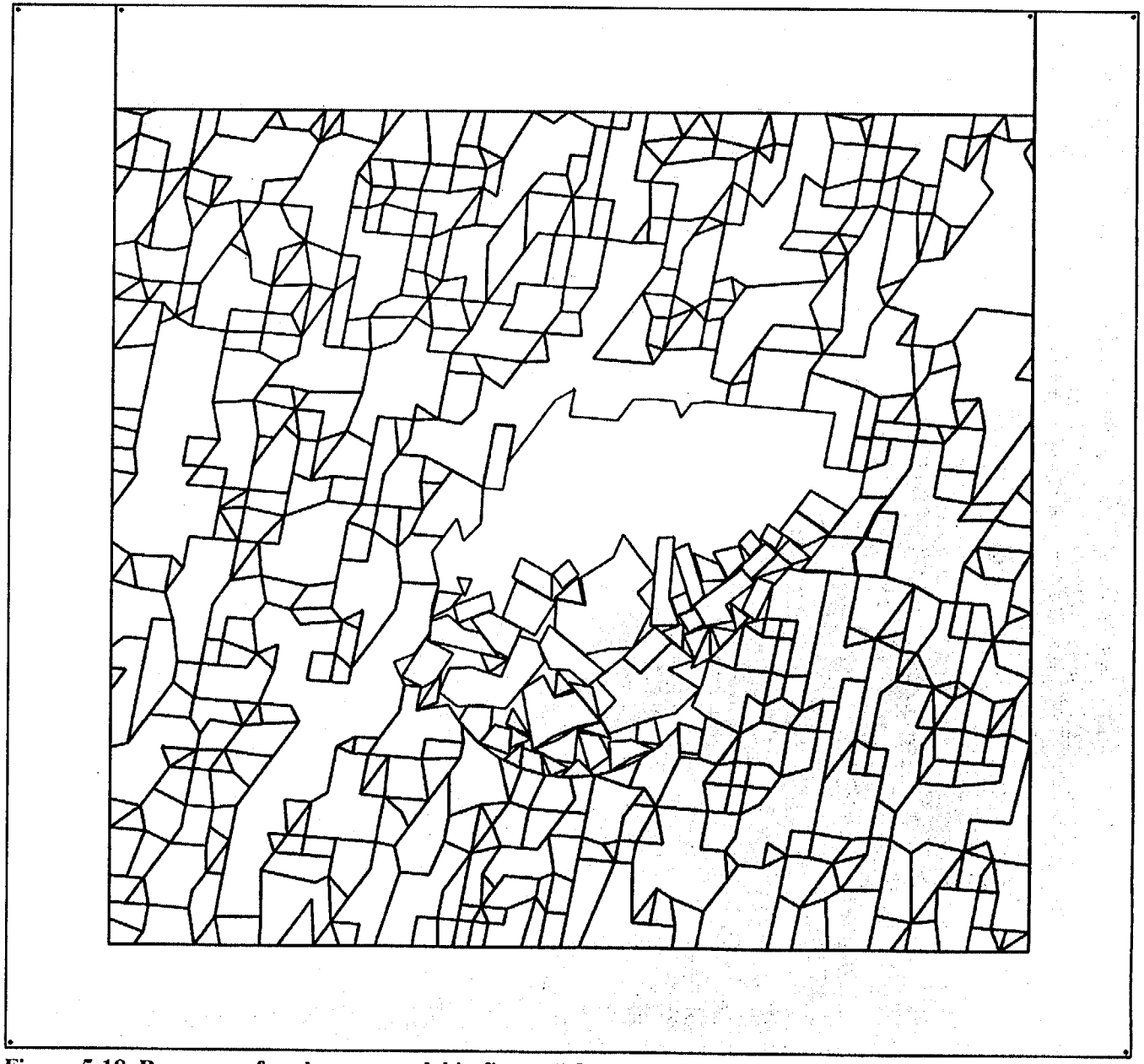

Figure 5-18. Response of rock-mass model in figure 5-8 to the seismic signal shown in figure 3-8

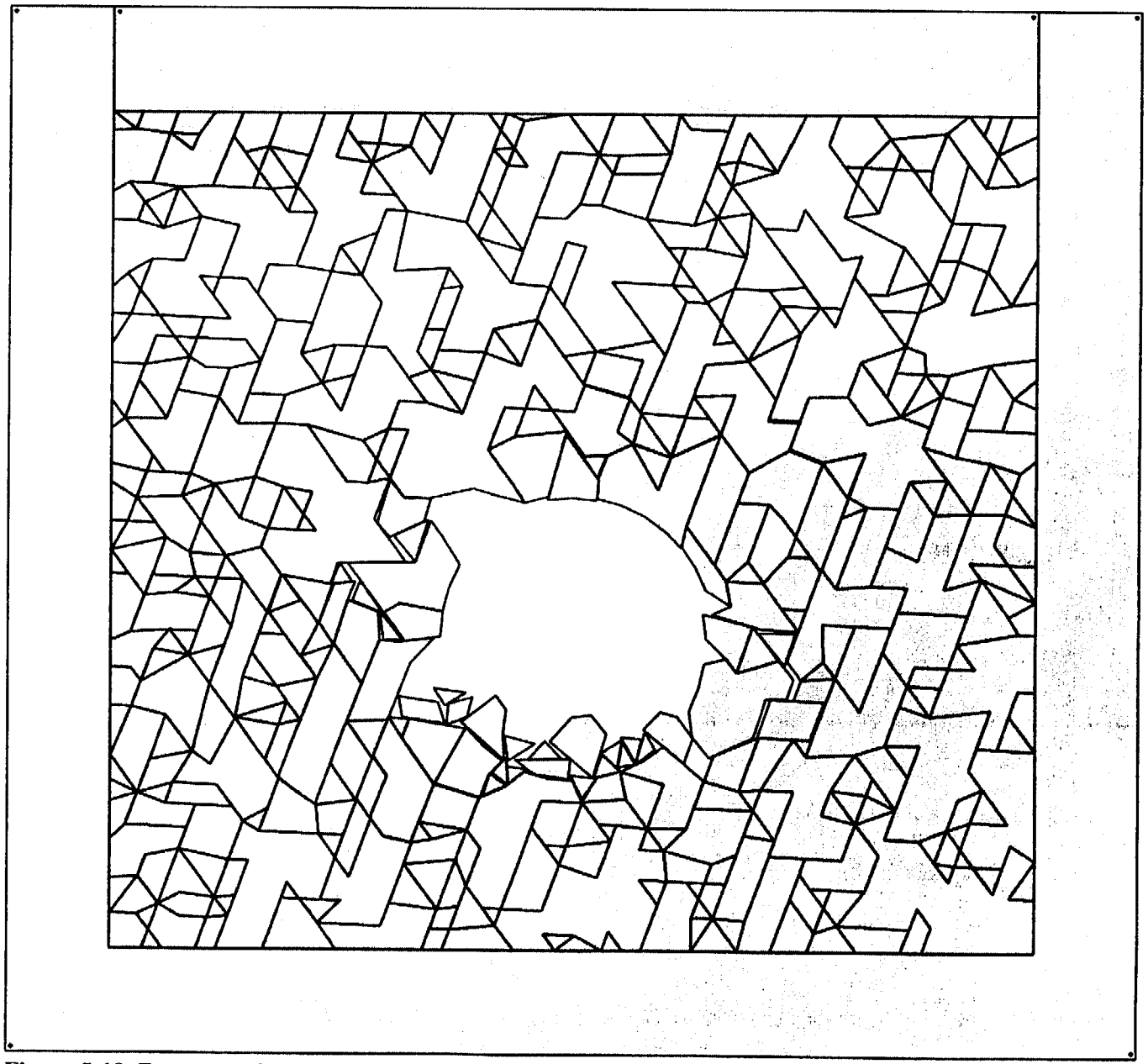

Figure 5-19. Response of rock-mass model in figure 5-9 to the seismic signal shown in figure 3-8

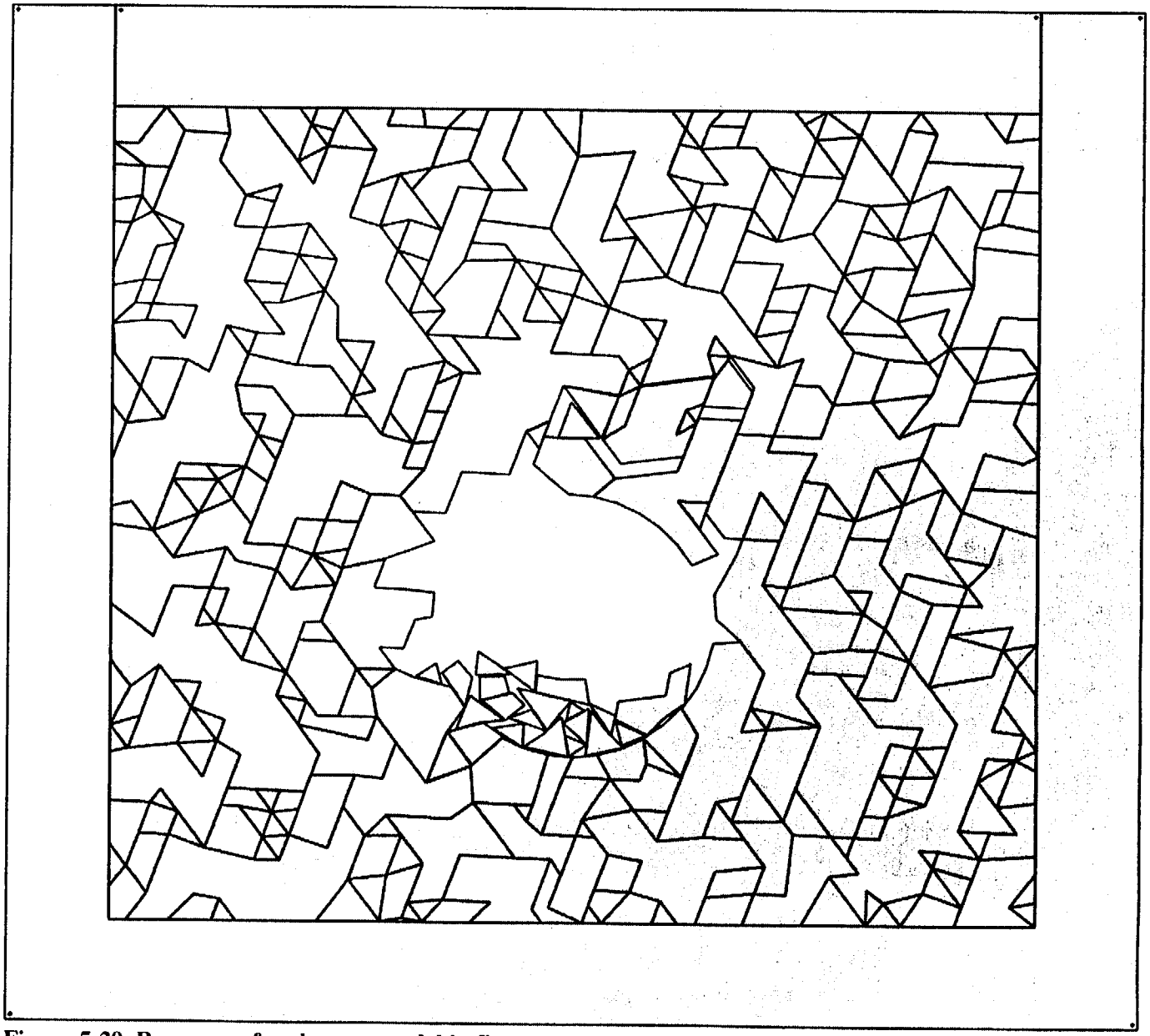

Figure 5-20. Response of rock-mass model in figure 5-10 to the seismic signal shown in figure 3-8

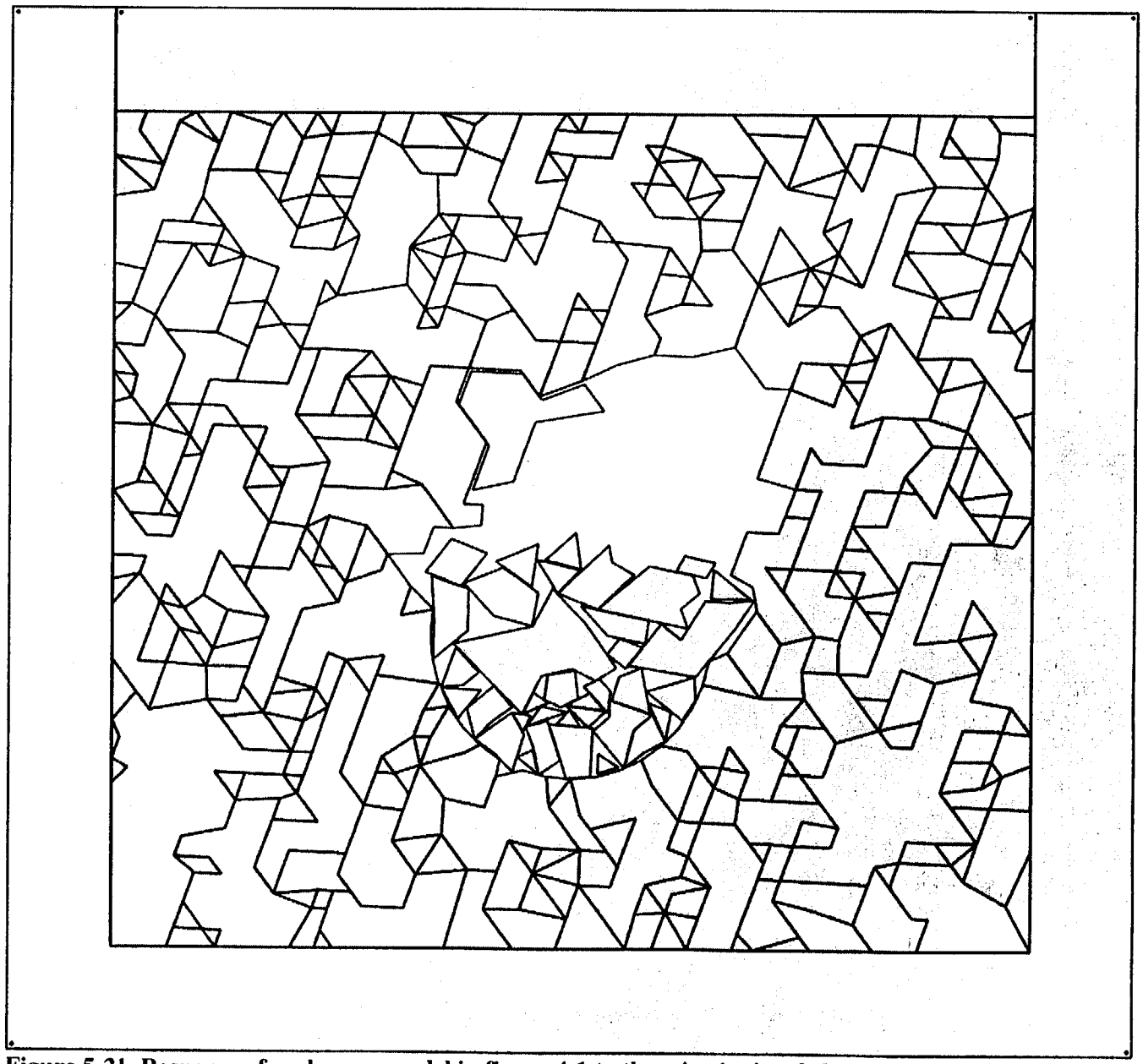

Figure 5-21. Response of rock-mass model in figure 4-1 to the seismic signal shown in figure 3-8

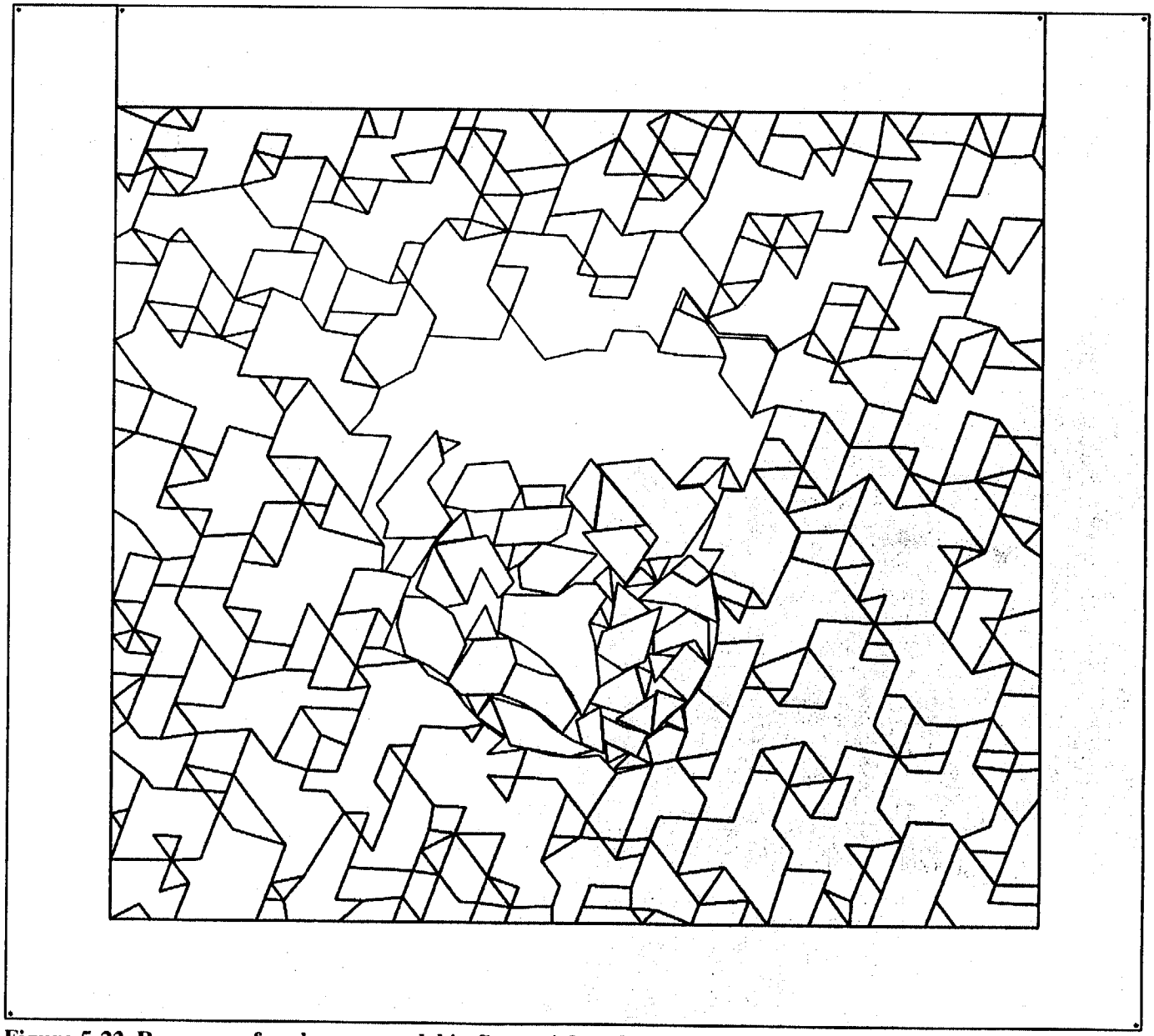

Figure 5-22. Response of rock-mass model in figure 4-2 to the seismic signal shown in figure 3-8

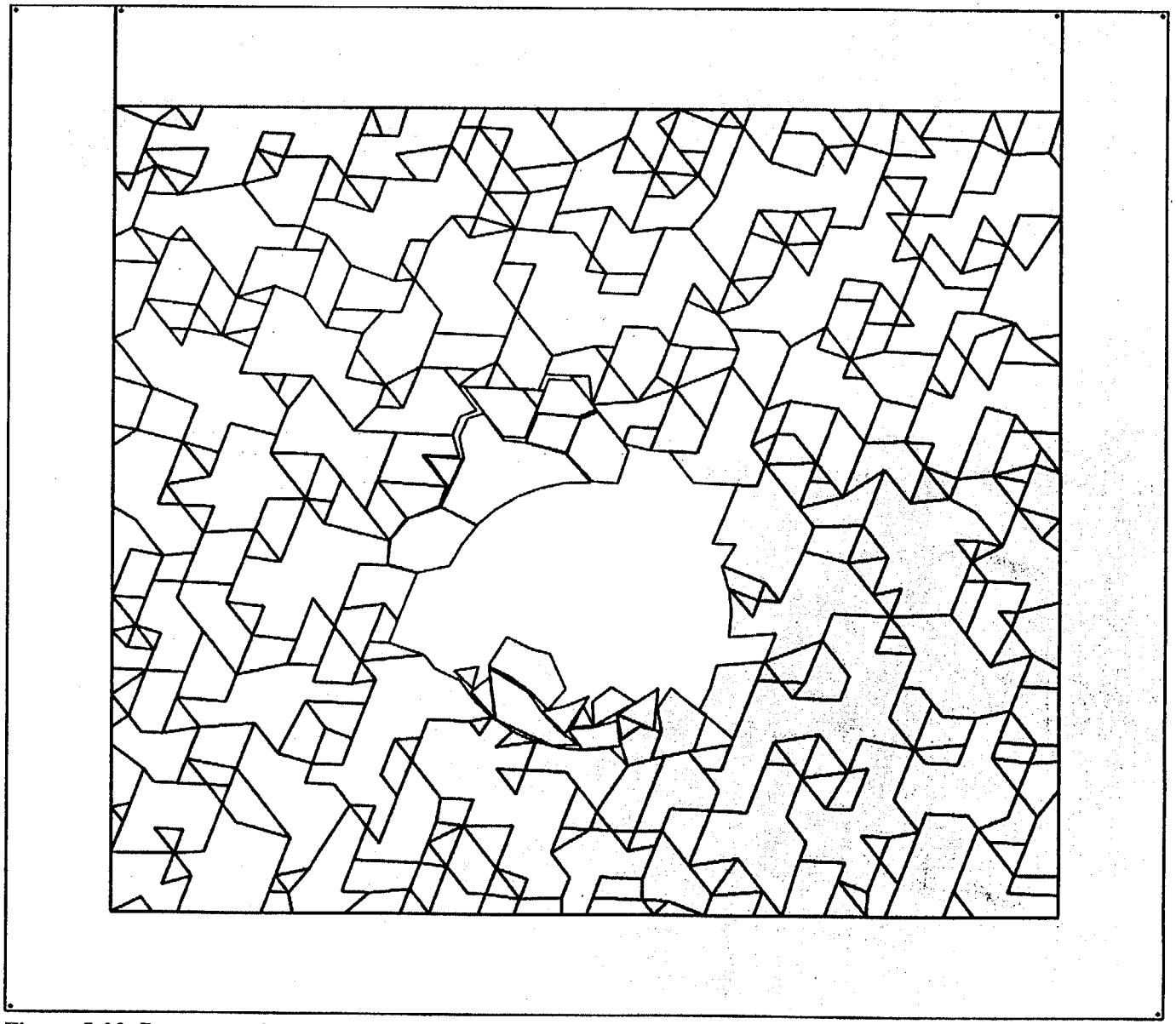

Figure 5-23. Response of rock-mass model in figure 4-2 to the seismic signal shown in figure 3-8 with a 1/5 scaling to the acceleration amplitudes

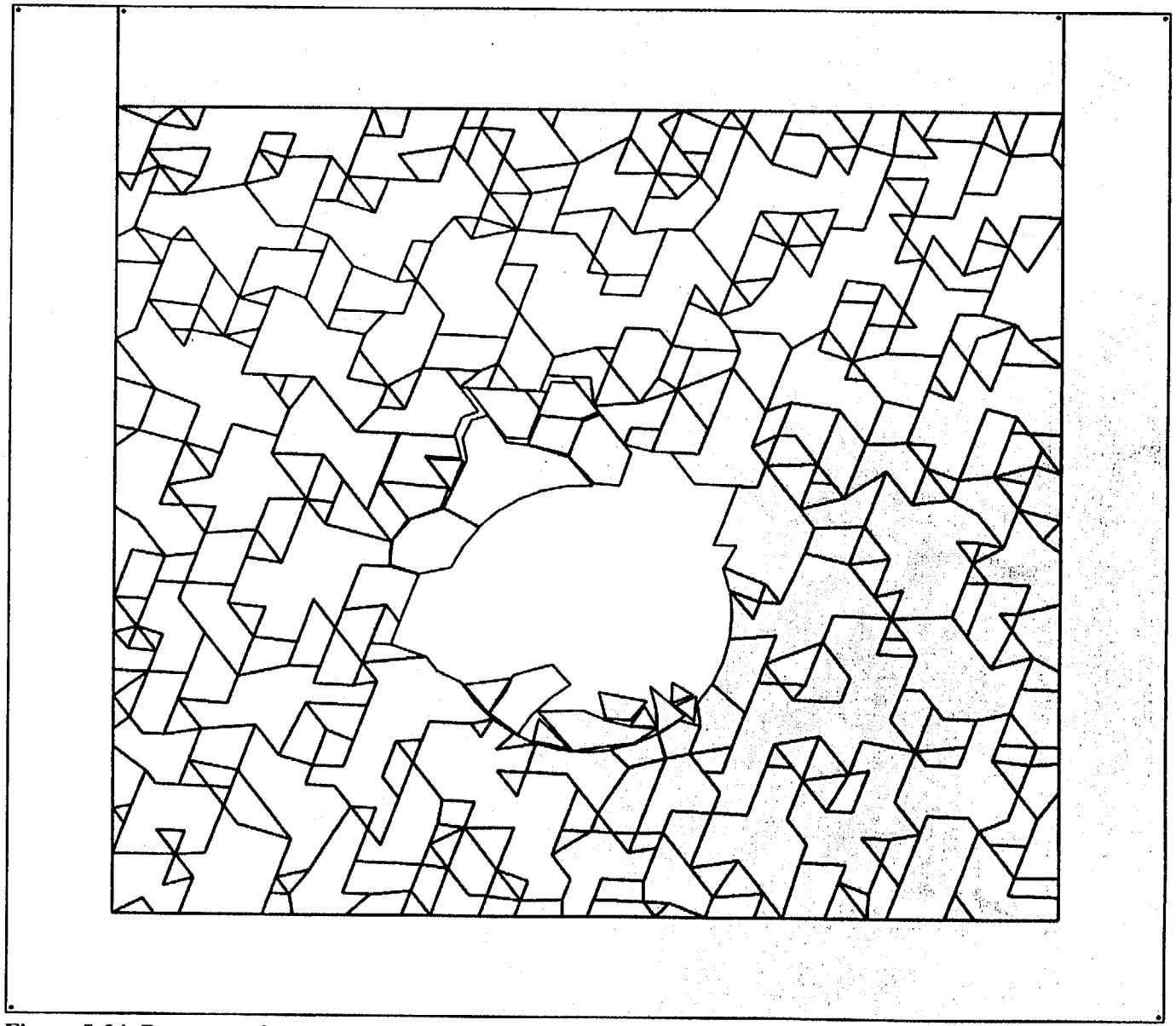

Figure 5-24. Response of rock-mass model in figure 4-2 to the seismic signal shown in figure 3-8 with a 2/5 scaling to the acceleration amplitudes

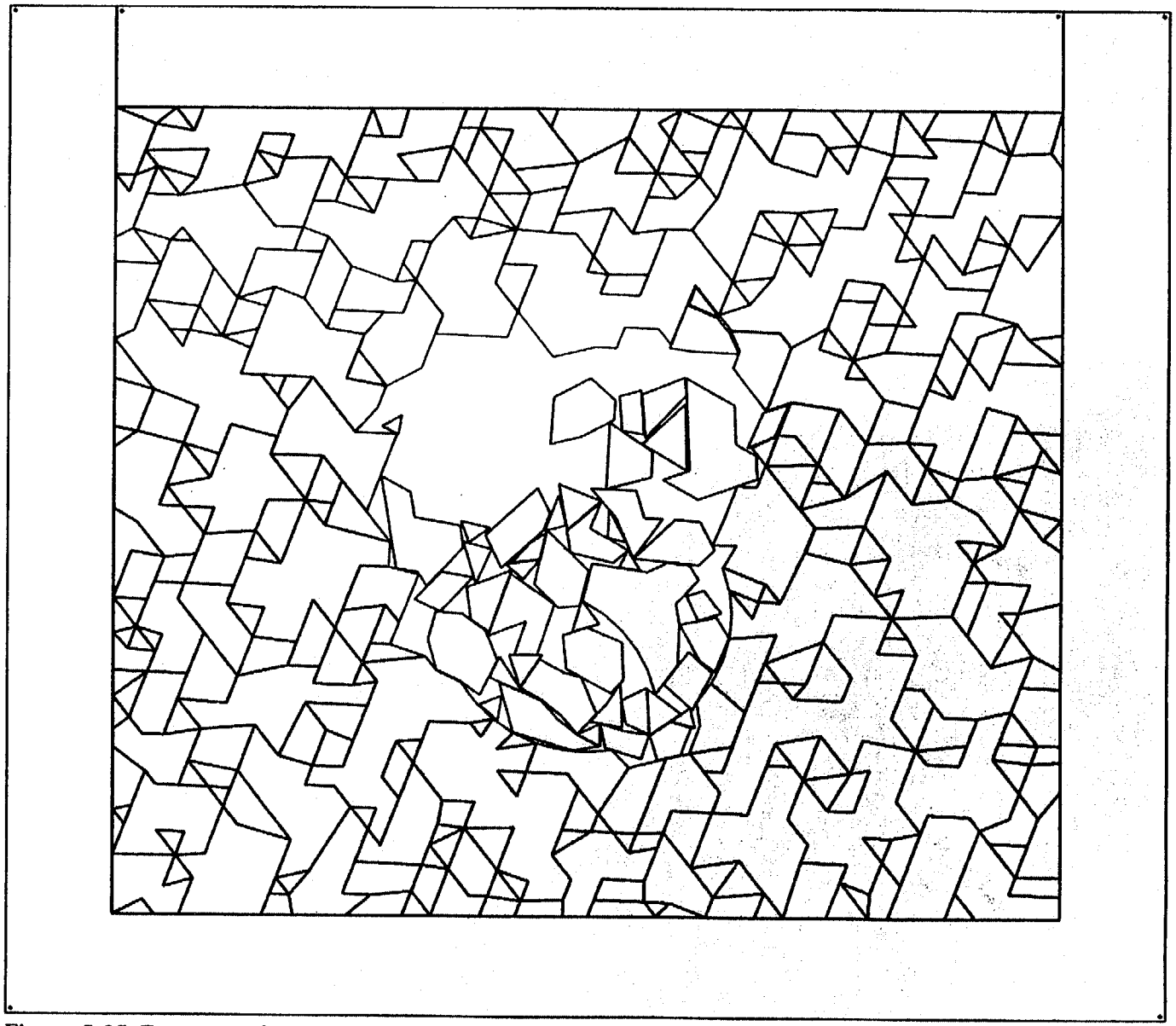

Figure 5-25. Response of rock-mass model in figure 4-2 to the seismic signal shown in figure 3-8 with a 1/2 scaling to the acceleration amplitudes

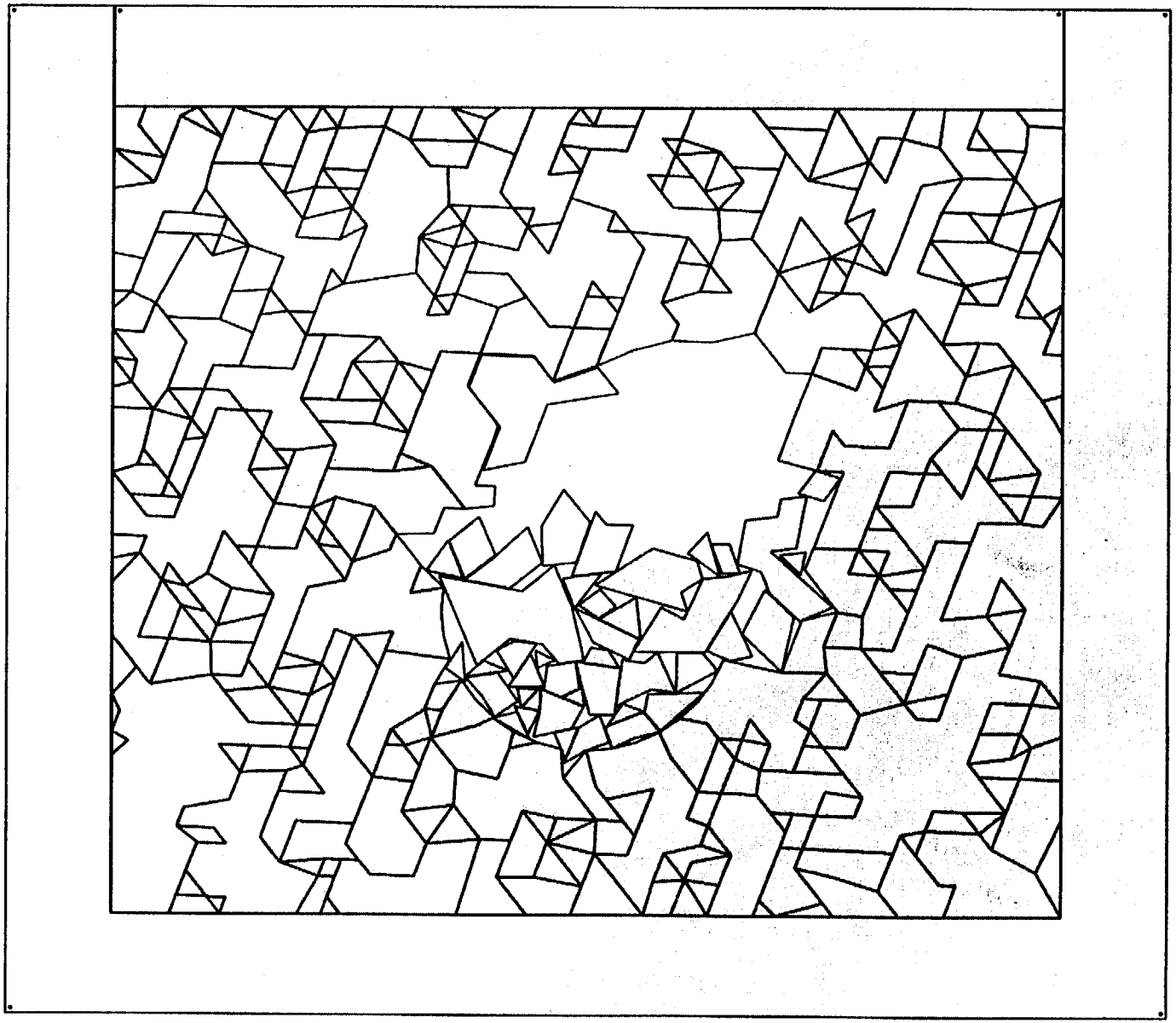

Figure 5-26. Response of rock-mass model in figure 4-1 to the seismic signal shown in figure 3-8 with a 1/5 scaling to the acceleration amplitudes

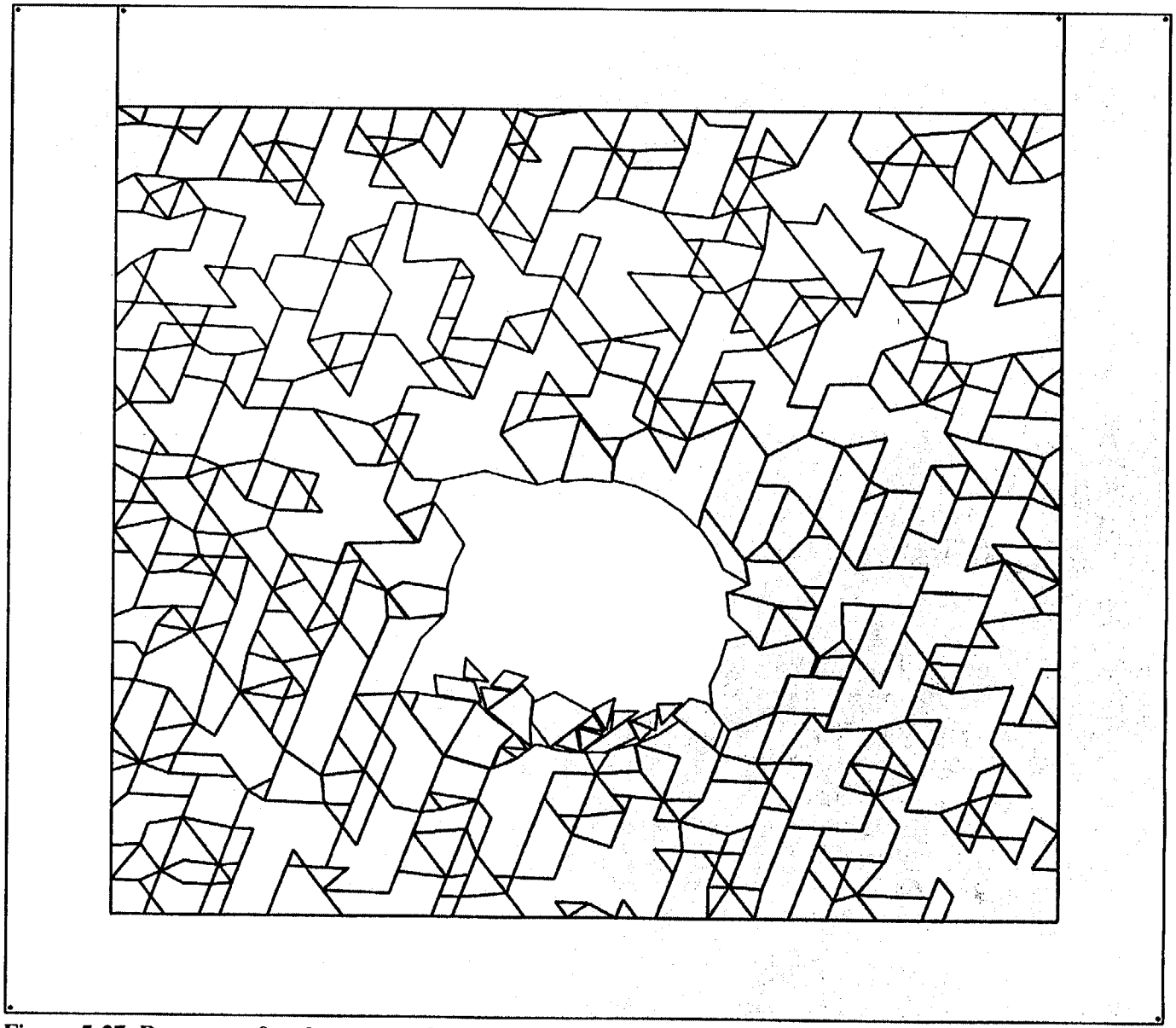

Figure 5-27. Response of rock-mass model in figure 5-9 to the seismic signal shown in figure 3-8 with a 1/5 scaling to the acceleration amplitudes

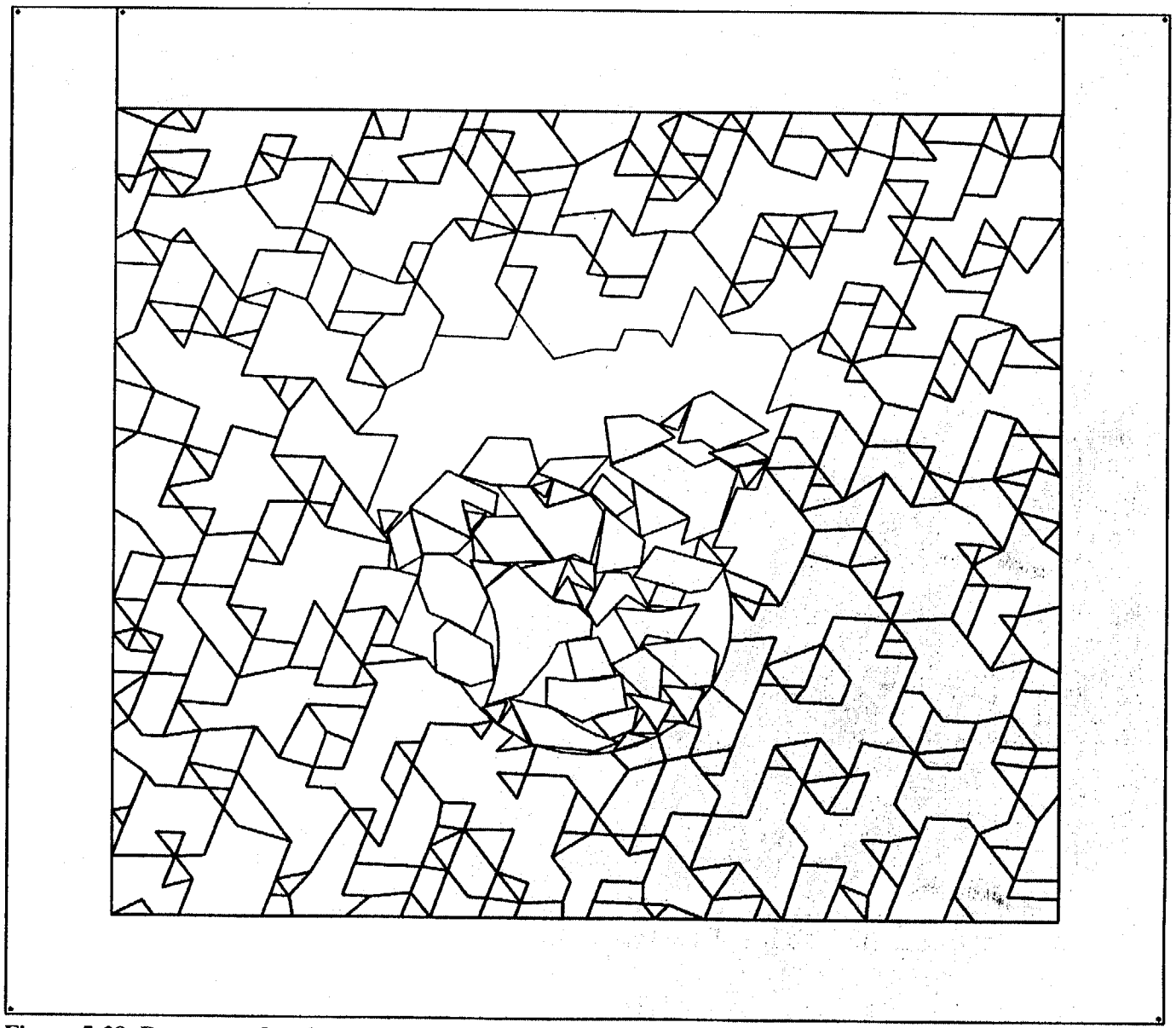

Figure 5-28. Response of rock-mass model in figure 4-2 to two episodes of earthquakes with identical seismic signals shown in figure 3-8 with a 1/5 scaling to the acceleration amplitudes

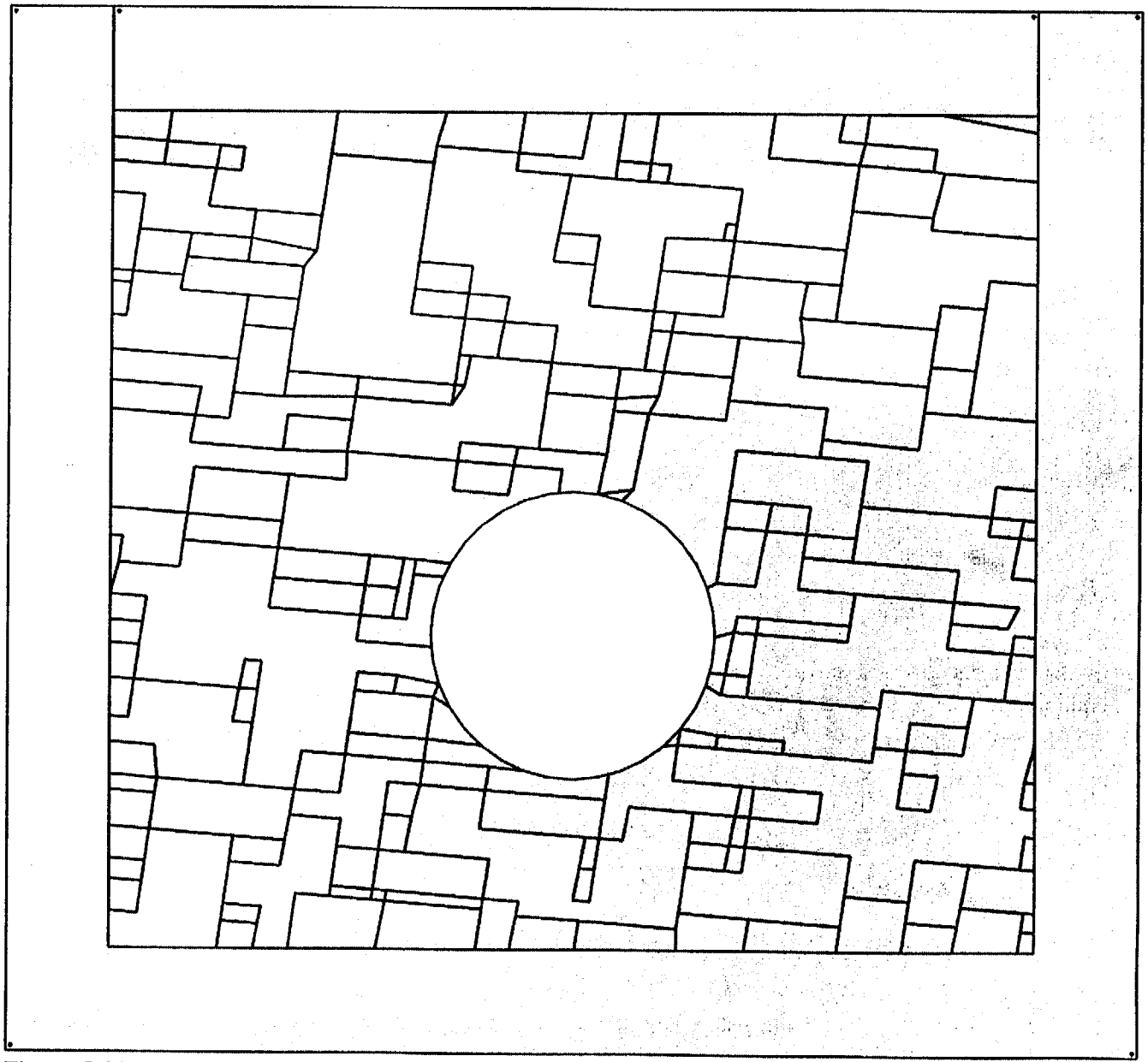

Figure 5-29. Discontinuous Deformation Analysis model realization 1 for large joint spacings

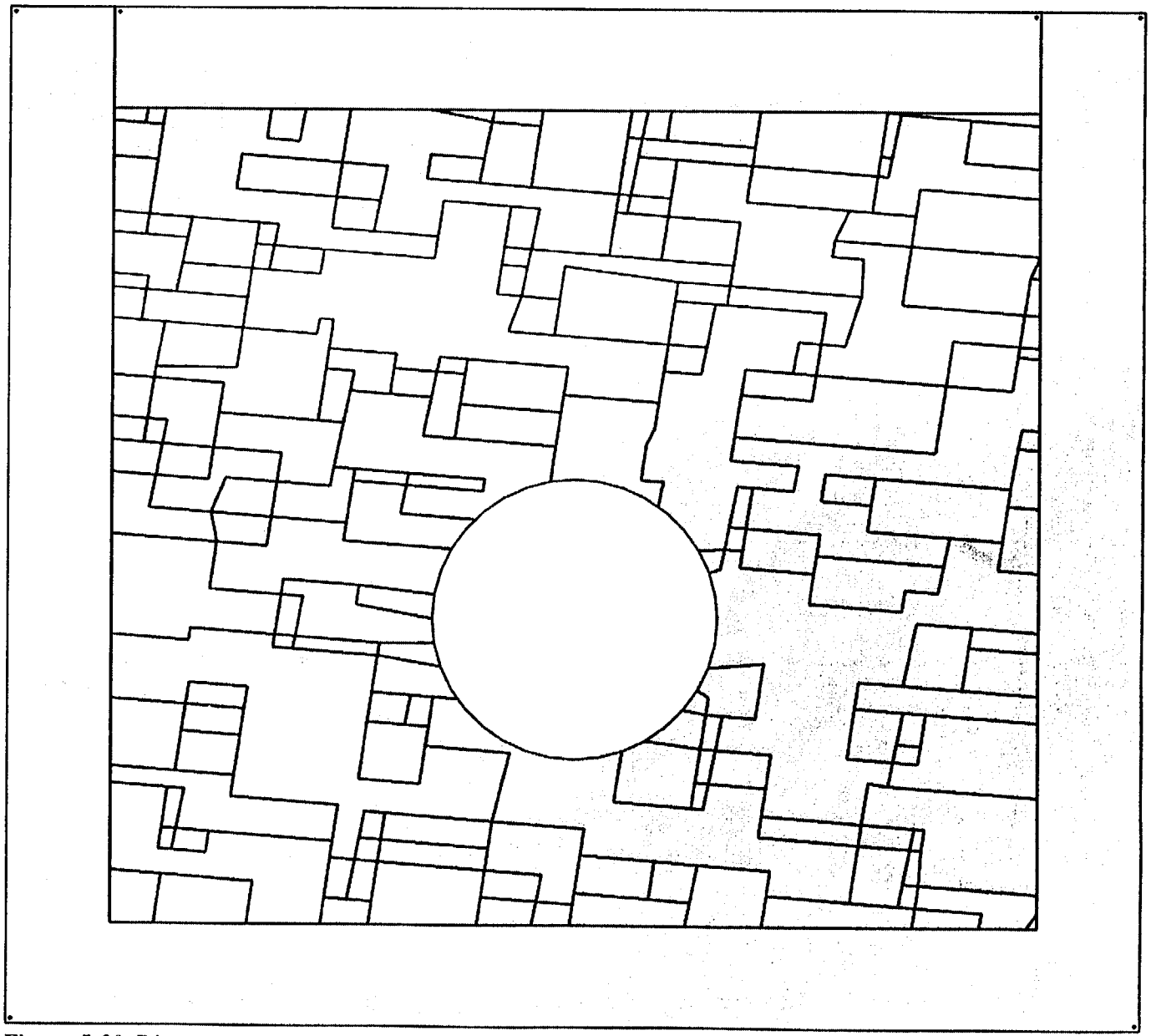

Figure 5-30. Discontinuous Deformation Analysis model realization 2 for large joint spacings

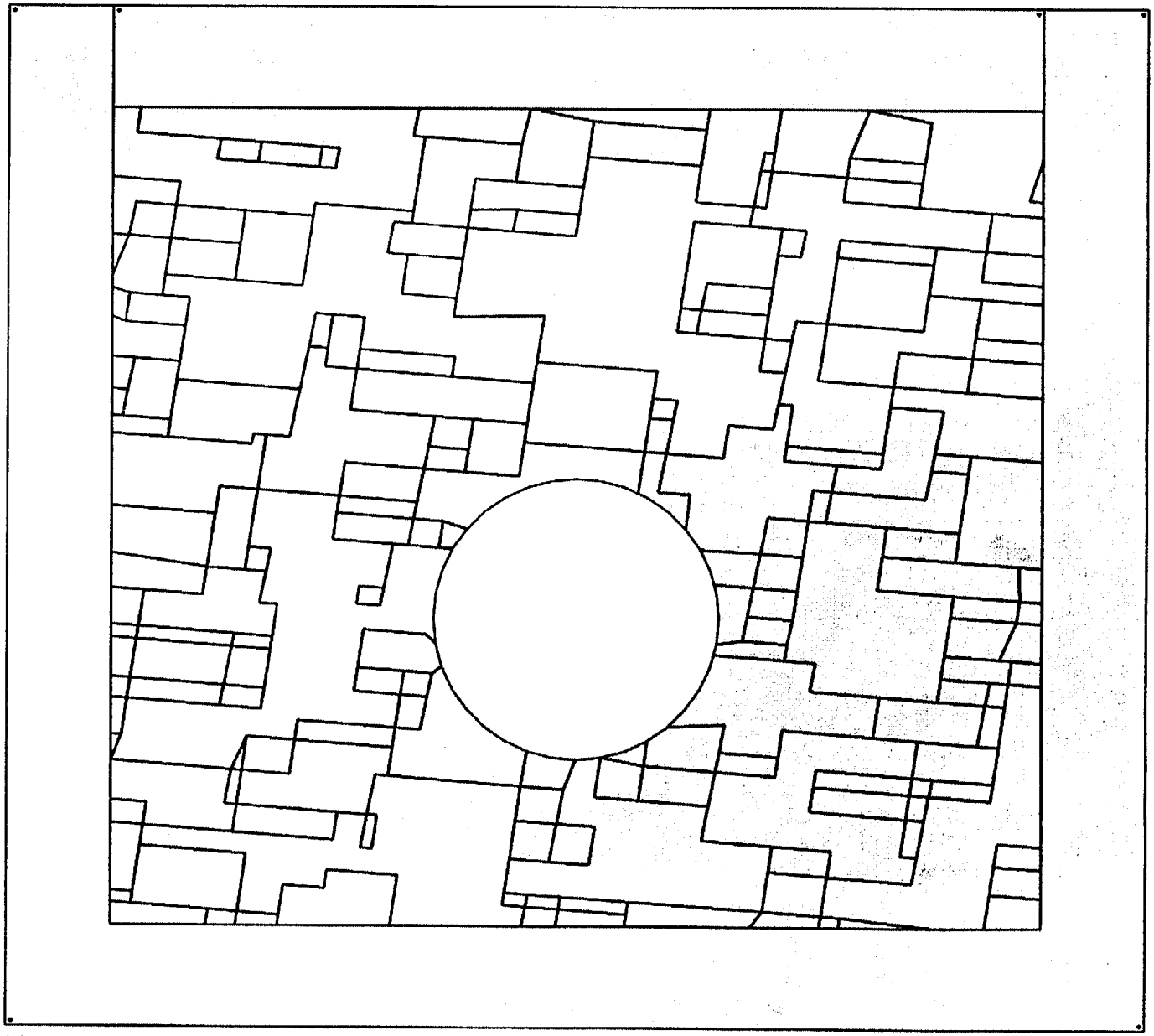

Figure 5-31. Discontinuous Deformation Analysis model realization 3 for large joint spacings

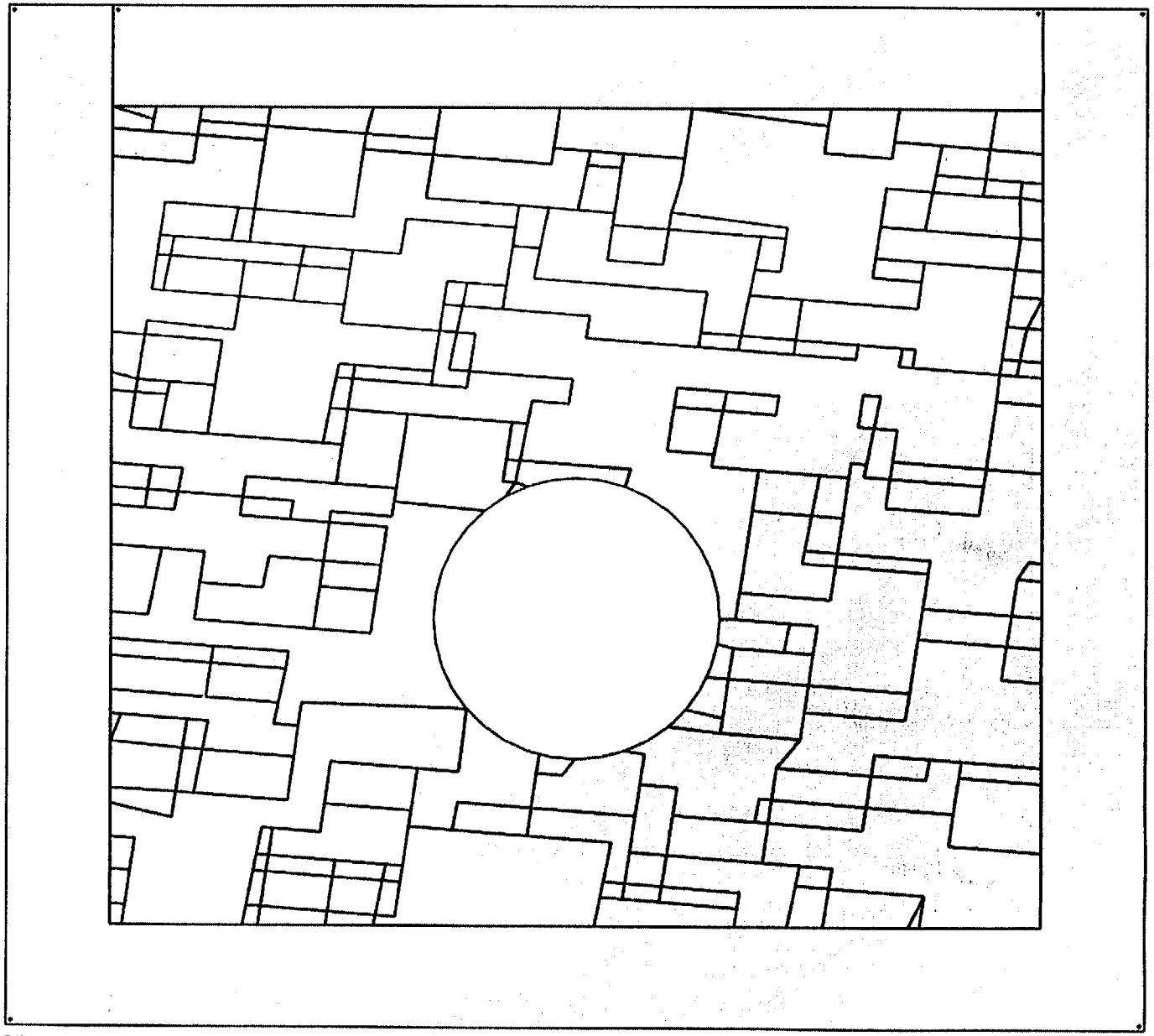

Figure 5-32. Discontinuous Deformation Analysis model realization 4 for large joint spacings

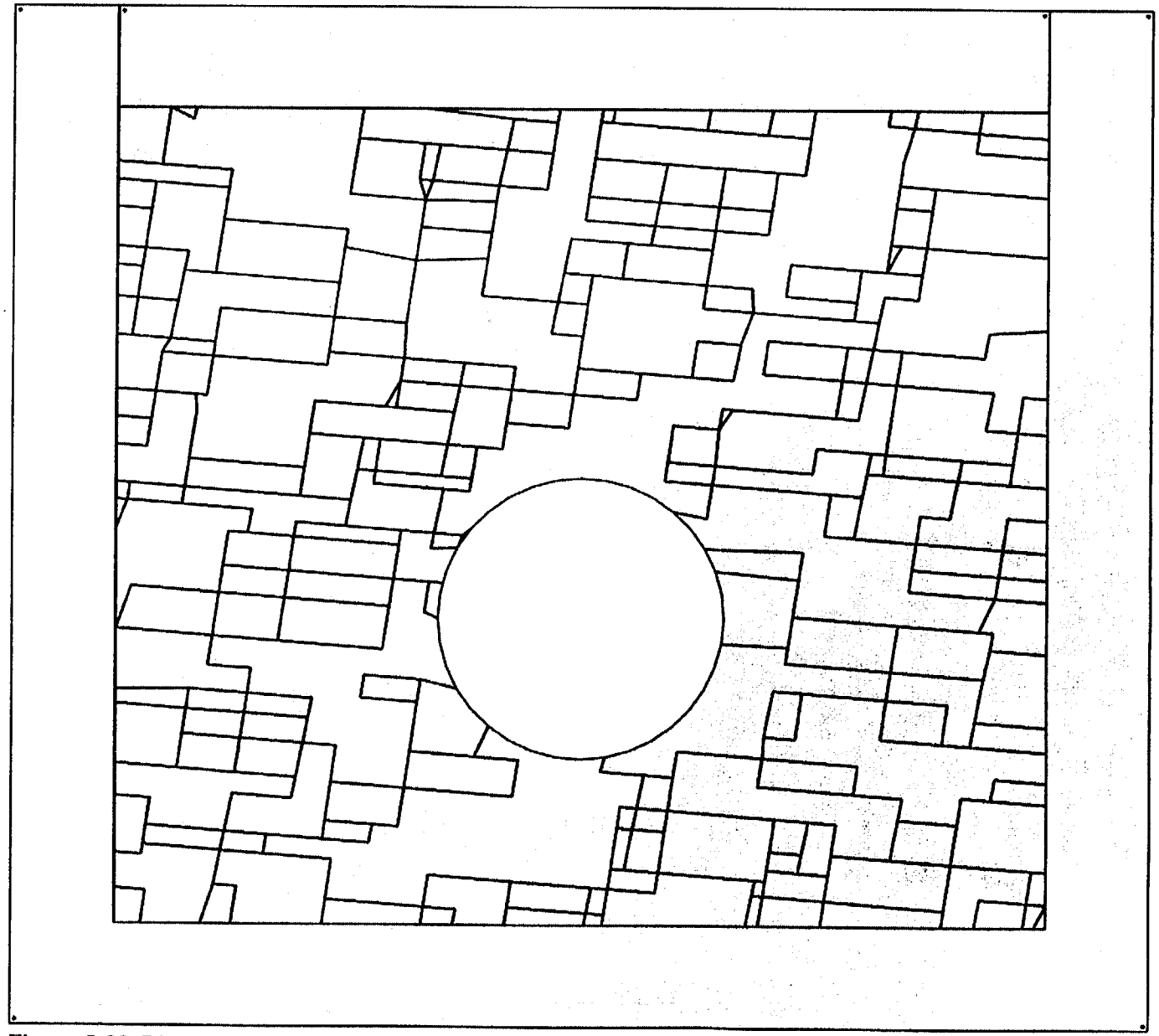

Figure 5-33. Discontinuous Deformation Analysis model realization 5 for large joint spacings

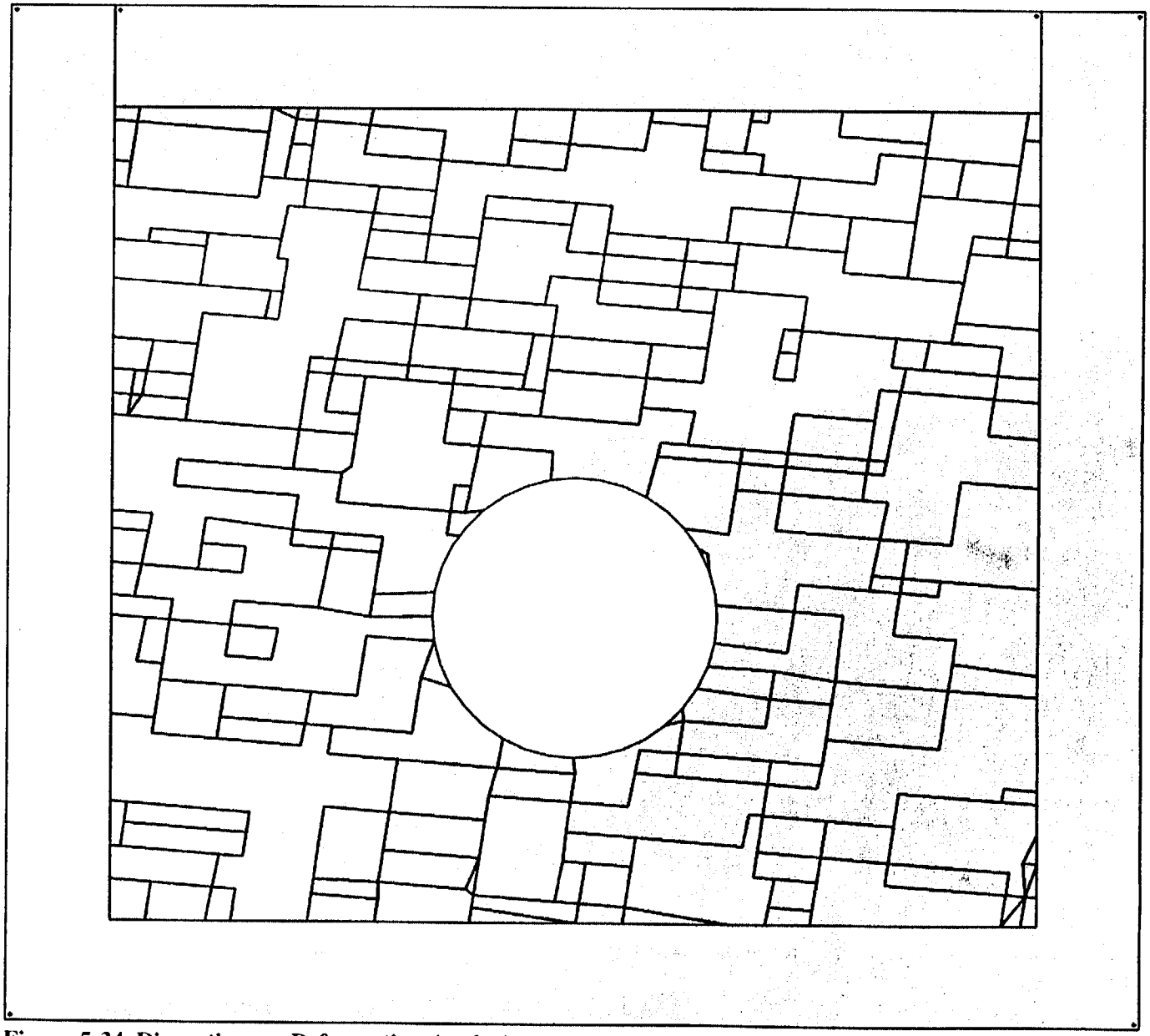

Figure 5-34. Discontinuous Deformation Analysis model realization 6 for large joint spacings

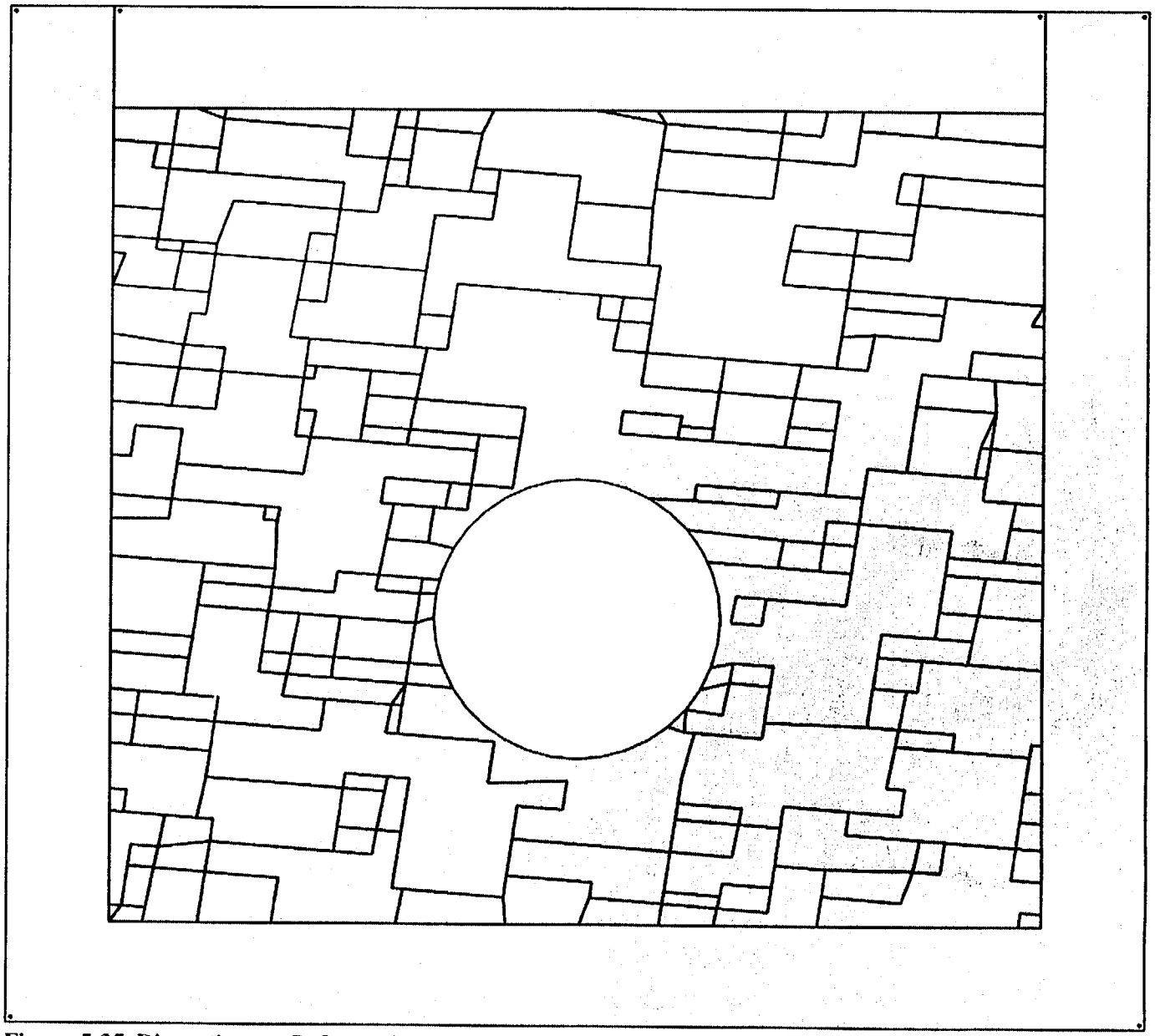

Figure 5-35. Discontinuous Deformation Analysis model realization 7 for large joint spacings

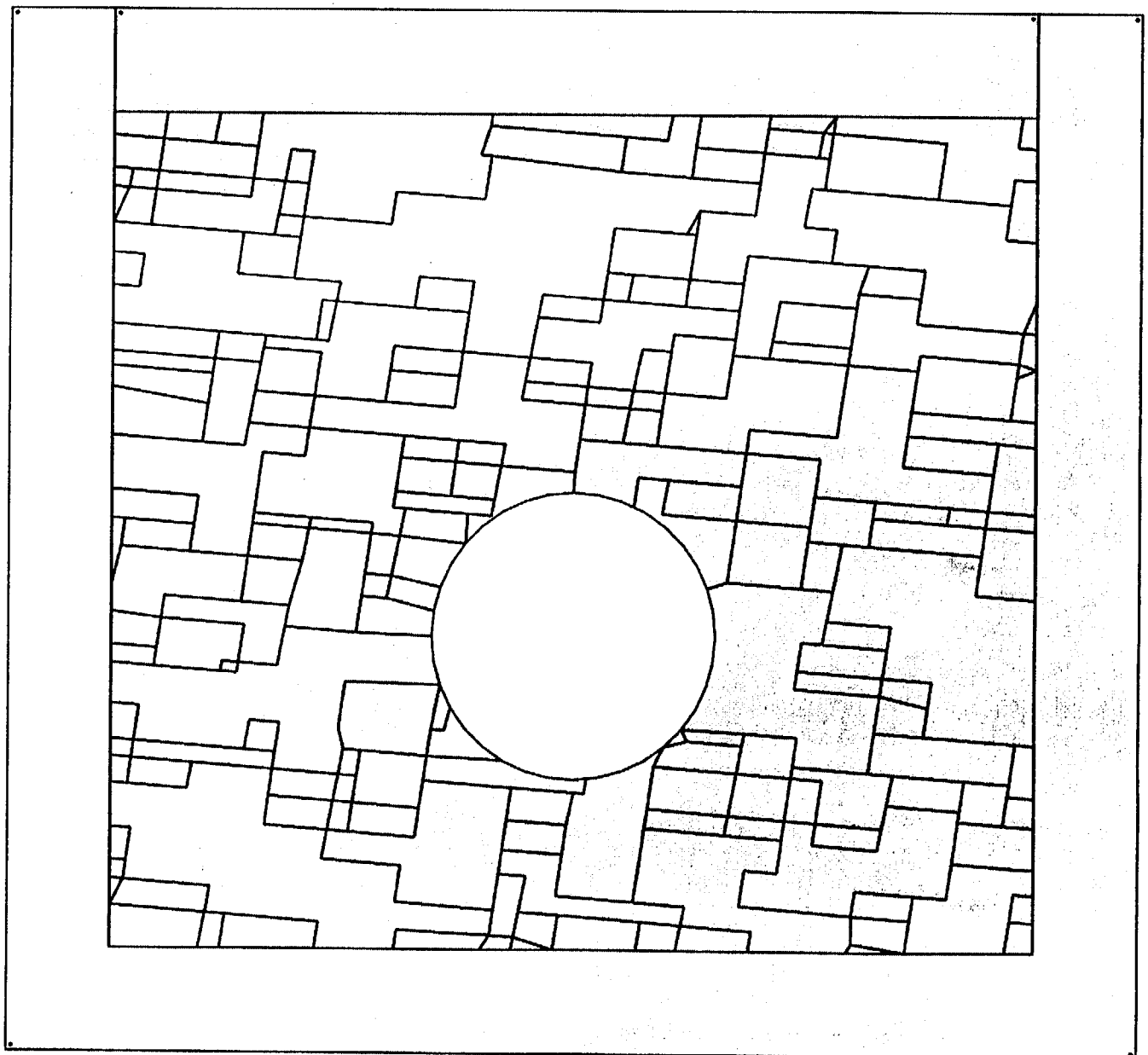

Figure 5-36. Discontinuous Deformation Analysis model realization 8 for large joint spacings

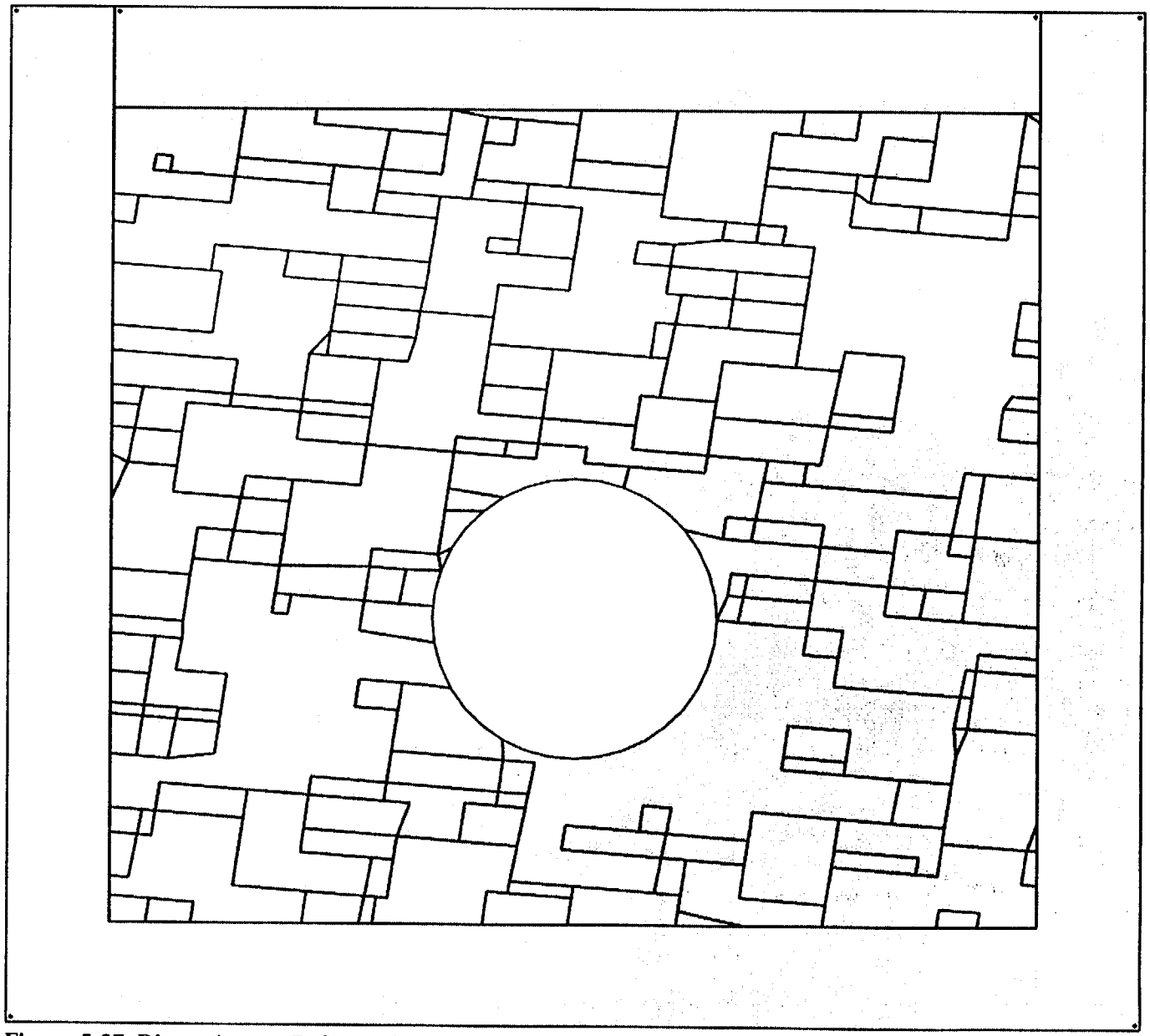

Figure 5-37. Discontinuous Deformation Analysis model realization 9 for large joint spacings

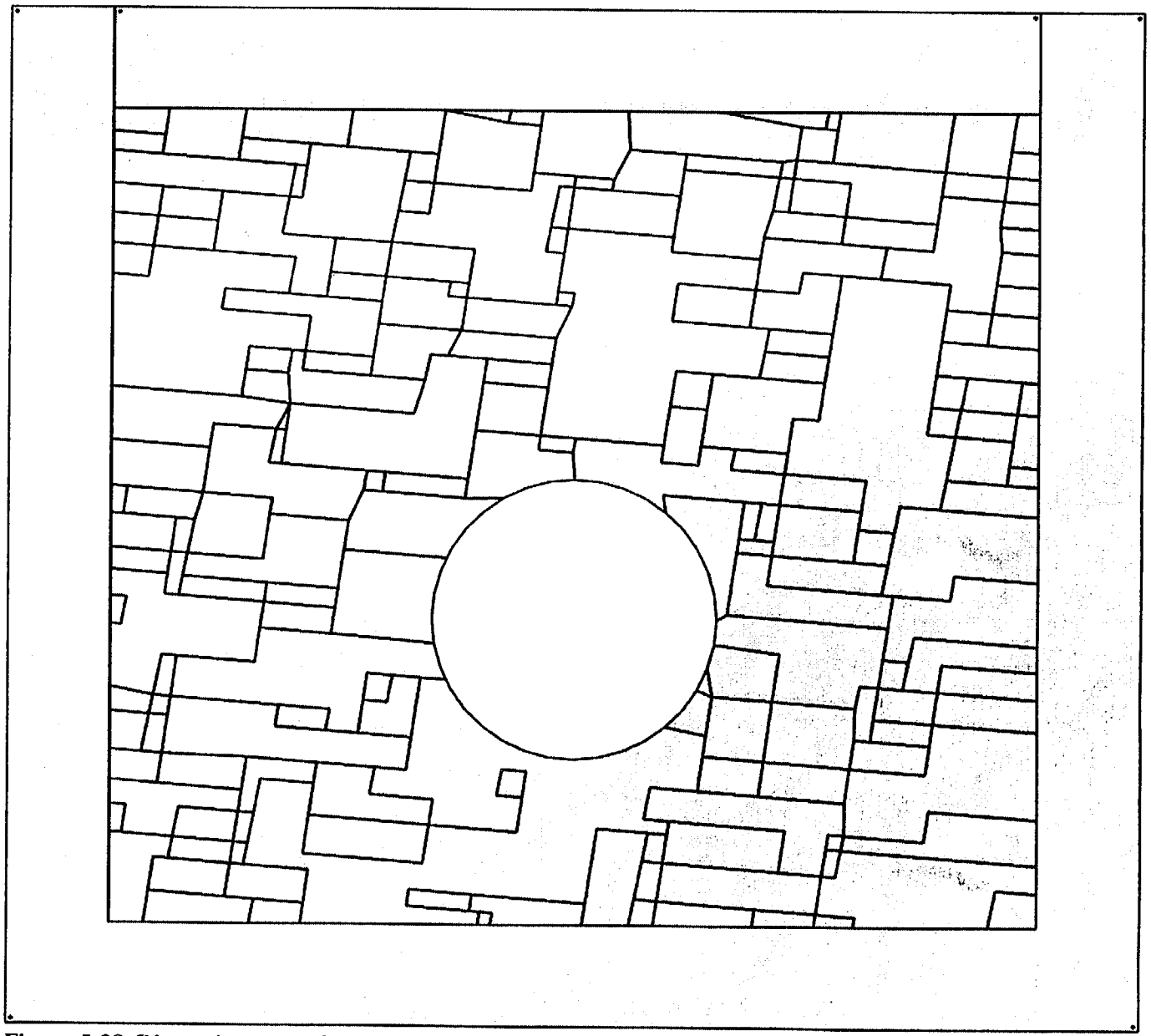

Figure 5-38. Discontinuous Deformation Analysis model realization 10 for large joint spacings

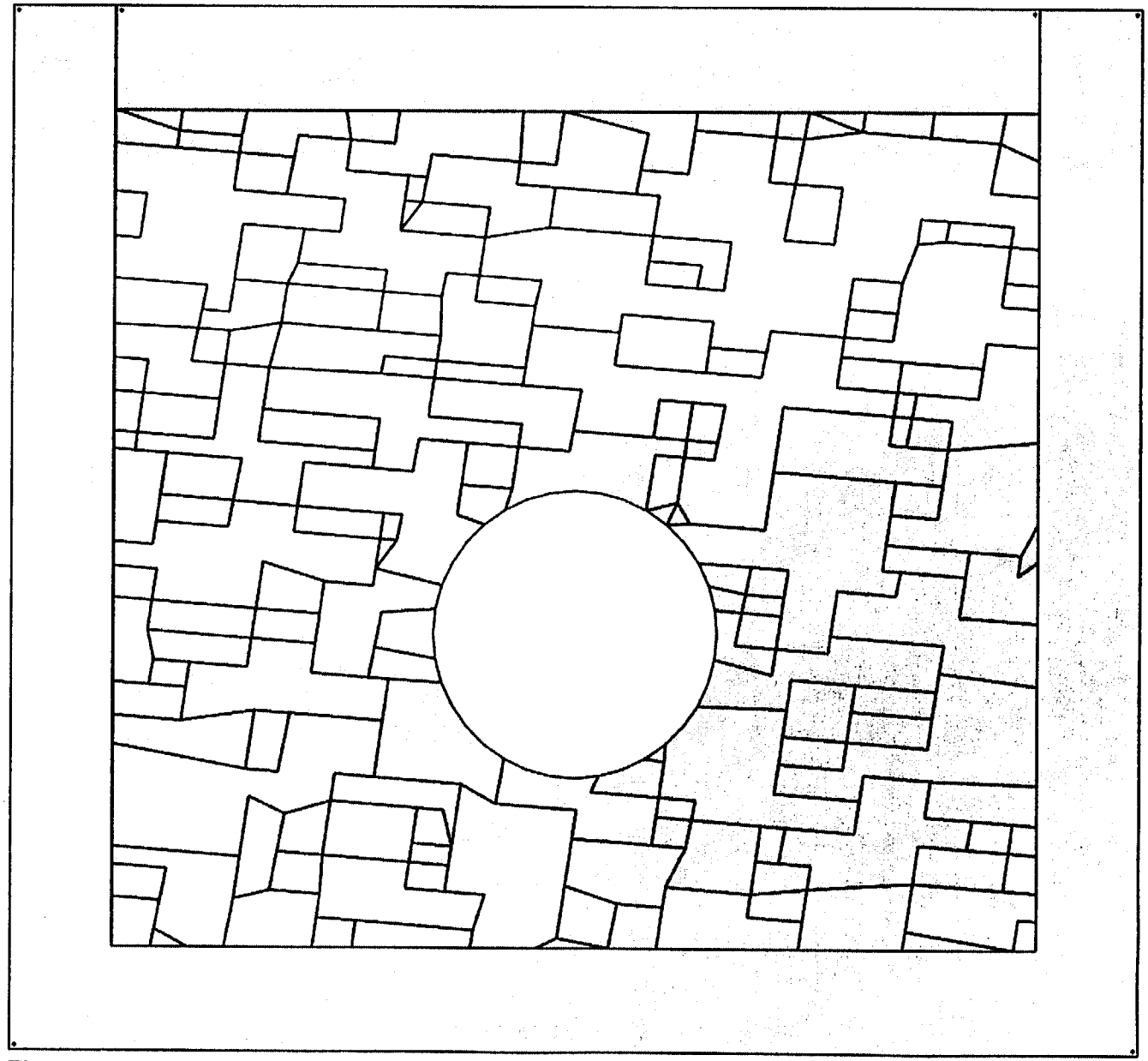

Figure 5-39. Discontinuous Deformation Analysis model realization 11 for large joint spacings

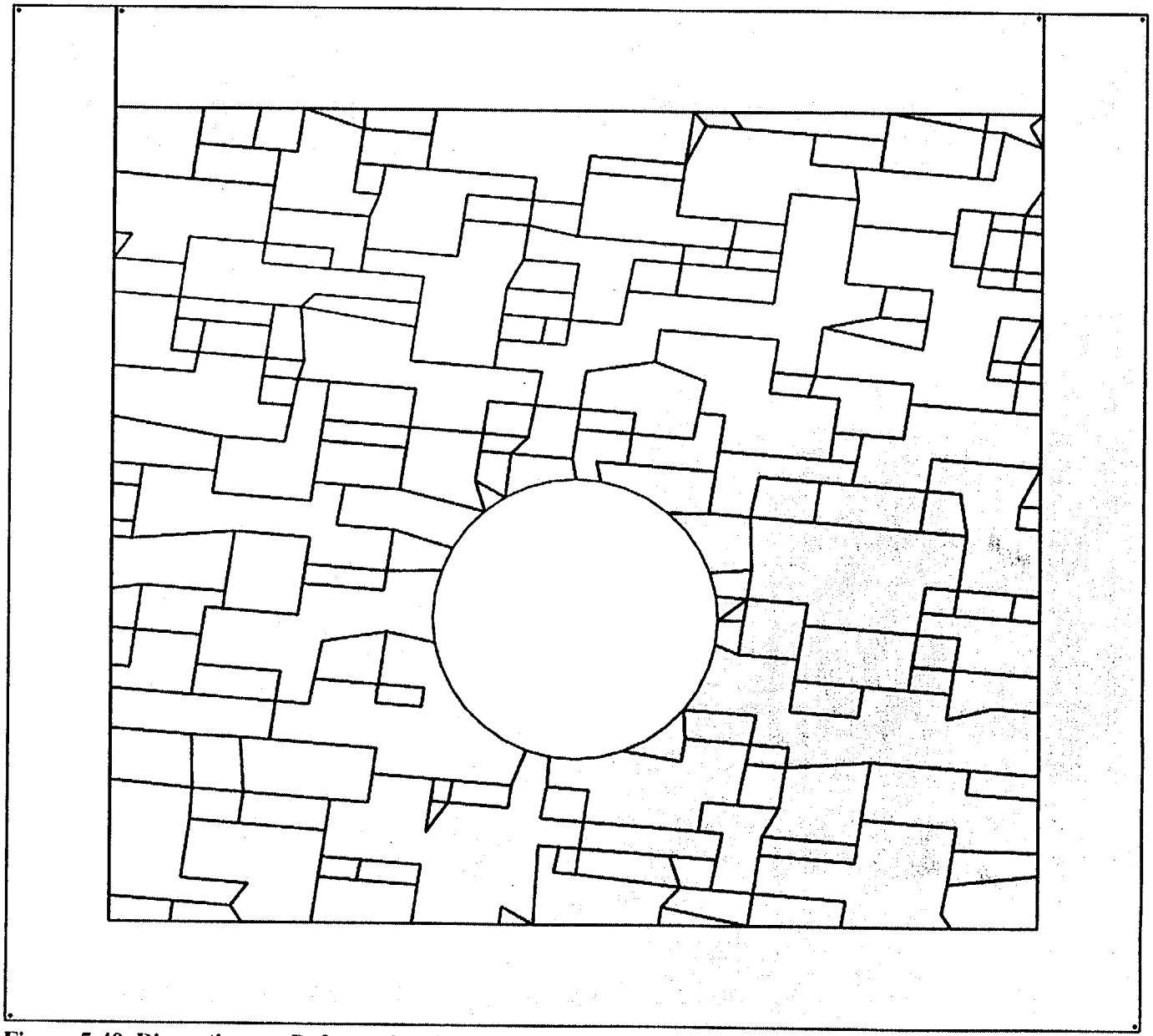

Figure 5-40. Discontinuous Deformation Analysis model realization 12 for large joint spacings

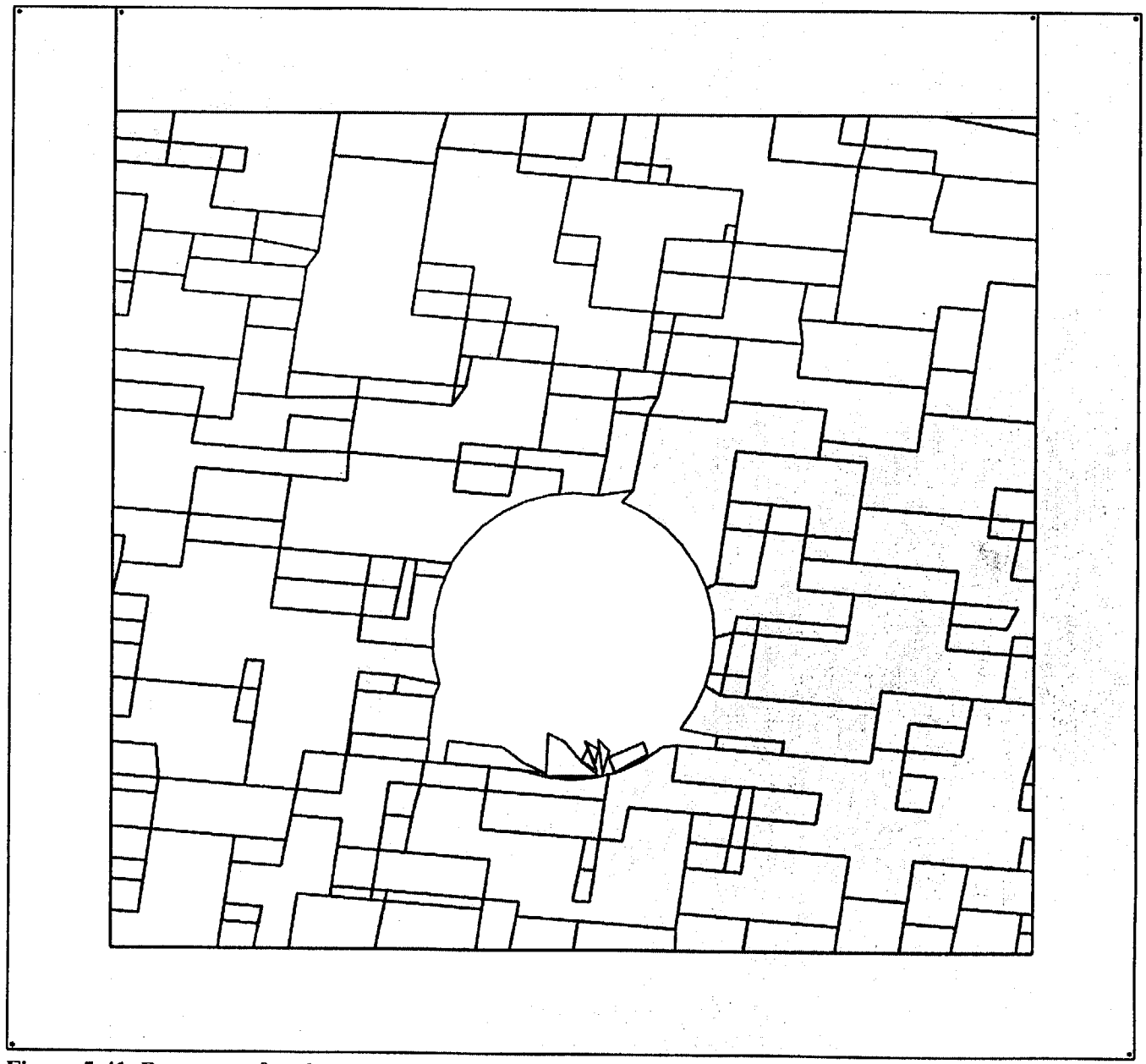

Figure 5-41. Response of rock-mass model in figure 5-29 to the seismic signal shown in figure 3-8

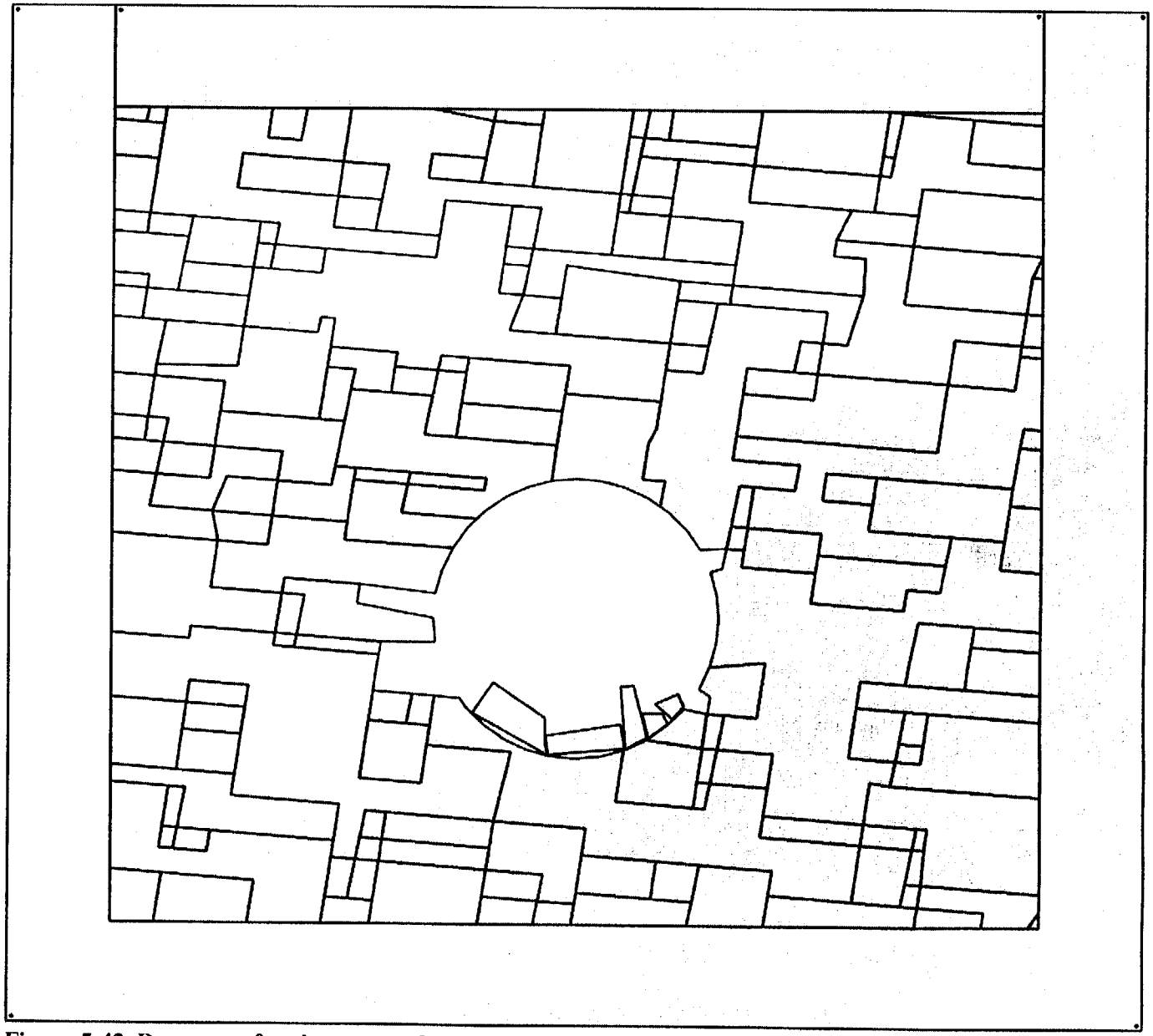

Figure 5-42. Response of rock-mass model in figure 5-30 to the seismic signal shown in figure 3-8

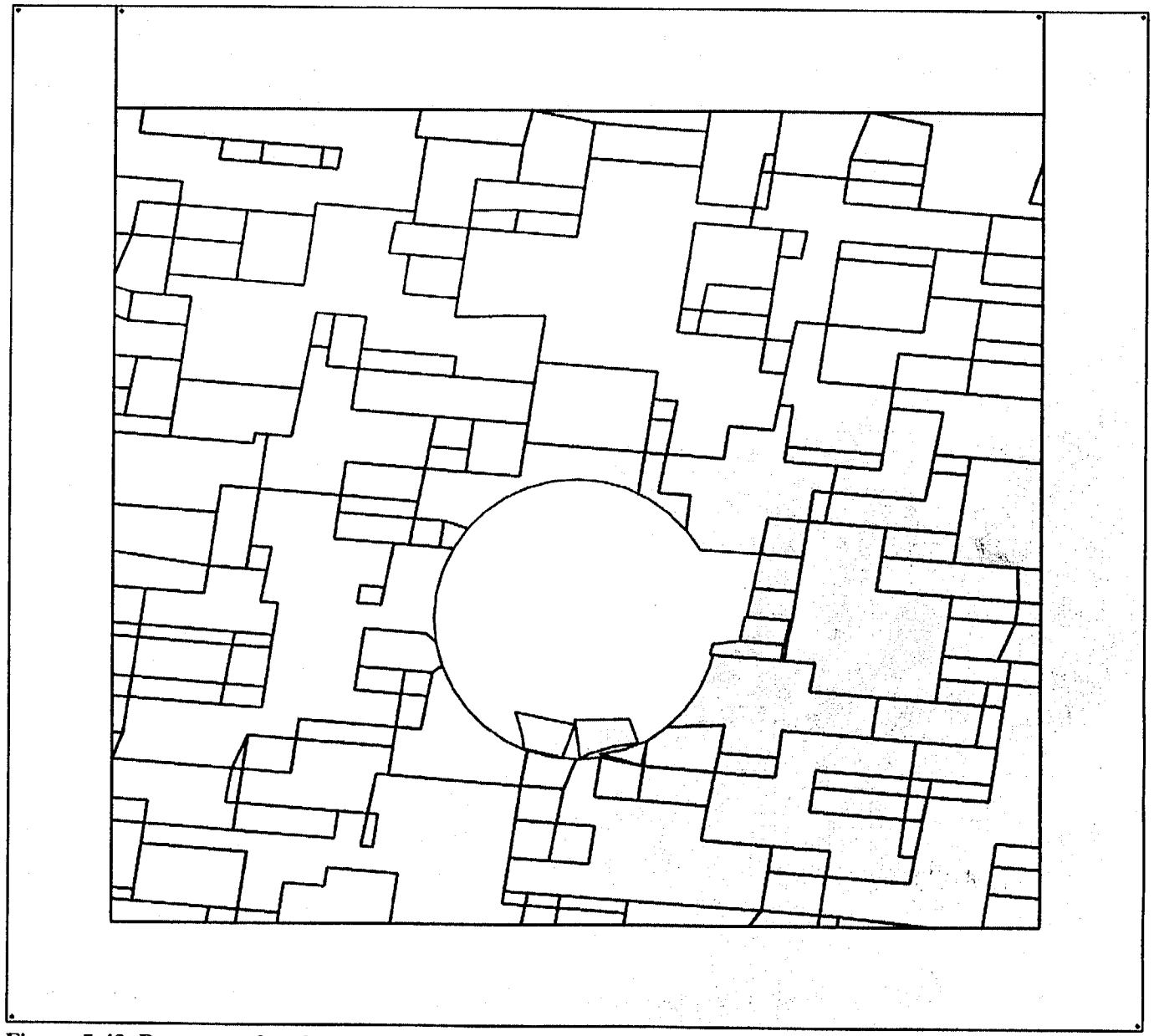

Figure 5-43. Response of rock-mass model in figure 5-31 to the seismic signal shown in figure 3-8

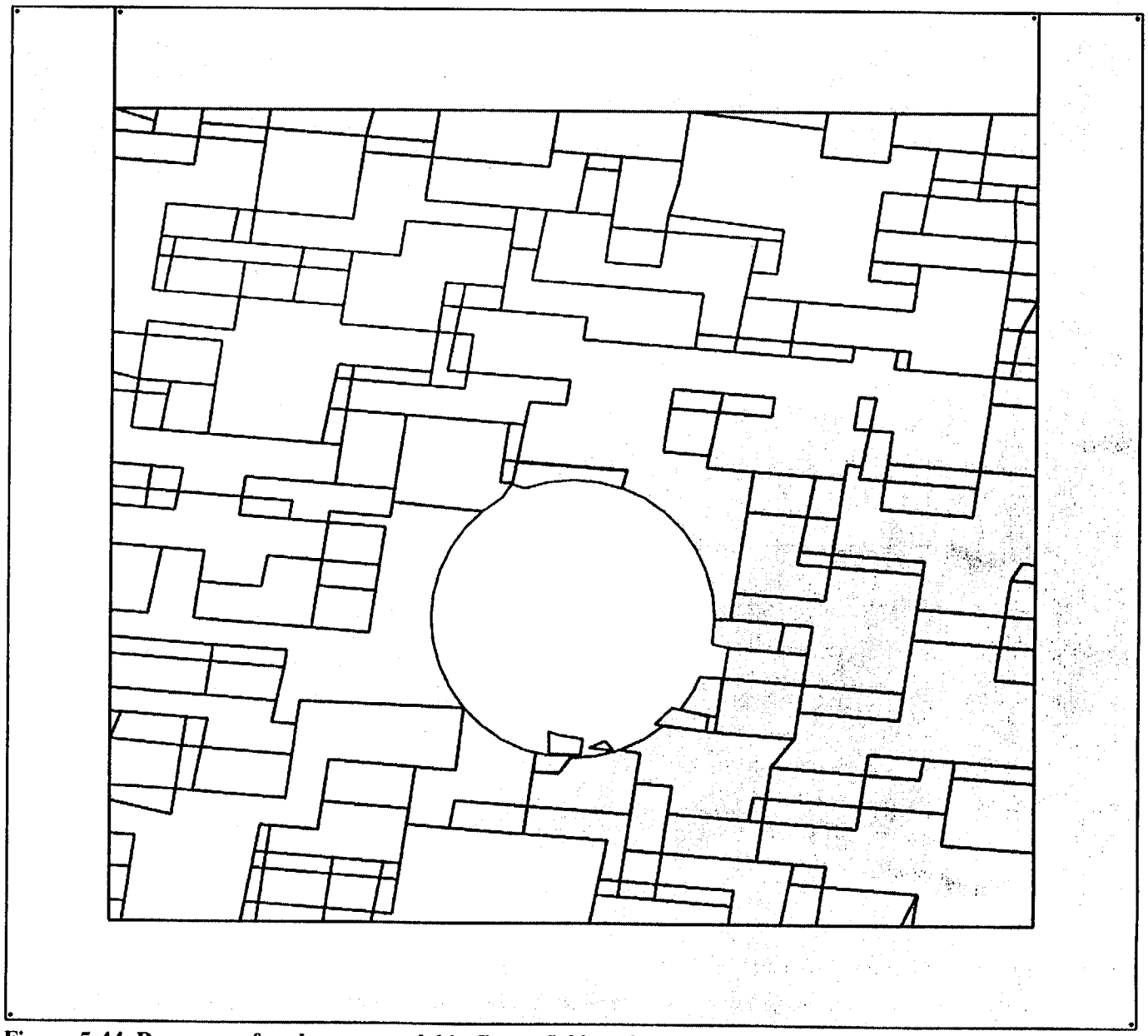

Figure 5-44. Response of rock-mass model in figure 5-32 to the seismic signal shown in figure 3-8

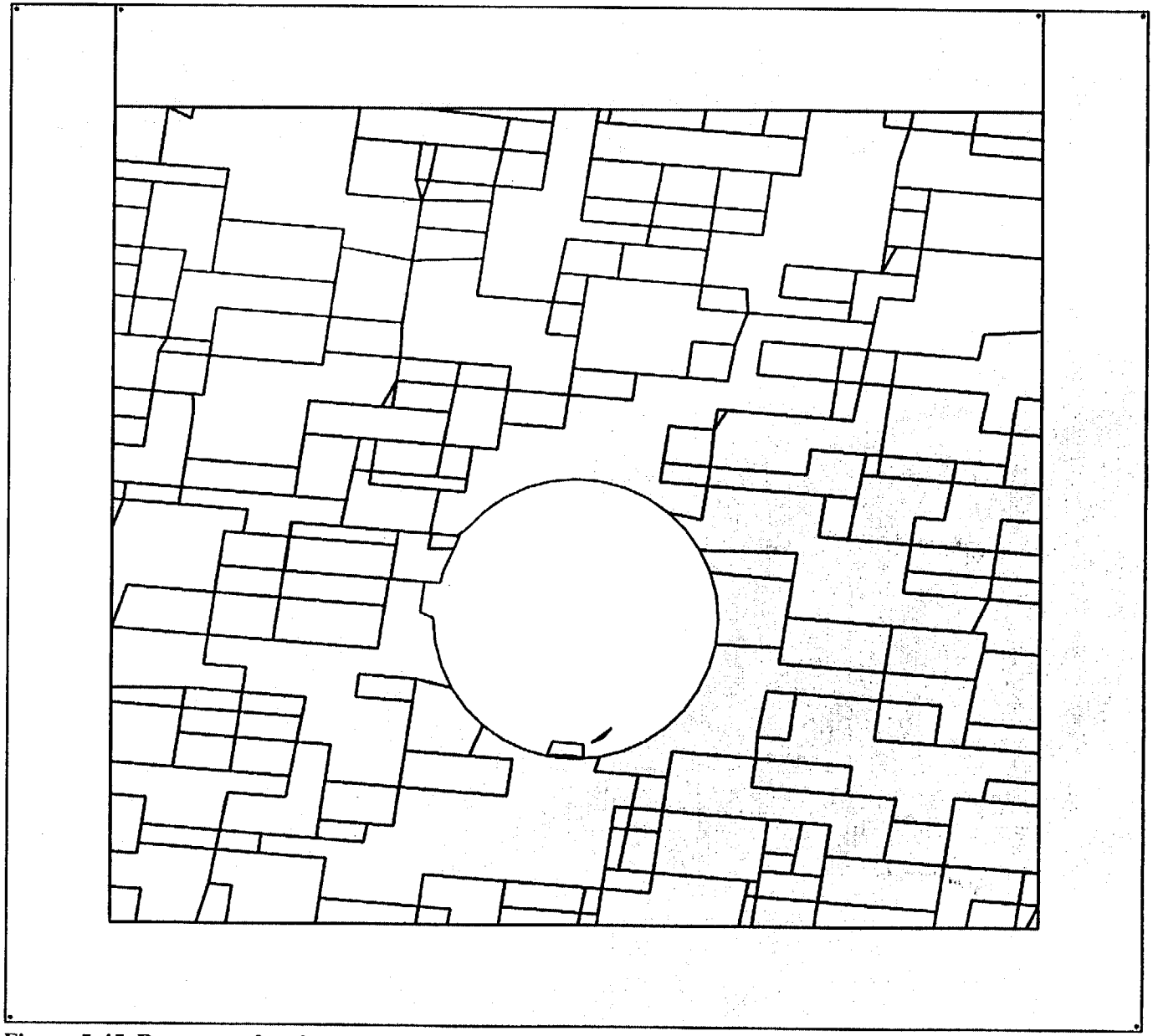

Figure 5-45. Response of rock-mass model in figure 5-33 to the seismic signal shown in figure 3-8

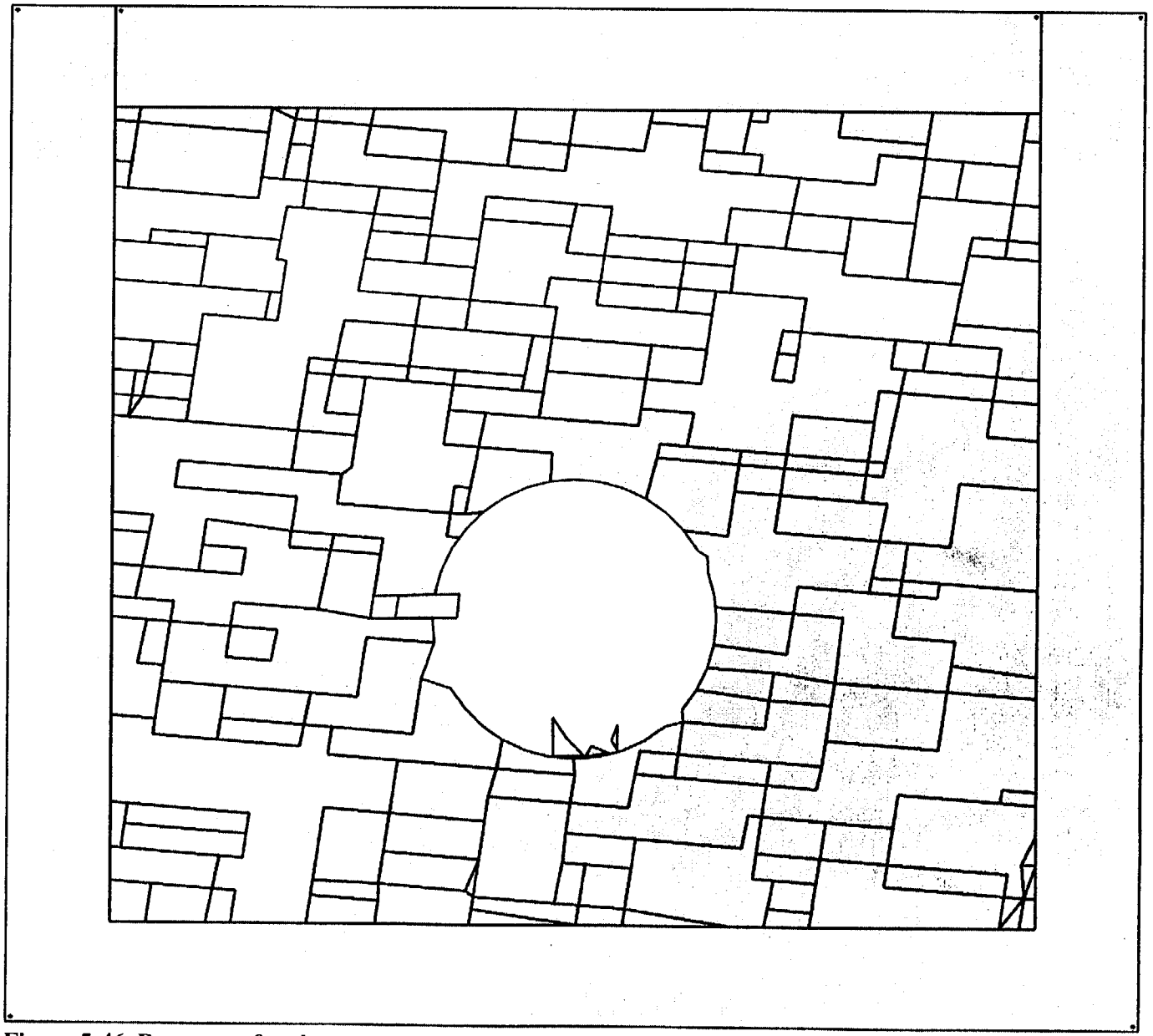

Figure 5-46. Response of rock-mass model in figure 5-34 to the seismic signal shown in figure 3-8

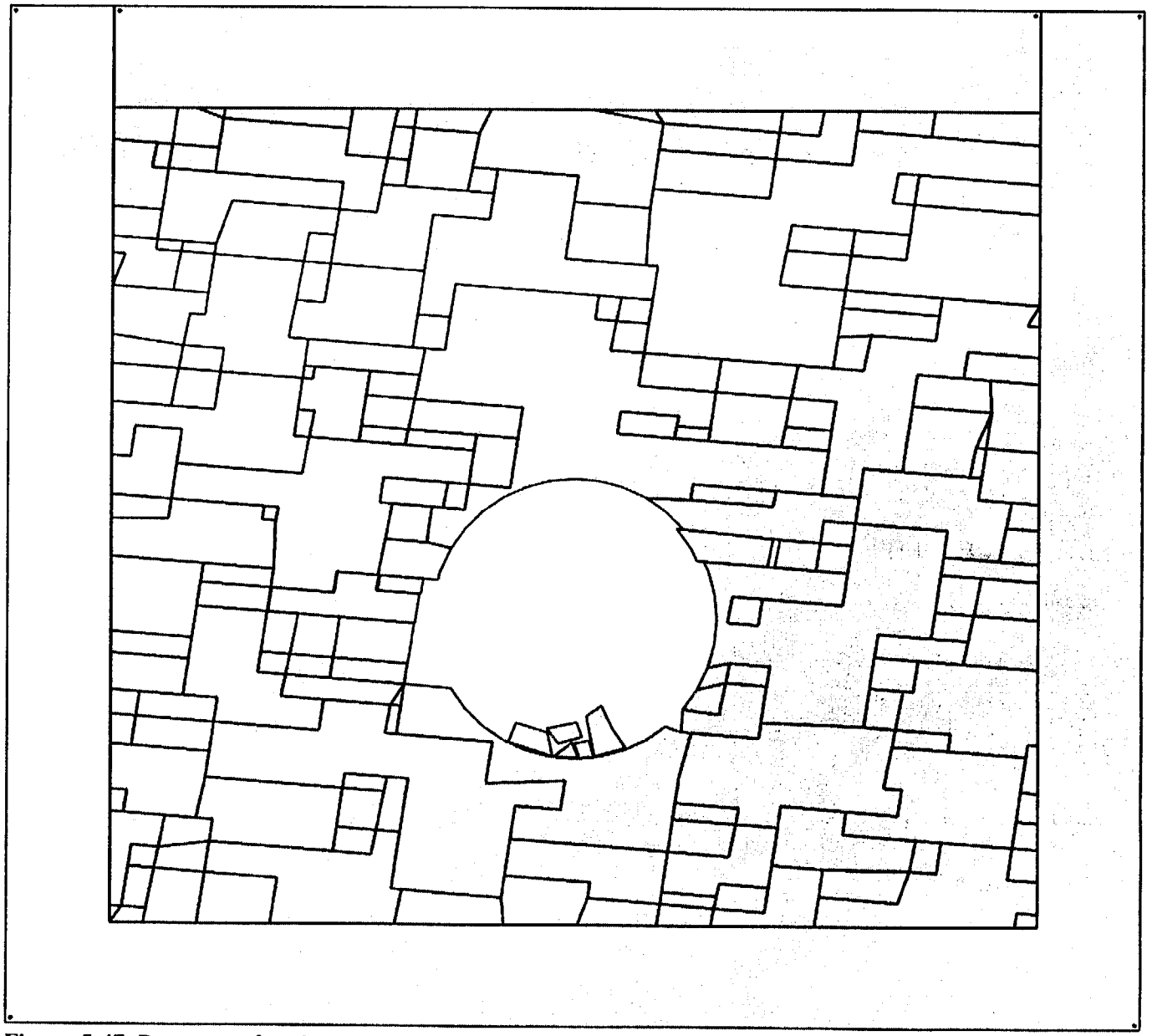

Figure 5-47. Response of rock-mass model in figure 5-35 to the seismic signal shown in figure 3-8

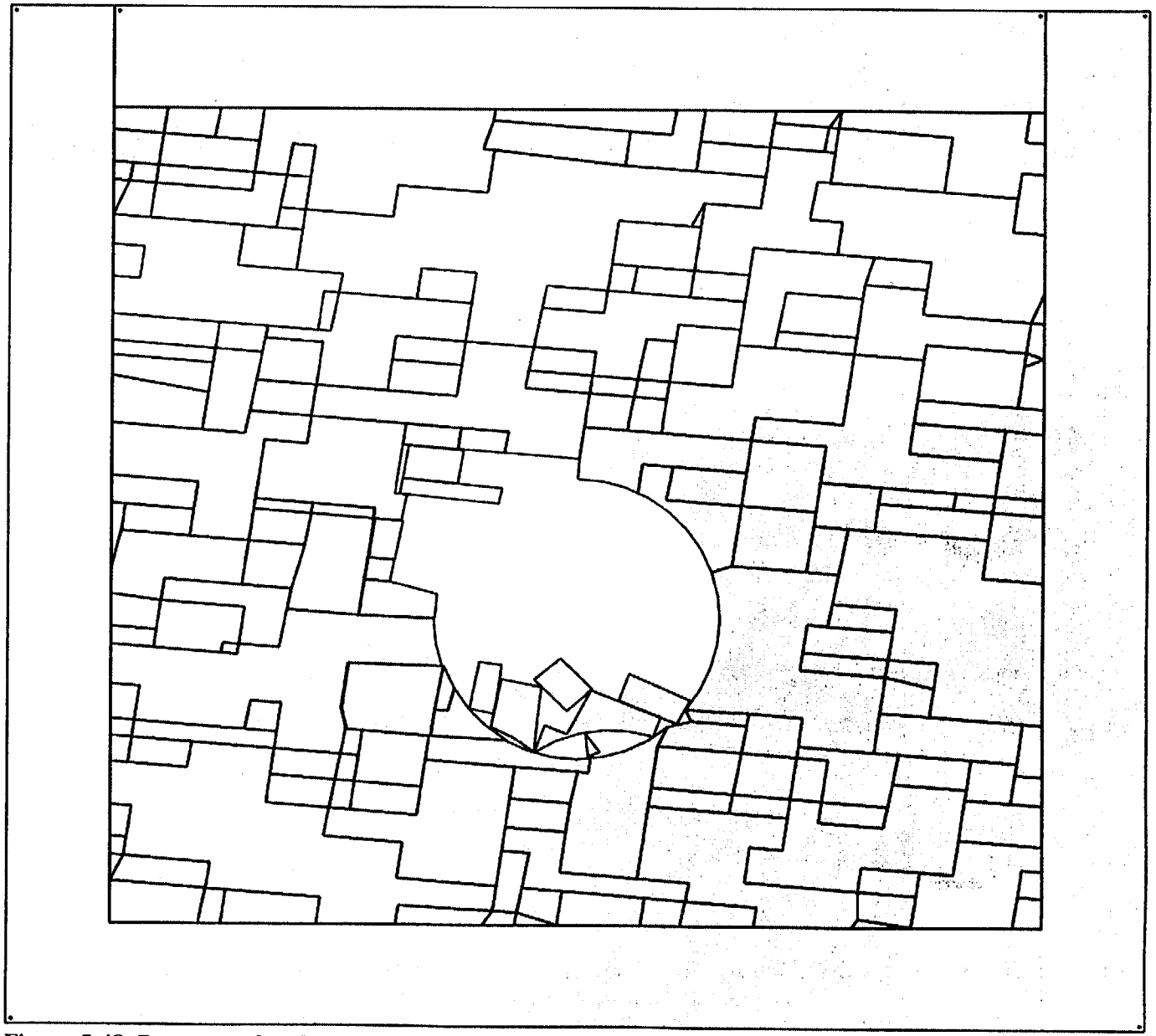

Figure 5-48. Response of rock-mass model in figure 5-36 to the seismic signal shown in figure 3-8

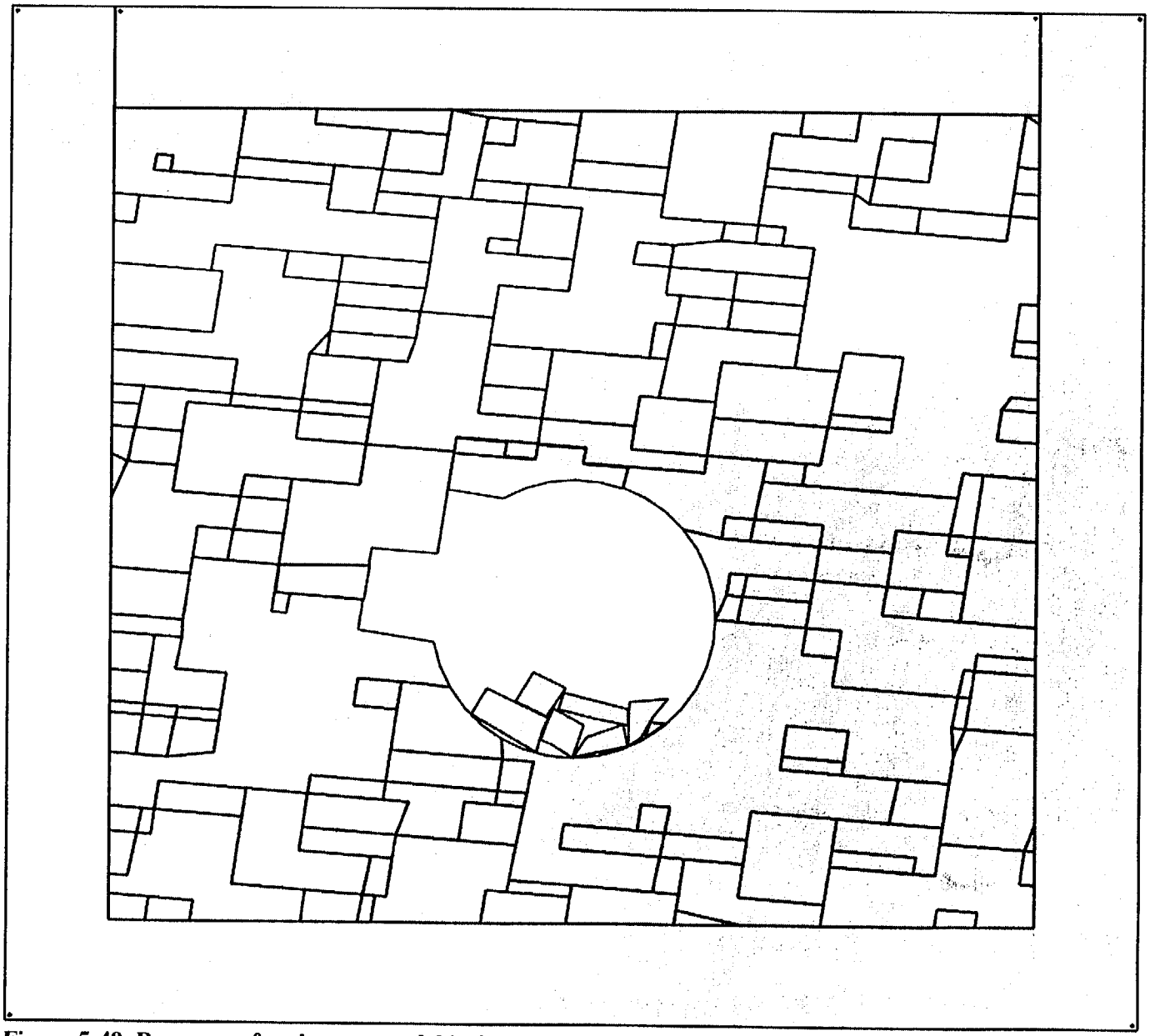

Figure 5-49. Response of rock-mass model in figure 5-37 to the seismic signal shown in figure 3-8

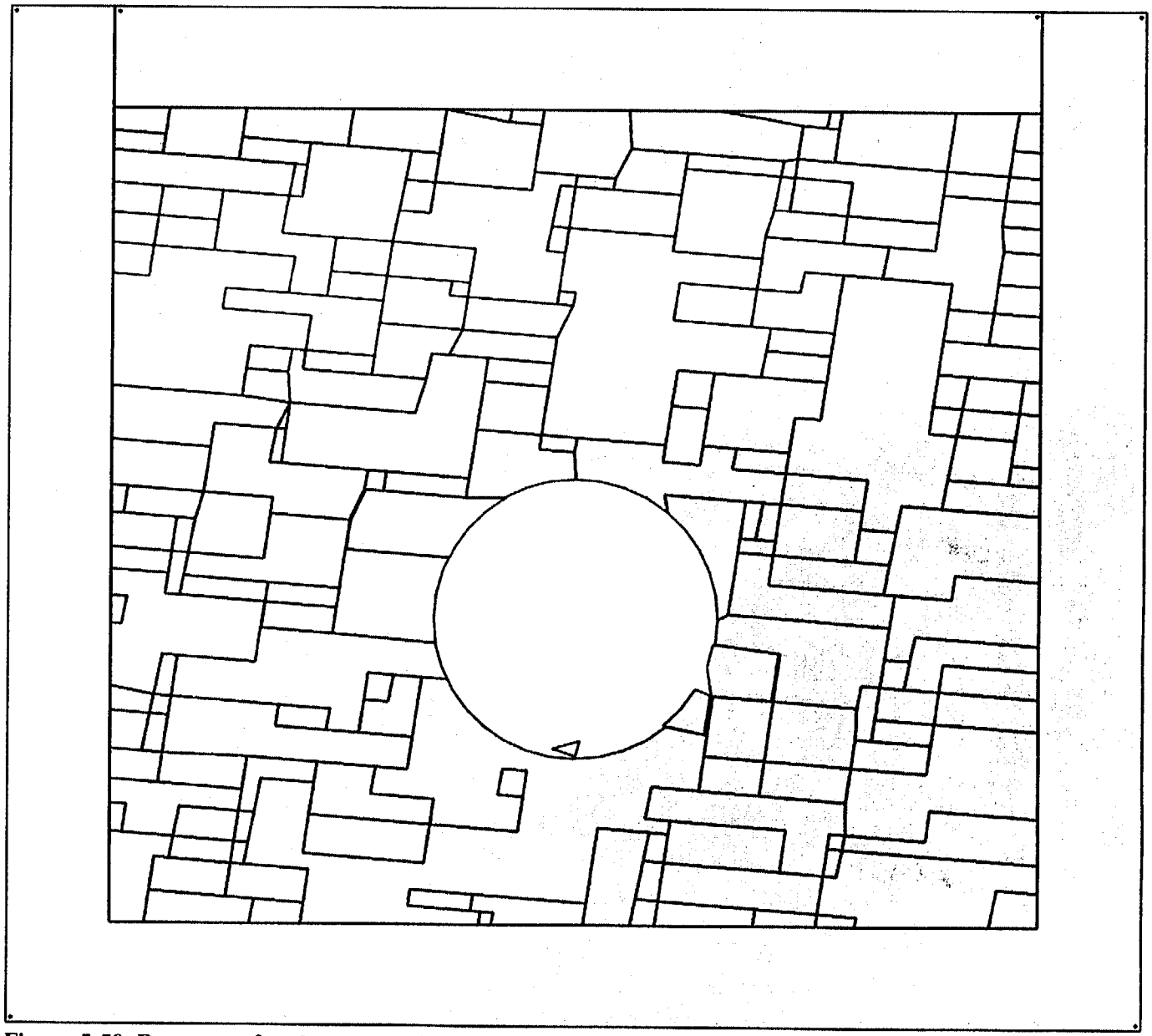

Figure 5-50. Response of rock-mass model in figure 5-38 to the seismic signal shown in figure 3-8

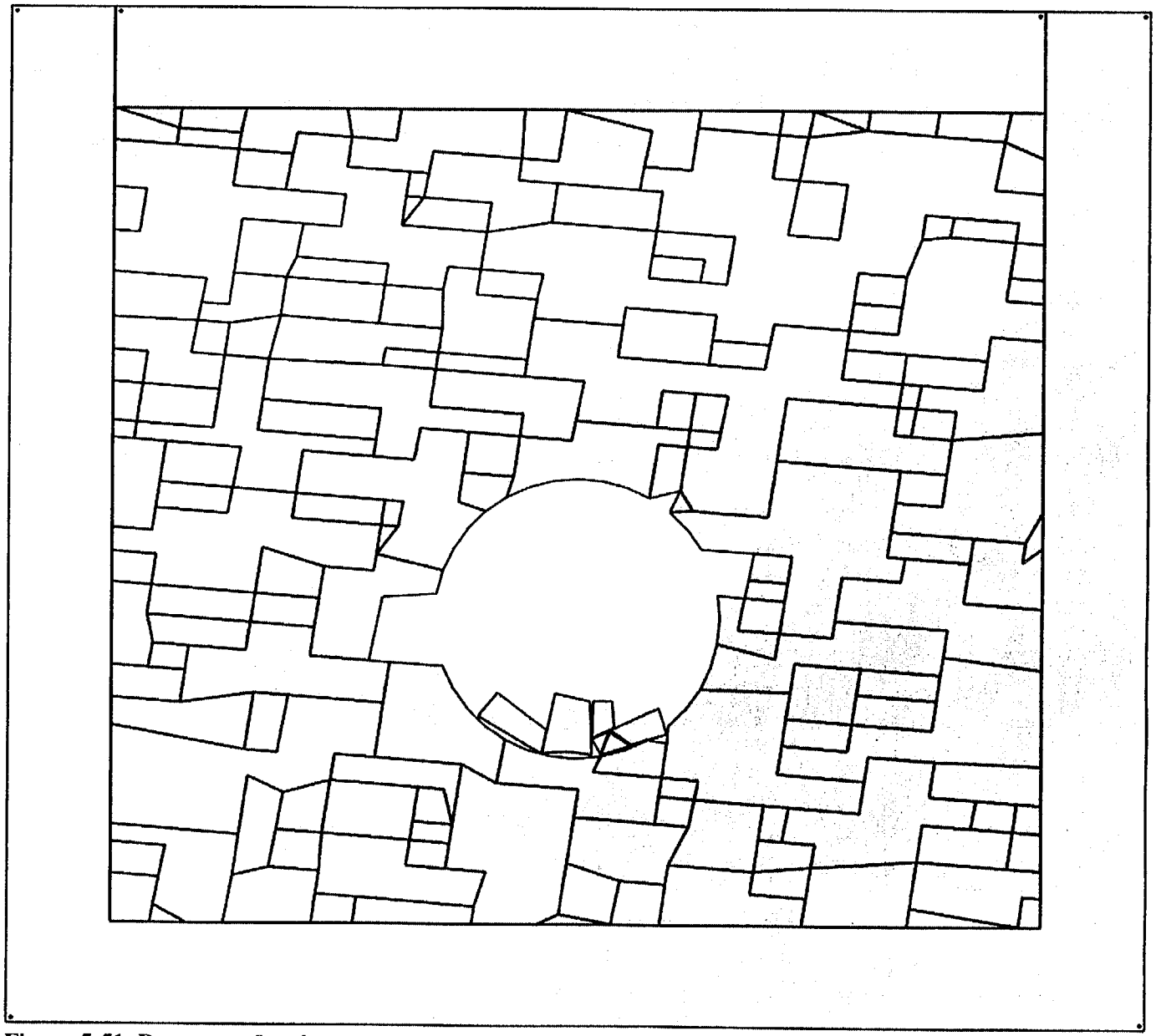

Figure 5-51. Response of rock-mass model in figure 5-39 to the seismic signal shown in figure 3-8

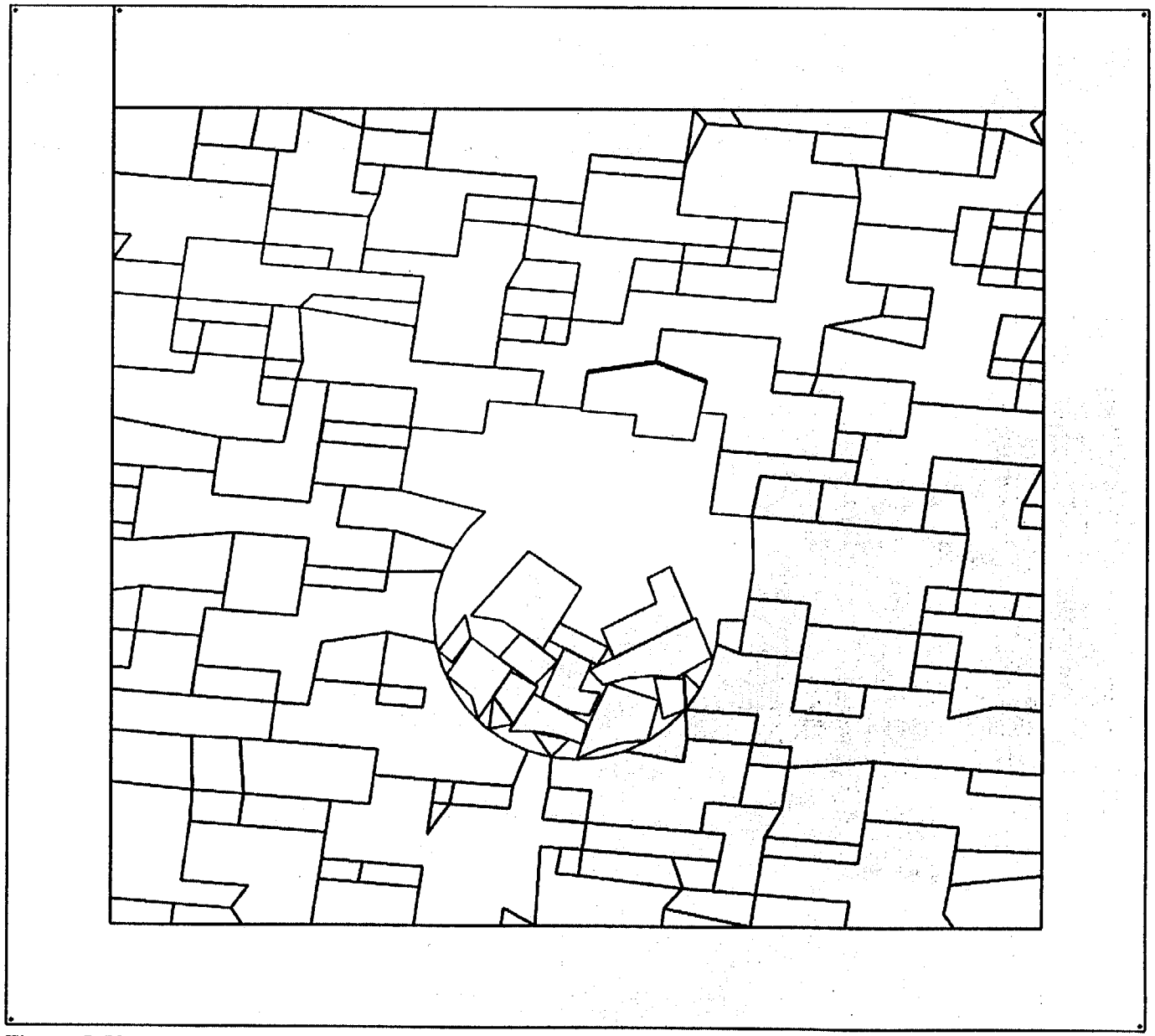

Figure 5-52. Response of rock-mass model in figure 5-40 to the seismic signal shown in figure 3-8

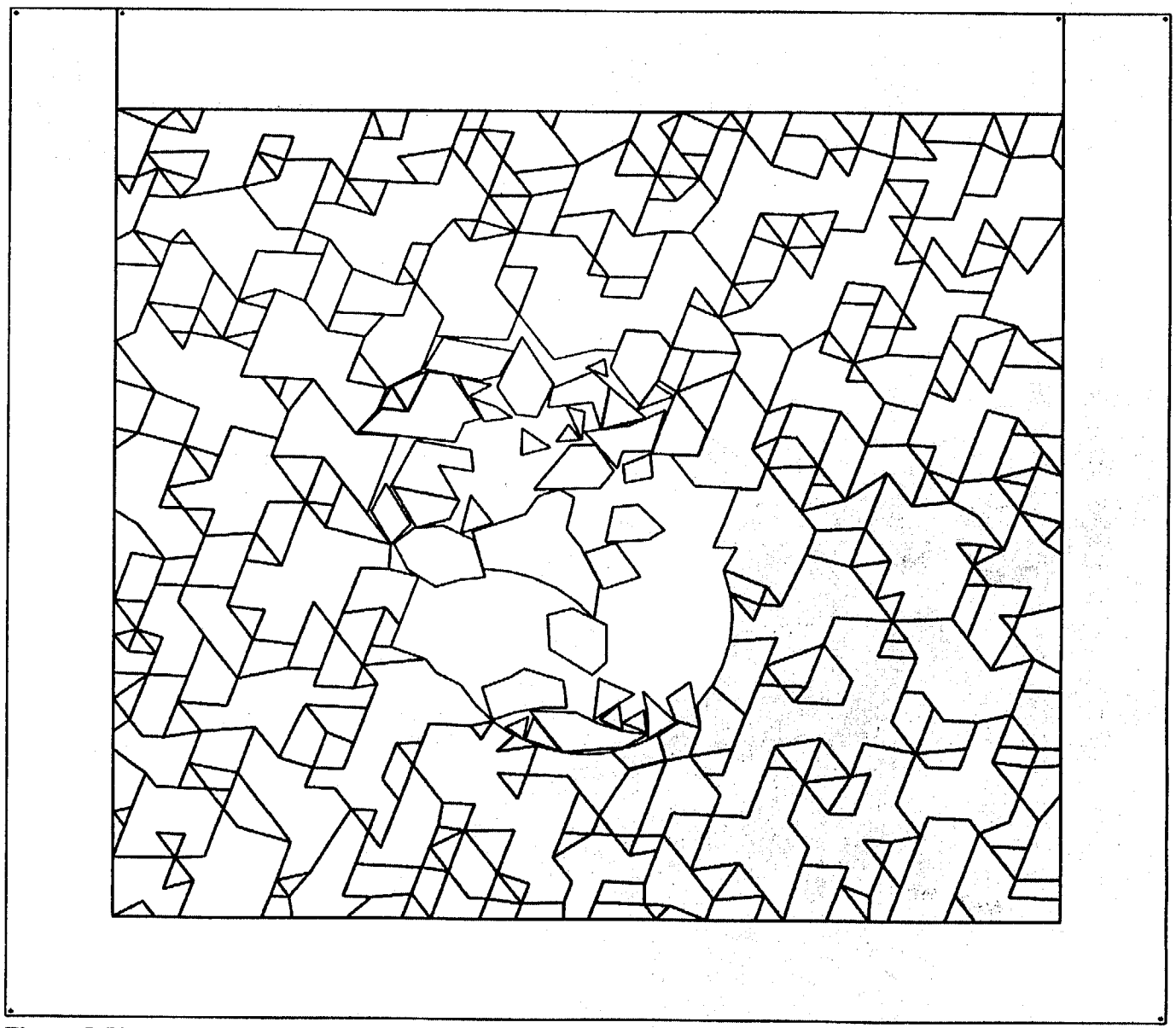

Figure 5-53. Response of rock-mass model in figure 4-2 to the seismic signal shown in figure 3-8 with a 2/5 scaling to the acceleration amplitudes and with a degraded joint friction angle from 39 to 30 degrees

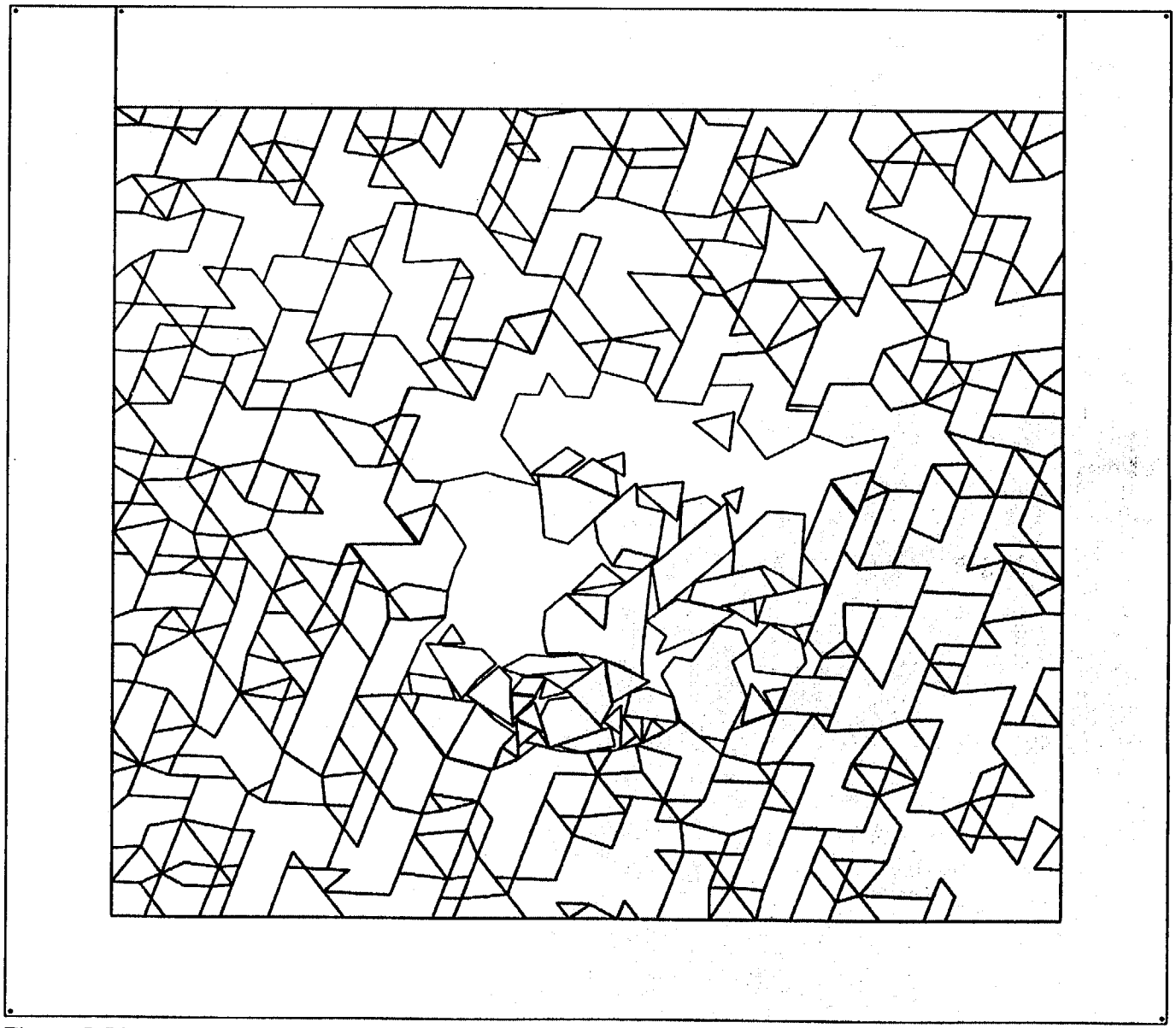

Figure 5-54. Response of rock-mass model in figure 5-9 to the seismic signal shown in figure 3-8 with a 2/5 scaling to the acceleration amplitudes and with a degraded joint friction angle from 39 to 30 degrees

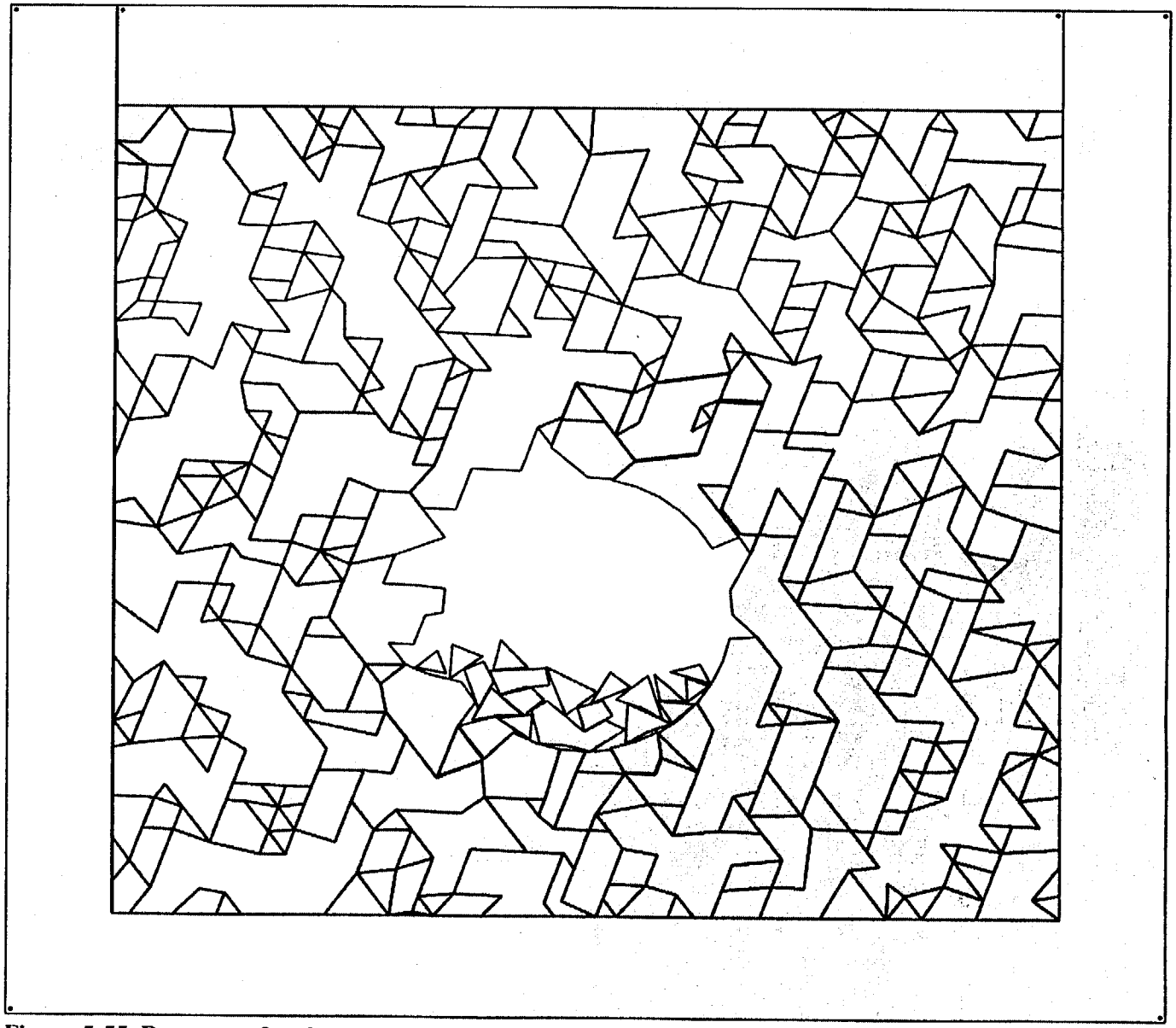

Figure 5-55. Response of rock-mass model in figure 5-10 to the seismic signal shown in figure 3-8 using the second order polynomial displacement function

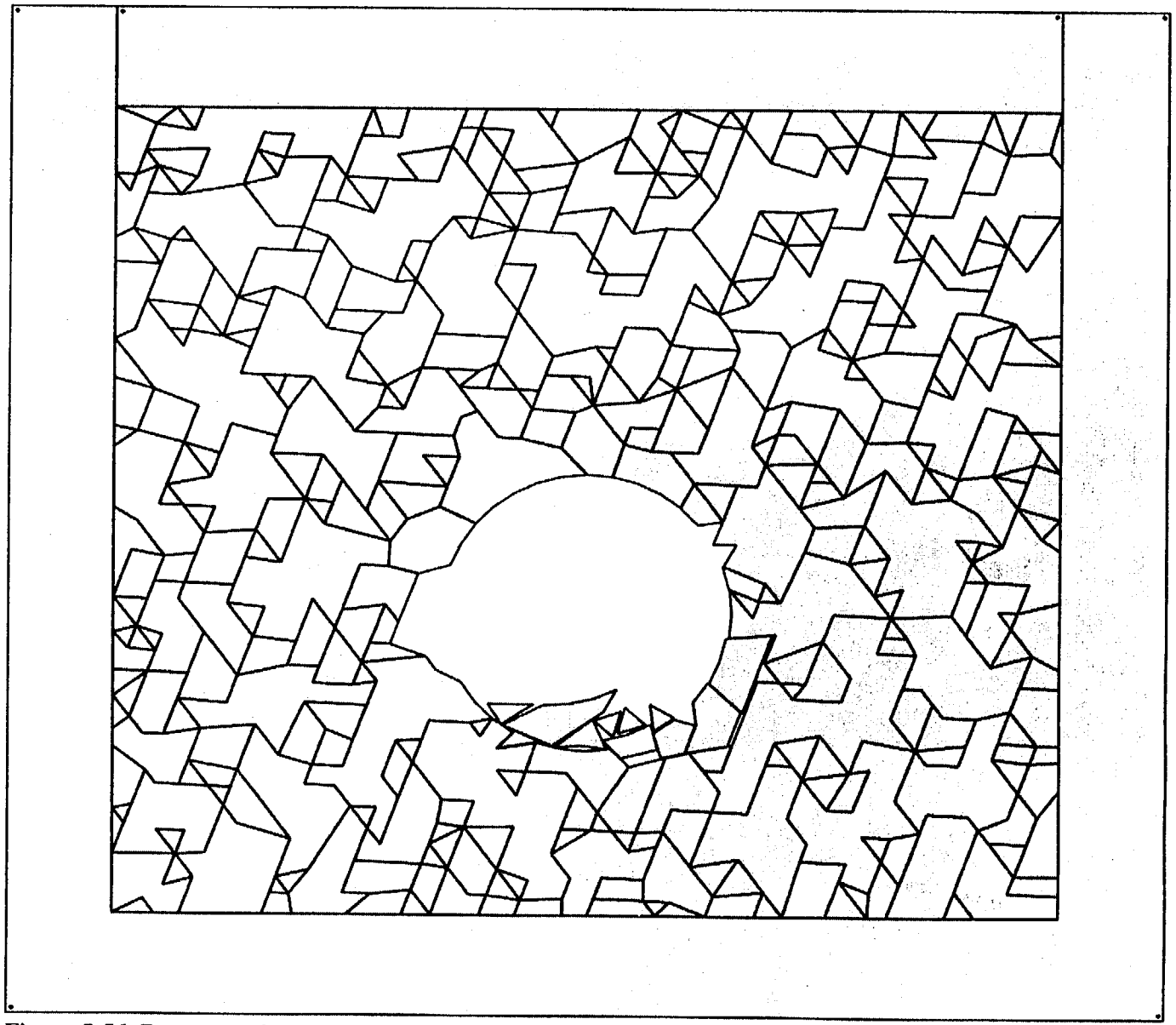

Figure 5-56. Response of rock-mass model in figure 4-2 to the seismic signal shown in figure 3-8 with a 1/2 scaling to the acceleration amplitudes using the second order polynomial displacement function

6 DISTRIBUTION OF ROCKFALL

As discussed in section 1, the primary objectives of this study are to (i) develop a database for rockfall with respect to magnitudes of ground motions and (ii) assess the change in drift geometry due to ground motions. The second objective is addressed in section 5 where the results indicated that changes in shapes of emplacement drifts due to seismicity varied dramatically for the small joint spacing cases after considerations of inherent variations in joint parameters. For the large joint spacing cases, however, the changes in drift geometry were much less dramatic than those for the small joint spacing cases simply due to the relatively stable nature of the emplacement drifts in the rock mass with large joint spacings. The findings on changes in drift geometry due to seismicity should be valuable input for assessing the effects of geometrical changes on fluid flow in the near-field environment. It should be noted that the conclusion drawn for the large joint spacing cases is based on analysis results that did not take into consideration the variations in joint orientations, especially joint dip angles. Investigation of the effects of joint orientation variations is currently under way. Preliminary findings suggest that inclusion of joint orientation variations in the analyses may affect the conclusion somewhat but may not be as dramatic as that found for the small joint spacing cases. The results of this investigation will be presented once they become available. Discussions related to the first objective are presented in the following subsections.

6.1 SIZE DISTRIBUTION

Rock masses with large joint spacings normally contain both small and large rock blocks. The large blocks were considerably bigger than the large blocks for rock masses with small joint spacings. It has been shown in section 5 that these rock masses appear to be kinematically more stable. Although seismically induced rockfall did take place occasionally, the number and size of rock blocks involved are relatively small. It should be pointed out that DDA analyzes deformation of blocky systems in a 2D domain. Determination of volume of rockfall for rock blocks from the DDA results is therefore not possible. Due to the inability to determine volumes of the fallen rock blocks for the 2D DDA analyses, it was decided that the size distributions be presented as volume per unit drift length.

Figure 6-1 shows the size distributions of rockfall induced by a ground motion with a PGA of 0.75 g for the 10 large joint spacing cases of the DDA realizations studied. This figure substantiates the discussion in section 5 that rockfall induced by seismicity for rock masses with large joint spacings involves small sizes of rock blocks. It can be noticed in the figure that more than 90 percent of the rock blocks that fell are smaller than 0.8 m^3 per unit drift length. The largest rock block that fell was approximately 1.1 m^3 per unit drift length. Figure 6-2 presents the accumulated rockfall distribution for the large joint spacing cases.

Figure 6-3 shows the size distributions of rockfall induced by ground motions with PGAs of 0.75 g and 0.3 g, and figure 6-4 provides the rockfall size distribution for ground motions with PGAs of 0.225 g, and 0.15 g. The number and size of large rock blocks could increase when more realizations are run. However, it is not expected that the volume distribution will change drastically. It can be observed that irrespective of magnitudes of ground motions, small sizes of rock blocks dominate rockfall events—with more than 90 percent of the block sizes smaller than 0.8 m^3 per unit drift length. However, rockfall occurred with block sizes bigger than 2 m^3 per unit drift length for cases with PGAs of 0.75 g and 0.3 g, based on the DDA realizations analyzed so far. The maximum rockfall size was approximately 3.1 m^3 per unit drift length for 0.75 g PGA ground motion and 1.7 m^3 per unit drift length for 0.3 g PGA. The rockfall sizes induced by

0.225 g and 0.15 g PGA ground motions were, in general, smaller than those induced by the 0.75 g and 0.3 g PGA ground motions. It should be noted that the size distributions for 0.3 g and 0.225 g PGA ground motions are based on limited modeling results. Figure 6-5 shows the accumulated occurrence of rockfall sizes associated with the four magnitudes of ground motions indicated in figures 6-3 and 6-4.

6.2 POTENTIAL AREAL COVERAGE

In developing an understanding of rockfall potential for emplacement drifts, two areas of primary interest are extent and areal coverage. The first area of interest was discussed in the previous subsection. The second item is discussed next.

It has been pointed out earlier that DDA is a 2D approach for analyzing the deformation of a blocky system. Therefore, assessing areal coverage of seismically induced rockfall based on DDA modeling results is not straightforward. The DDA modeling results for all realizations presented in this report showed some amount of rockfall. The extent of rockfall varied from realization to realization. Figure 6-6 shows the accumulated volumes per unit drift length of rockfall for various DDA realizations formed using large joint spacings. These realizations were subjected to a ground motion with a PGA of 0.75 g. The figure indicates the amount of rockfall for the first two realizations is practically negligible. In fact, the total volumes of rockfall available for the first five realizations could be considered sufficiently small that their effect, if any, can be neglected without affecting performance. Because the total volumes of rockfall are made of several rock blocks, individually the effects are even smaller. It should be noted that this result does not include formation of new blocks due to thermal load and long-term strength degradation of blocks. If thermally induced stresses are sufficiently high to fracture rock blocks, more rockfall could occur and the sizes of blocks that fall could potentially increase as well.

Figure 6-7 shows the accumulated volumes per unit drift length of rockfall due to a 0.75 g PGA ground motion for various DDA realizations formed using small joint spacings. The calculation for accumulated volumes of rockfall for other levels of ground motion is not meaningful due to a limited number of realizations analyzed in this study. Therefore, they are not presented in this report. More results are being generated. Examination of figure 6-7 indicates that the potential effect of the rockfall associated with realization 1 may be neglected; however, the significance of potential effects of other realizations may require further evaluation. Consistent with the discussion presented in section 5, it can be observed from figures 6-6 and 6-7 that the total volume per unit drift length, in general, is significantly bigger for the small joint spacing cases than for the large joint spacing cases.

Figures 6-6 and 6-7 present the total volumes of rockfall due to a particular event. Rockfall may include a wide range of block sizes. The effect of these individual rock blocks is obviously not the same as that of one rock block having a volume equal to the total volume. Observing the DDA results obtained thus far on rockfall, it may be concluded that multiple rock blocks falling in unison (i.e., considered as a single block) were rare. The resulting increase in volume when compared to the individual blocks was small.

However, multiple blocks falling in a short period of time due to ground motion will result in multiple impacts on drip shields and WPs. It is not clear what the effect will be with this mode of rockfall. However, it is likely that the integral effect on the performance of drip shields and WPs may fall in between the effect of an individual block and that of multiple blocks falling in unison. Some study in this regard may be needed.

It should be noted that, when considering the effect of an individual rock block, its size and initial location relative to the drip shield and WP are two important parameters. Determination of block size and initial location of the block is straightforward. However, an approach will need to be developed to include this information in the SEISMO module.

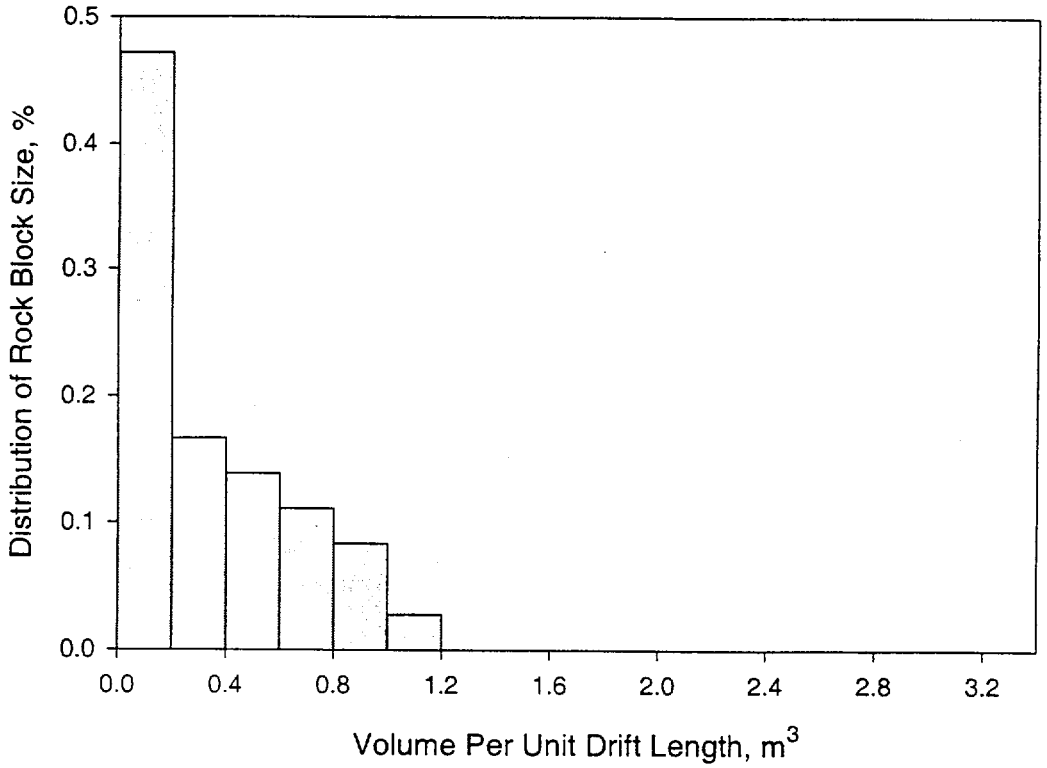

Figure 6-1. Size distributions of seismically induced rockfall for large joint spacing cases subjected to a 0.75-g peak ground acceleration ground motion

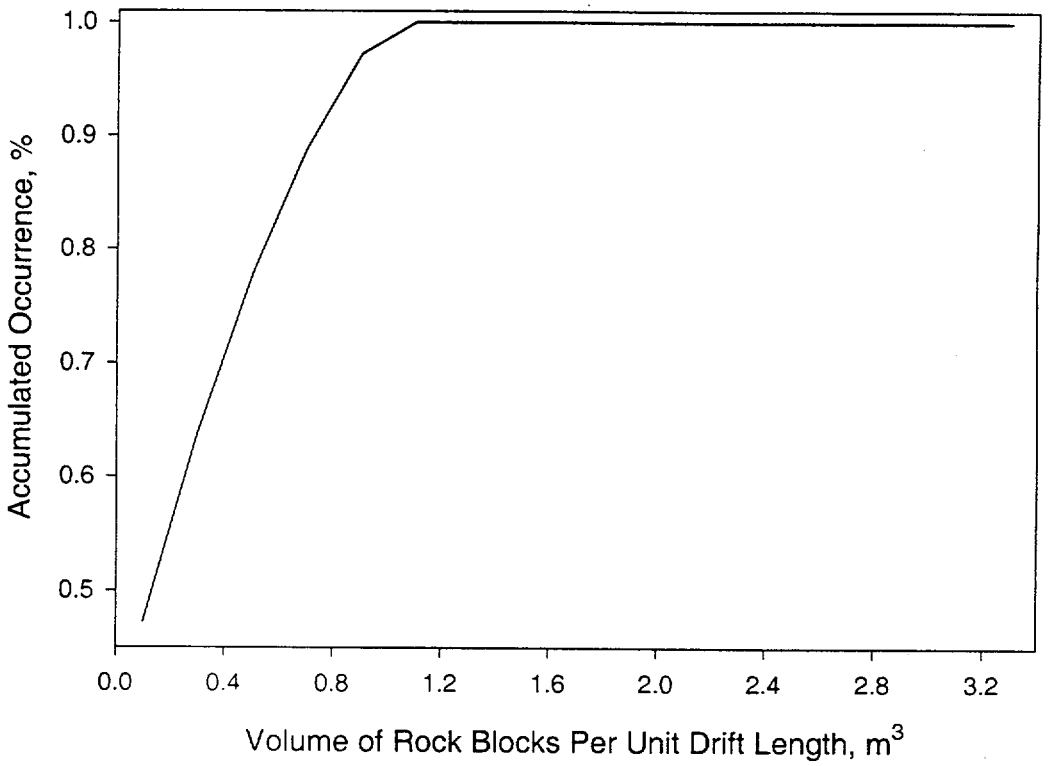

Figure 6-2. Cumulative distribution of rockfall sizes for large joint spacing cases subjected to a 0.75-g peak ground acceleration ground motion

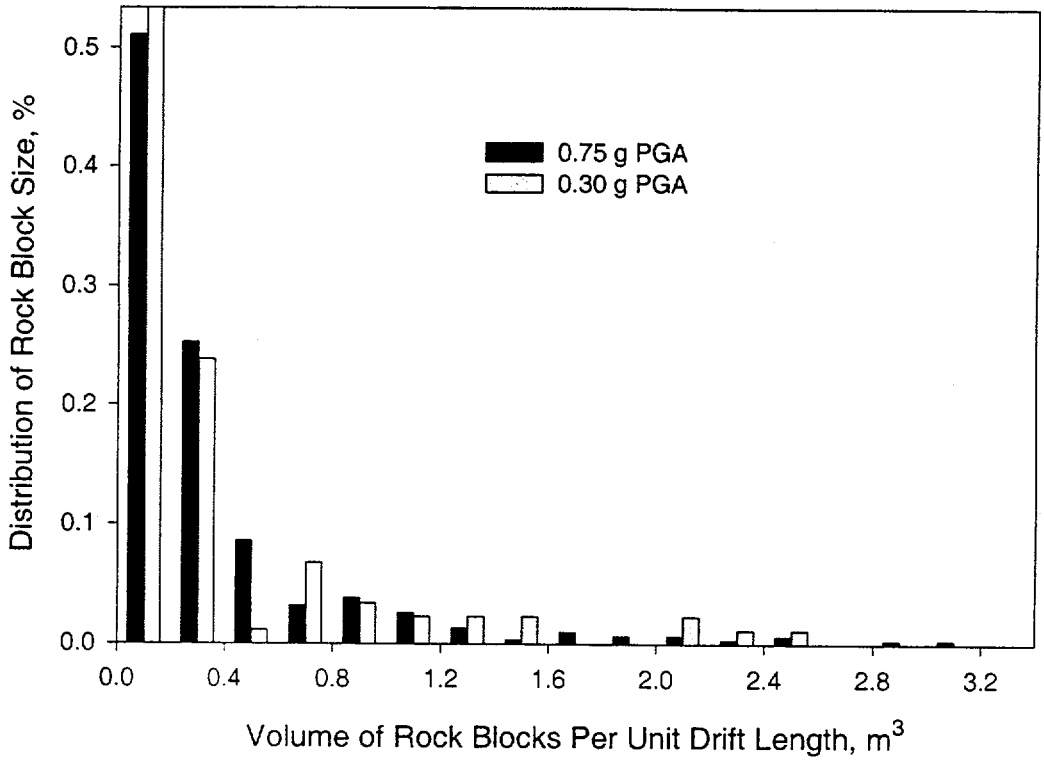

Figure 6-3. Size distributions of rockfall for small joint spacing cases subjected to 0.75-g and 0.3-g peak ground acceleration ground motions

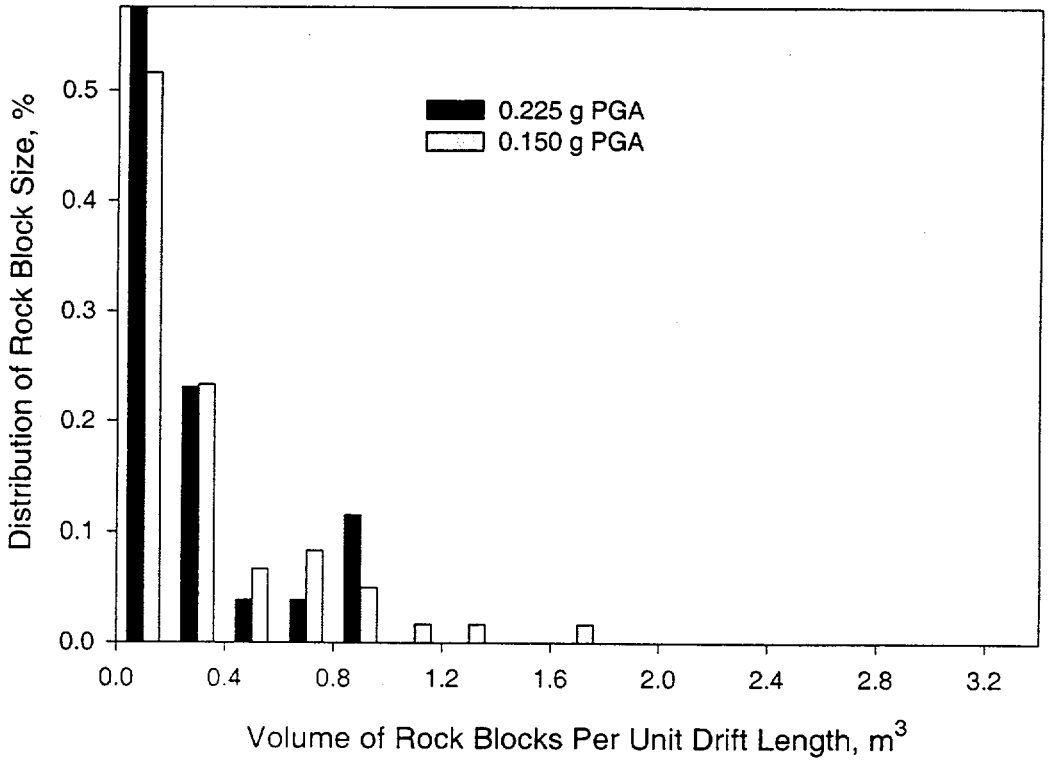

Figure 6-4. Size distributions of rockfall for small joint spacing cases subjected to 0.225-g and 0.15-g peak ground acceleration ground motions

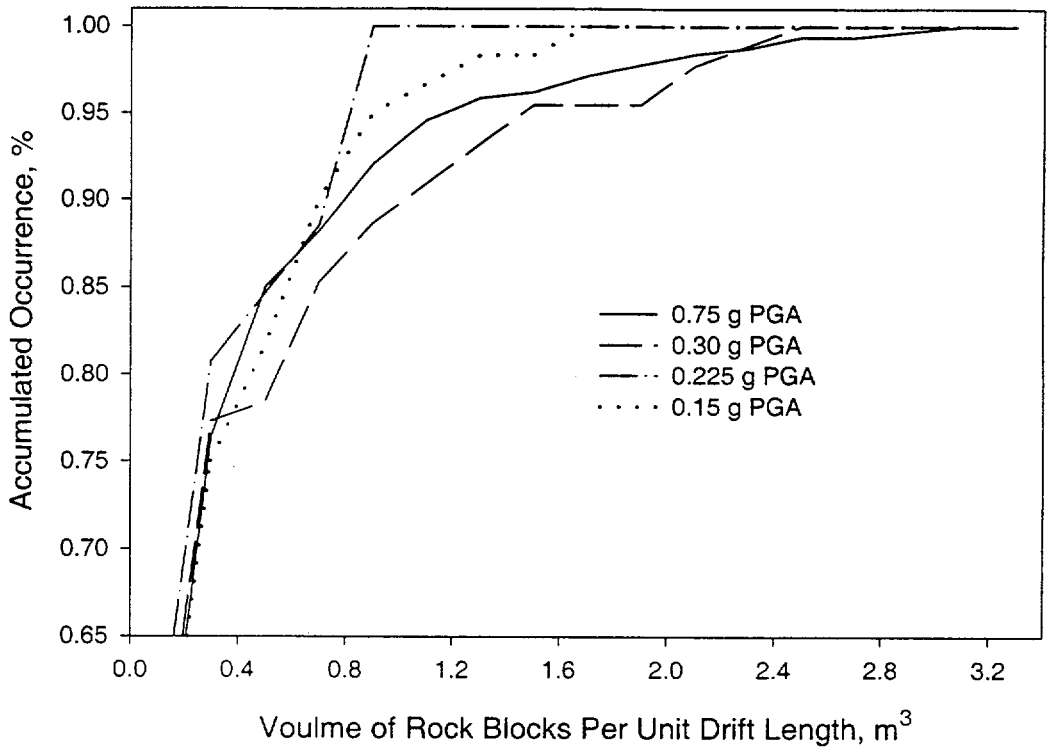

Figure 6-5. Cumulative distribution of rockfall for small joint spacing cases subjected to 0.75-g, 0.3-g, 0.225-g, and 0.15-g peak ground acceleration ground motions

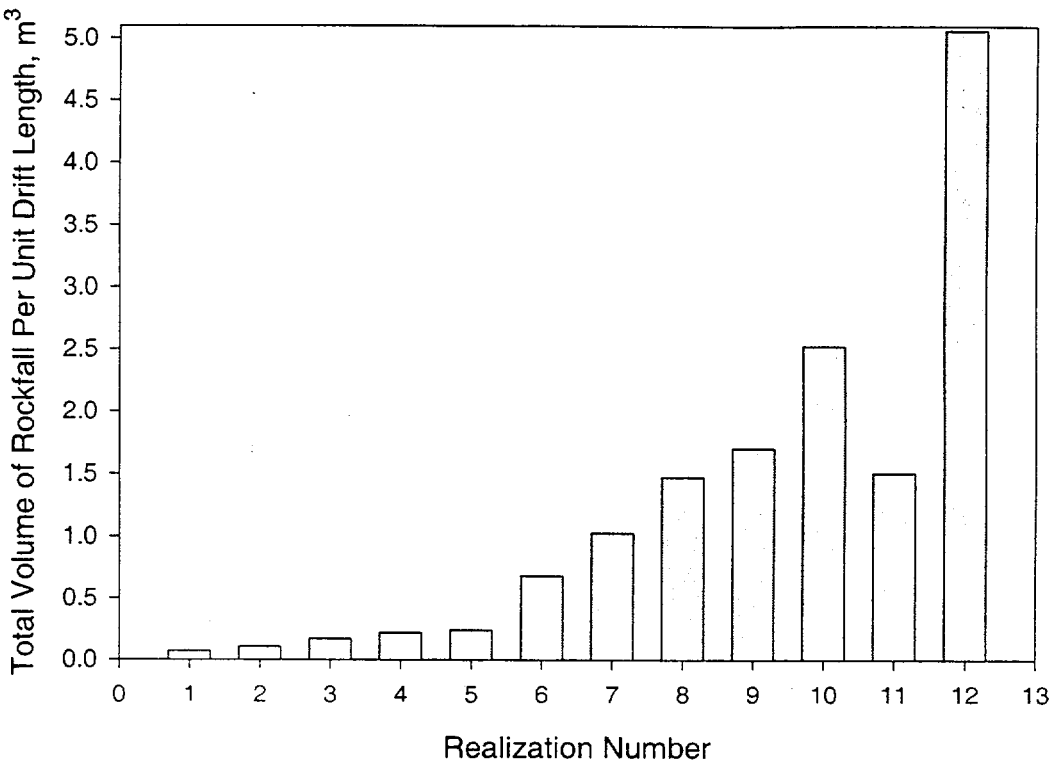

Figure 6-6. Total amount of rockfall for each Discontinuous Deformation Analysis model realization for large joint spacing cases

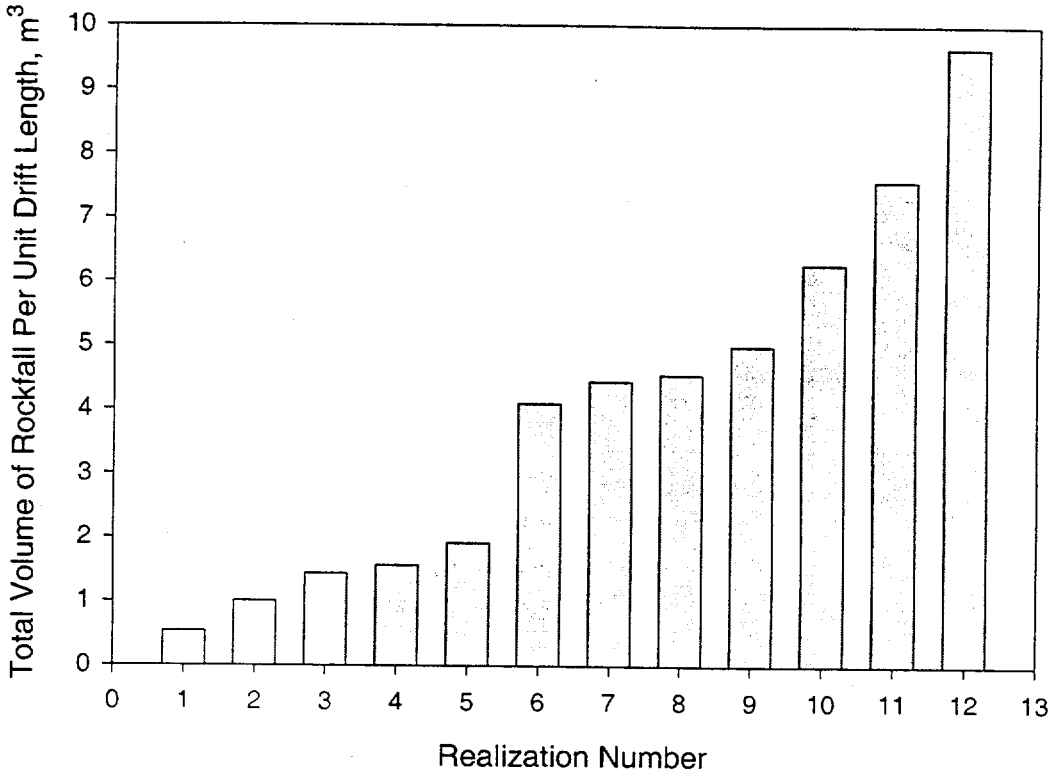

Figure 6-7. Total amount of rockfall for each Discontinuous Deformation Analysis model realization for small joint spacing cases

7 CONCLUSIONS

The investigation of seismically induced rockfall in emplacement drifts attempts to develop a database on rockfall potential for different levels of ground motions, evaluate the effects of the characteristics of ground motion on drift stability, and assess the effects of such rockfall on emplacement drift geometry. 2D DDA computer codes were used to evaluate rockfall induced by various magnitudes of input ground motion for the emplacement drifts located in the TSw2 thermo-mechanical unit with both small and large joint spacings. Simulation of earthquake ground motion in this study was approximated by applying the forces induced by ground accelerations directly to the blocks as body forces. Propagation of waves through the DDA model domain was not simulated.

Thermal load was not included in the analysis because DDA is not capable of simulating formation of new blocks that may be the primary failure mechanism at YM. The effects of long-term degradation on joint shear strength (in the form of joint friction angle because joint cohesion was assumed to be 0 in this study) were analyzed in this investigation.

In analyzing seismically induced rockfall in the emplacement drifts, realizations of the DDA model were formed from the same joint information, specifically considering the variations associated with joint spacing, joint length, and joint bridge (gap). In generating these realizations, the joint spacing, length, and bridge were assumed to be uniformly distributed with a ±35 percent variation about the mean values.

Sinusoidal velocity waves with a frequency of 10 Hz, duration of 3 s, and amplitudes equal to the appropriate levels of PGVs were used by the CRWMS M&O (2000a,b) to study ground control and drift degradation. The DDA results suggested that the rock-mass responses to ground motions cannot be sufficiently captured using the sinusoidal waves specified when compared to the actual ground motion time histories. Consequently, the CRWMS M&O may need first to demonstrate that the sinusoidal waves mentioned can bound the effects induced by the site-specific ground motion time histories developed for the proposed YM site. If this demonstration is insufficient, site-specific or a modified sinusoidal wave should be used for ground control and drift degradation analyses.

This study suggested that the responses of rock masses depend on the geometries of the blocky systems. The damage of drifts ranges from a few small rock blocks that fall into the drifts to a substantial collapse of the drifts. Consequently, analyses should be performed on a sufficient number of realizations to assess the stability of drifts so that the conditions for the most critical damage can be identified for the purposes of ground support design and drift degradation assessment. The rock masses with large joint spacings were found to be more stable and the extent of rockfall was, in general, less than that with small joint spacings.

The DDA results showed that magnitudes of ground motion have an effect of drift stability, and the extent of such effect is geometry-dependent. The physical effects could be in the forms of additional rockfall or accumulation of joint slip as the magnitude increases, and it is often a combination of the two.

The DDA results for the effects of repeated earthquakes indicated that the second earthquake, in some cases, could cause significantly more damage to the drifts even if this episode had the same magnitude as the first one. This result demonstrates that repeated ground motions could have a detrimental effect on excavation stability. This result also confirms the findings from laboratory and field studies: the fundamental failure

mechanism of an excavation subjected to repeated episodes of seismic events is accumulation of joint deformations.

More than 90 percent of the rock blocks that fell were small for both large and small joint spacing cases. The effect of these types of rockfall on the performance of drip shields and WPs may be small. Based on limited modeling results, the maximum rock block sizes identified from the realizations performed for the large and small joint spacing cases were approximately 1.1 and 3.1 m^3 per unit drift length, respectively. These values may change when more modeling results become available. Note that the rock block size is presented in volume per unit drift length in this report because the actual rock block volume falling on one waste package cannot be estimated from a 2D analysis. The rock block volume will depend on the joint spacing in the third dimension. It should be noted that the results were based on the assumption that joints with joint trace length smaller than 1 m have no effect on seismically induced rockfall. The presence of these joints could potentially increase the possibility of forming relatively smaller blocks that may make the condition relatively less stable, hence, increase the potential for rockfall. These joints were not included in the analyses because data on them are not available.

Long-term degradation of joint shear strength could significantly decrease stability of the drifts. Consequently, in assessing rockfall of the emplacement drifts during the postclosure period, long-term degradation of joint shear strength needs to be considered. Another important factor that may significantly change the findings presented in this report regarding rockfall size and extent is the presence of thermal load. This is especially true for the large joint spacing cases where large blocks surrounding the drifts are kinematically stable without the influence of thermal load. If the thermally induced stresses are high, breaking these large blocks becomes possible. If fracturing of these large blocks occurs, kinematically unstable conditions may result and thus increase rockfall potential. It is therefore imperative to include this intact rock failure mechanism when assessing rockfall potential at YM.

8 REFERENCES

Ahola, M.P., R. Chen., H. Karimi., S.M. Hsiung, and A.H. Chowdhury. *A Parametric Study of Drift Stability in Jointed Rock Mass. Phase I: Discrete Element Thermal-Mechanical Analysis of Unbackfilled Drifts*. San Antonio, TX: Center for Nuclear Waste Regulatory Analyses. 1996.

Barrett. L.H. *Basis for Department of Energy Design Selection*. Letter (September 10) to J. L. Cohon. Washington, DC: U.S. Department of Energy. 1999.

Barton, N., and H. Hansteen. Very large span openings at shallow depth: Deformation magnitudes from jointed models and finite element analysis. *Proceedings of the Fourth Rapid Excavation and Tunneling Conference, Atlanta, Georgia*. 2: 1,331–1,353. 1979.

Brown, E.T., and J.A. Hudson. Fatigue failure characteristics of some models of jointed rock. *Earthquake Engineering and Structural Dynamics* 2: 379–386. 1974.

Chen, G., and Y. Ohnishi. 1999. Practical Computing Formulas of Simplex Integration, *Proceedings of the 3rd International Conference on Analysis of Discontinuous Deformation from Theory to Practice*, Ed., B. Amadei, 75-84, Vail, CO.

Civilian Radioactive Waste Management System Management and Operating Contractor. *Yucca Mountain Site Geotechnical Report*. B00000000–01717–5705–00043. Volume 1. Revision 01. Las Vegas, NV: Civilian Radioactive Waste Management System Management and Operating Contractor. 1997a.

Civilian Radioactive Waste Management System Management and Operating Contractor. *Configuration of Empirical Design Methodologies*. BABEE0000–01717–5705–00002. Revision 00. Las Vegas, NV: Civilian Radioactive Waste Management System Management and Operating Contractor. 1997b.

Civilian Radioactive Waste Management System Management and Operating Contractor. *Probabilistic Seismic Hazard Analysis for Fault Displacement and Vibrational Ground Motion at Yucca Mountain, Nevada*. Final Report. Las Vegas, NV: Civilian Radioactive Waste Management System Management and Operating Contractor. 1998.

Civilian Radioactive Waste Management System Management and Operating Contractor. *License Application Design Report*. B00000000–01717–4600–00123. Revision 01. Las Vegas, NV: Civilian Radioactive Waste Management System Management and Operating Contractor. 2000a.

Civilian Radioactive Waste Management System Management and Operating Contractor. *Repository Safety Strategy: Plan to Prepare the Postclosure Safety Case to Support Yucca Mountain Site Recommendation and Licensing Considerations*. TDR–WIS–RL–000001. Revision 03. Las Vegas, NV: Civilian Radioactive Waste Management System Management and Operating Contractor. 2000b.

Civilian Radioactive Waste Management System Management and Operating Contractor. *Drift Degradation Analysis*. ANL–EBS–MD–000027. Revision 01. Las Vegas, NV: Civilian Radioactive Waste Management System Management and Operating Contractor. 2000c.

Civilian Radioactive Waste Management System Management and Operating Contractor. *Ground Control for Emplacement Drifts for SR*. ANL–EBS–GE–000002. Revision 00. Las Vegas, NV: Civilian Radioactive Waste Management System Management and Operating Contractor. 2000d.

Civilian Radioactive Waste Management System Management and Operating Contractor. *Fracture Geometry Analysis for the Stratigraphic Units of the Repository Host Horizon*. ANL–EBS–GE–000006. Revision 00. Las Vegas, NV: Civilian Radioactive Waste Management System Management and Operating Contractor. 2000e.

Cruden, D.M.A. Theory of brittle creep in rock under uniaxial compression. *Journal of Geophysical Research*. 75(17). 1970.

Goodman, R.E., and G.H. Shi. *Block Theory and Its Application to Rock Engineering*. Englewood Cliffs, NJ: Prentice-Hall, Inc. 1985.

Griggs, D.T. The creep of rock. *Journal of Geology* XLVII(3): 225–250. 1939.

Hardy, H.R. Time-dependent deformation and failure of geologic materials. *Proceedings of the Tenth Symposium on Rock Mechanics*. Berkeley, CA: The University of California, Berkeley. 137–175. 1969.

Hsiung, S.M., W. Blake, A.H. Chowdhury, and T.J. Williams. Effects of mining-induced seismic events on a deep underground mine. *PAGEOPH* 139(3/4): 741–762. 1992.

Hsiung, S.M., D.D. Kana, M.P. Ahola, A.H. Chowdhury, and A. Ghosh. *Laboratory Characterization of Rock Joints*. NUREG/CR–6178. Washington, DC: U.S. Nuclear Regulatory Commission. 1994.

Hsiung, S.M., J.D. Fox, and A.H. Chowdhury. Effects of repetitive seismic loads on underground excavations in jointed rock mass. *Proceedings of the Seventh International Conference on Radioactive Waste Management and Environmental Remediation, Nagoya, Japan*. 1999.

Hsiung, S.M., G.H. Shi, and A.H. Chowdhury. *Assessment of Seismically Induced Rockfall in the Emplacement Drifts of the Proposed Repository at Yucca Mountain—Progress Report*. San Antonio, TX: Center for Nuclear Waste Regulatory Analyses. 2000.

Hughson, D., and F. Dodge. The effect of cavity wall roughness on seepage into underground openings. *EOS, Transactions. American Geophysical Union*. Supplement H51B–02: 80(17). 1999.

Law, H.K., and I.P. Lam. Application of Key Block Theory and DDA at Yerba Buena Island Tunnel Portals Under Earthquake Loading, *Proceedings of the Third International Conference on Analysis of Discontinuous Deformation (ICADD–3) from Theory to Practice*. B. Amadei ed. Alexandria, VA: American Rock Mechanics Association: 181–190. 1999.

Ma, M.Y. Development of Discontinuous Deformation Analysis: The first ten years (1986 to 1996). *Proceedings of the Third International Conference on Analysis of Discontinuous Deformation (ICADD–3) from Theory to Practice*. B. Amadei, ed. Alexandria, VA: American Rock Mechanics Association: 17–32. 1999.

Mohanty, S., T.J. McCartin, and D.W. Esh. *Total-system Performance Assessment (TPA) Version 4.0 Code Module Descriptions and User's Guide*. San Antonio, TX: Center for Nuclear Waste Regulatory Analyses. 2000.

Newmark, N.M. Effects of Earthquakes on Dams and Embankments. *Geotechnique*. XV(2), 139–160. 1965.

Scholz, C.H. Mechanism of creep in brittle rock. *Journal of Geophysical Research* 73: 3,295–3,302. 1968.

Sharma, S., and W.R. Judd, Underground opening damage from earthquakes. *Engineering Geology* 30: 263–276. 1991.

Shi, G.H. Block system modeling by discontinuous deformation analysis. *Topics in engineering*: Volume 11. C.A. Brebbia and J.J. Conner, eds. Boston, MA: Computational Mechanics Publications. 1993.

Shi, G.H. 1994. Modeling Dynamic Rock Failure by Discontinuous Deformation Analysis with Simplex Integration, *Proceedings of the 1st North American Rock Mechanics Symposium*, Austin, TX.

Shi, G.H. Discontinuous Deformation Analysis–Technical Note. *First International Forum on Discontinuous Deformation Analysis, Berkeley, California*. 1996.

Shi, G.H. *Discontinuous Deformation Analysis–User's Manual*. Belmont, CA. 1998.

Shi, G.H. Applications of discontinuous deformation analysis and manifold method. *Proceedings of the Third International Conference on Analysis of Discontinuous Deformation (ICADD–3) from Theory to Practice*. B. Amadei, ed. Alexandria, VA: American Rock Mechanics Association: 3–15. 1999.

U.S. Department of Energy. *Viability Assessment of a Repository at Yucca Mountain, Overview*. DOE/RW–0508. Las Vegas, NV: U.S. Department of Energy, Office of Civilian Radioactive Waste Management. 1998a.

U.S. Department of Energy. *Viability Assessment of a Repository at Yucca Mountain. Volume 2: Preliminary Design Concept for the Repository and Waste Package*. DOE/RW–0508 V2. Las Vegas, NV: U.S. Department of Energy, Office of Civilian Radioactive Waste Management. 1998b.

Wawersik, W.R. Time-dependent rock behavior in uniaxial compression. *Proceedings of the Fourteenth Symposium on Rock Mechanics, Pennsylvania State University*. 85–106. 1972.

Wilder. D.G., and J.L. Yow. *Geomechanics of the Spent Fuel Test—Climax*. UCRL–53767. Livermore, CA: Lawrence Livermore National Laboratory. 1987.